

D-33192
Version 8.0

Earth Observing System (EOS) Tropospheric Emission Spectrometer (TES)



Data Validation Report (Version F08_12 data)

Editors:

Robert Herman and Gregory Osterman

Contributors:

Matthew Alvarado, Christopher Boxe, Kevin Bowman, Karen Cady-Pereira, Tony Clough, Annmarie Eldering, Brendan Fisher, Dejian Fu, Robert Herman, Daniel Jacob, Line Jourdain, Le Kuai, Susan Kulawik, Michael Lampel, Qinbin Li, Jennifer Logan, Ming Luo, Inna Megretskaya, Ray Nassar, Gregory Osterman, Susan Paradise, Vivienne Payne, Hank Revercomb, Nigel Richards, Mark Shephard, Dave Tobin, Solene Turquety, Felicia Vilrotter, Kevin Wecht, Helen Worden, John Worden, Lin Zhang

December 31, 2019

JPL

Jet Propulsion Laboratory
California Institute of Technology
Pasadena, California

© 2019. All rights reserved.

Earth Observing System (EOS) Tropospheric Emission Spectrometer (TES)



Data Validation Report (Version F08_12 data)

Approved by:

Kevin Bowman
TES Principal Investigator
Jet Propulsion Laboratory

Richard Lay
TES Ground Data Systems Manager
Jet Propulsion Laboratory

For the Reader:

In order to successfully interpret TES data one must account for the variable vertical sensitivity of the TES product and the a priori constraints used to help convert measured radiances to vertical profiles of tropospheric composition.

Biases in the data can also vary with altitude. Comparisons between TES data and earth atmosphere models can also be challenging because of possible logarithmic differences between the data product, a priori, and model fields.

We therefore recommend that the scientist interested in TES data read Chapter 9 of the Level 2 TES Data User's Guide Version 7.0 (Herman et al., 2018) on how to interpret and use TES data AND any published papers in which the data are used (all published papers using TES data are listed on the TES website). For example, these papers will discuss how biases are addressed or how logarithmic differences between TES data and model fields affect scientific interpretation.

Users should also read the quality statement associated with the version of the data. For most scientific applications a data user should select data using the master data quality flag ("speciesretrievalquality") and a check on the sensitivity with the DegreesOfFreedomForSignal data field. If these checks are removing too much data over the area of interest then the user should contact a member of the TES science team on how to use a subset of flags.

Revision History:

Version	Date	Description/Comments
1.0	8/15/2005	Initial Version of Validation Report for time frame “launch + 1 year”
2.0	1/4/2007	Validation Report for F03_03 data
3.0	11/5/2007	Validation Report for F04_04 data
4.0	11/23/2011	Validation Report for F05_05, F05_06, F05_07 data
5.0	4/8/2012	Validation Report for F06_08, F06_9 data
6.0	6/20/2014	Validation Report for F07_10 data
7.0	5/30/2018	Validation Report for F08_11 data
8.0	12/31/2019	Validation Report for F08_12 data

TABLE OF CONTENTS

1. OVERVIEW OF TES PRODUCT VALIDATION.....	1
1.1 APPLICABLE DOCUMENTS.....	3
2. AN OVERVIEW OF THE TES INSTRUMENT AND DATA PRODUCTS	4
2.1 INSTRUMENT DESCRIPTION.....	4
2.2 TES OBSERVATION MODES	4
2.2.1 <i>Global Surveys</i>	4
2.2.2 <i>Special Observations</i>	5
2.3 TES SCAN IDENTIFICATION NOMENCLATURE.....	7
2.4 DERIVED PRODUCTS AND DATA VISUALIZATION.....	7
2.5 WHERE TO OBTAIN TES DATA	7
2.6 FILE FORMATS AND DATA VERSIONS	8
2.7 TES STANDARD L2 PRODUCTS.....	11
2.8 REFERENCES	12
2.8.1 <i>TES References</i>	12
3. EXECUTIVE SUMMARY	14
3.1 REFERENCES	18
3.1.1 <i>TES References</i>	18
3.1.2 <i>General References</i>	21
4. TES LEVEL 1B RADIANCE DATA PRODUCTS AND LEVEL 2 IRK.....	23
4.1 LEVEL 2 PRODUCT: OZONE BAND INSTANTANEOUS RADIATIVE KERNEL (IRK)	23
4.2 SINGLE SOUNDING COMPARISON BETWEEN V008 AND V007	27
4.3 REFERENCES	30
4.3.1 <i>TES LIB Radiance Validation References</i>	30
4.3.2 <i>TES Level 2 IRK References</i>	30
4.3.3 <i>TES References</i>	30
5. NADIR OZONE VALIDATION.....	31
5.1 OVERVIEW	31
5.2 TES OZONESONDE COMPARISONS.....	33
5.3 REFERENCES	34
5.3.1 <i>Primary TES Nadir Ozone References</i>	34
5.3.2 <i>TES References</i>	34
5.3.3 <i>General References</i>	36
6. VALIDATION OF TES RETRIEVALS OF CARBON MONOXIDE.....	39
6.1 OVERVIEW	39
6.2 INSTRUMENT PERFORMANCE BEFORE AND AFTER OPTICAL BENCH WARM-UP	39
6.3 PROBLEMS IN FILTER 1A1 SIGNAL USED FOR CO RETRIEVAL SINCE 2011	40
6.4 COMPARISONS OF TES V008 TO V007 IN CO RETRIEVAL	41
6.5 GLOBAL DISTRIBUTIONS OF CO FROM TES MEASUREMENTS.....	43
6.6 CO VALIDATION: COMPARISONS TO IN SITU AIRCRAFT MEASUREMENT.....	44

6.7	CO VALIDATION: COMPARISONS TO MOZAIC, ACE, MLS, AND AIRS DATA SETS	44
6.8	CO VALIDATION: COMPARISONS TO MOPITT DATA	45
6.9	CO VALIDATION: SUMMARY	49
6.10	REFERENCES	50
6.10.1	<i>TES Carbon Monoxide References</i>	50
7.	VALIDATION OF TES NADIR TEMPERATURE RETRIEVALS WITH RADIOSONDES	51
7.1	EXECUTIVE SUMMARY	51
7.2	DETAILS OF TES V008 TATM RETRIEVAL	51
7.3	A PRIORI CONSTRAINT VECTOR	51
7.4	VALIDATION STATUS OF V008 NADIR TEMPERATURE	52
7.5	COMPARISON OF TES V008 NADIR TEMPERATURE WITH V007 NADIR TEMPERATURE....	53
7.6	TES TEMPERATURE RETRIEVAL STABILITY 2006-2011	54
7.7	REFERENCES	54
7.7.1	<i>TES Temperature References</i>	54
7.7.2	<i>TES References</i>	54
7.7.3	<i>General References</i>	56
8.	SEA SURFACE TEMPERATURE.....	57
8.1	REFERENCES	57
8.1.1	<i>TES References</i>	57
9.	WATER VAPOR	58
9.1	EXECUTIVE SUMMARY	58
9.2	BACKGROUND AND RECOMMENDATION	58
9.3	A PRIORI CONSTRAINT VECTOR	58
9.4	COMPARISON OF TES V008 WATER VAPOR WITH IN SITU RADIOSONDES	59
9.5	COMPARISON OF TES V008 WATER VAPOR WITH V007 WATER VAPOR	60
9.6	REFERENCES	60
9.6.1	<i>TES H₂O References</i>	60
9.6.2	<i>TES References</i>	61
9.6.3	<i>General References</i>	61
10.	HDO/H₂O.....	63
10.1	COMPARISON OF V008 TO V007 HDO/H ₂ O	63
10.2	REFERENCES	64
10.2.1	<i>TES HDO/H₂O References</i>	64
10.2.2	<i>TES References</i>	64
11.	VALIDATION OF NADIR METHANE	65
11.1	REFERENCES	65
11.1.1	<i>TES CH₄ References</i>	65
11.1.2	<i>General References</i>	65
12.	CLOUD PRODUCTS	66
12.1	REFERENCES	66

12.1.1	TES References	66
13.	CARBON DIOXIDE VALIDATION.....	67
13.1	OVERVIEW OF CURRENT VALIDATION STATUS OF TES V008 CO ₂	67
13.2	REFERENCES	67
13.2.1	TES CO ₂ References	67
13.2.2	General References.....	68
14.	MINOR SPECIES: AMMONIA (NH₃), METHANOL (CH₃OH) AND FORMIC ACID (HCOOH).....	69
14.1	OBJECTIVES AND DATA	69
14.2	AMMONIA (NH ₃) ANALYSIS	71
14.3	METHANOL (CH ₃ OH) ANALYSIS.....	73
14.4	FORMIC ACID (HCOOH) ANALYSIS	75
14.5	REFERENCES	77
14.5.1	TES NH ₃ , CH ₃ OH and HCOOH References.....	77
15.	PEROXYLACETYL NITRATE (PAN) VALIDATION	78
15.1	REFERENCES	80
15.1.1	TES PAN References.....	80
16.	NADIR CARBONYL SULFIDE (OCS) VALIDATION	82
16.1	SAMPLING DENSITY.....	82
16.2	GLOBAL PATTERN	82
16.3	COMPARISON WITH HIPPO OBSERVATION DATA	83
16.4	REFERENCES	84
16.4.1	TES OCS References.....	84
17.	HYDROGEN CYANIDE (HCN) VALIDATION.....	85
17.1	REFERENCES	85
17.1.1	TES HCN References	85
	APPENDICES.....	86
A.	ACRONYMS.....	86

LIST OF FIGURES

Figure 4-1	O ₃ LWRE global pattern averaged seasonally.....	25
Figure 4-2	The same as Figure 4-1 but global pattern averaged seasonally for H ₂ O LWRE.....	26
Figure 4-3	The same as Figure 4-1 and Figure 4-2 but global pattern averaged seasonally for TSUR IRK.....	26
Figure 4-4	Top: forward model flux segments (every 3 cm ⁻¹) for 970-1120 cm ⁻¹ . Red for V007 and black for V008. Bottom: the same as top but for L1B data.	27

Figure 4-5 O ₃ LIRK, H ₂ O LIRK, TATM IRK, Cloud OD LIRK, and Emissivity IRK comparisons between V008 and V007.....	28
Figure 4-6 The comparisons of V007 (red) and V008 (black) O ₃ , H ₂ O, TATM profiles in the left column. Their differences in the right column.....	29
Figure 5-1 The global distribution of coincident TES (black plus) and WOUDC ozonesonde (blue diamond) measurements. Their latitude range is from 73.26°S to 81.82°N and time spans from 2004 to 2016, though only years 2005-2010 are used in this analysis.	32
Figure 5-2 TES-ozonesonde percent differences. (Left) Individual profile of differences between TES V007 and ozonesonde for 2005-2010 are shown in grey, mean and one standard deviation ranges are overlaid in solid red and dash red lines, respectively. (Right) The same plot for the new version of TES data (V008).....	33
Figure 6-1 Time series of measured normalized Integrated Spectral Magnitude (ISM) (top panel), beamsplitter temperature (middle panel), and average DOFS for 30°N-30°S latitude. The ISM is normalized to 1.0 at the beginning of the time series.....	40
Figure 6-2 Time series of the percentage of ‘good quality CO retrievals’ per month. Note that V007 data processing was still in progress when this figure was prepared.....	41
Figure 6-3 TES CO Volume Mixing Ratio V008 minus V007 in percent for run 5800, an along track Step and Stare observation campaign taken 2007-07-26 over mid-east Asia and E Europe.....	42
Figure 6-4 Histograms of percent differences between TES CO V008 and V007 from Global Survey run2147 taken 2004-09-20/21.	42
Figure 6-5 TES CO Global Distributions at 681.3 hPa for the Four Typical Months, Jan, April, July, and Oct 2007.	43
Figure 6-6 TES (left column) and down-sampled MOPITT (right column) CO VMRs at 681 hPa. The corresponding date is one TES Global Survey, Sept 20-21, 2004. Top panels are TES and MOPITT CO VMRs at or near TES geolocations. Bottom panels are horizontally interpolated CO VMR maps with footprints in white dots. TES data version is V008 and MOPITT data is V008 Thermal Infrared (TIR) only.....	46
Figure 6-7 Comparisons of CO VMR reported by TES and MOPITT at 681 hPa and 215 hPa respectively. The left panels are the ‘direct’ comparisons. The right panels are the comparisons after the TES CO being adjusted to MOPITT a priori profile and MOPITT CO profiles being adjusted by applying TES averaging kernels (Luo et al., 2007a).....	47
Figure 7-1 Temperature differences between TES V008 TATM and NOAA ESRL radiosondes with observation operator applied: (left) all good quality comparisons, (right) comparisons filtered by average cloud effective optical depth < 0.1. Shown are individual temperature differences (thin grey lines), bias (solid red line), rms (dashed red line), and the TES observation error (solid blue line).....	53
Figure 7-2 Histogram of nadir temperature differences between TES V008 and V007 retrievals for TES Global Survey run id 2147 at (left) the 681.3 hPa pressure level and (right) 215.4 hPa pressure level. Figure prepared by Ming Luo using code developed by Mark Montero.....	54

Figure 9-1 Water vapor percent differences between TES V008 retrievals and radiosondes (with averaging kernel applied) from the NOAA ESRL database for two latitude ranges, the Arctic (left) and Northern midlatitudes (right). Matches are selected for TES geolocation coincidence within 100 km distance and -0.5 to +1.5 hours of radiosonde launch time. In each panel, N individual matches are shown (thin grey lines) with bias (thick red line) and bias±rms (thin red lines). Percent differences are calculated as 100(TES-radiosonde)/TES. Figure prepared by Ming Luo.	59
Figure 9-2 Histogram of water vapor percent differences between TES V008 and V007 retrievals for TES Global Survey run id 2147 at (left) the 681.3 hPa pressure level and (right) 215.4 hPa pressure level. Figure prepared by Ming Luo using code developed by Mark Montero.....	60
Figure 10-1 TES V008 Delta-D minus V007 Delta-D as a function of latitude.....	63
Figure 14-1 Surface temperature from V007 and V008 for run 5800 (Step and Stare) vs latitude: (left, top) and the difference between V008 and V007 (left, bottom). Histogram of the V008-V007 differences for run 2147 (GS) (right).....	70
Figure 14-2 Atmospheric temperature differences between V008 and V007 for run 5800 (Step and Stare) (left) and for run 2147 (GS) (right).	70
Figure 14-3 Water vapor differences between V008 and V007 for run 5800 (Step and Stare) (left) and for run 2147 (GS) (right).....	71
Figure 14-4 NH ₃ Information from V007 and V008 vs latitude for run 5800 (Step and Stare): DOFs (left, top) and the difference between V008 and V007 (left, bottom). Total column NH ₃ (right, top) and the differences between V007 and V008 (right, bottom).	72
Figure 14-5 NH ₃ differences between V008 and V007 for run 5800 (Step and Stare) (left) and histogram of differences for run 2147 (GS) at 825 hPa (right).....	72
Figure 14-6 Ozone differences between V008 and V007 for run 5800 (Step and Stare) (left) and for run 2147 (GS) (right).....	73
Figure 14-7 CH ₃ OH differences between V008 and V007 for run 5800 (Step and Stare) (left) and for run 2147 (GS) (right).....	73
Figure 14-8 CH ₃ OH information from V007 and V008 vs latitude: DOFs (top) and the difference between V008 and V007 (bottom); run 5800 (left) and run 2147 (right).....	74
Figure 14-9 CH ₃ OH total column from V007 and V008 vs latitude for run 5800 (Step and Stare): total column (left, top) and the difference between V008 and V007 (left, bottom); total column scatter plot for run 2147 (GS) (right): red line is linear fit, dashed line is 1:1.	74
Figure 14-10 HCOOH differences between V008 and V007 for run 5800 (Step and Stare) (left) and for run 2147 (GS) (right).....	75
Figure 14-11 HCOOH information from V007 and V008 vs latitude: DOFs (top) and the difference between V008 and V007 (bottom); run 5800 (left) and run 2147 (right).....	76
Figure 14-12 HCOOH total column from V007 and V008 vs latitude for run 5800 (Step and Stare): total column (left, top) and the difference between V008 and V007 (left, bottom); total column scatter plot for run 2147 (GS) (right): red line is linear fit, dashed line is 1:1.	76

Figure 15-1 Examples of elevated CO and PAN in boreal burning plumes (previously identified by Alvarado et al. (2010) and shown in Payne et al. (2014)) seen in TES special observations made during the July 2008 phase of the ARCTAS campaign. These are the V008 retrievals. CO plots show the retrieved CO at 510 mbar, while PAN plots show the average retrieved VMR for retrieval levels between 800 hPa and the tropopause. Colored points show the cases where the degrees of freedom for signal (DOFS) was greater than 0.6 for the PAN retrieval. 79

Figure 15-2 Comparison between V007 and V008 global PAN results for October 2006. PAN values shown here represent the average VMR for retrieval levels between 800 mbar and the tropopause. Panels (a) and (b) show individual PAN retrievals for V007 and V008 respectively, while panels (c) and (d) show gridded results for V007 and V008 respectively. 80

Figure 16-1 The maps of the sampling density for four seasons. Left for V007 and right for V008. 82

Figure 16-2 The global data with quality control in four seasons. 83

Figure 16-3 Comparisons between HIPPO and TES matched OCS in V007 and V008. Left column is the HIPPO path during each campaign. The middle and right column shows the HIPPO free tropospheric OCS in blue and TES OCS in red. 84

Figure 17-1 Retrieved TES HCN for October, 2006. A large HCN signal is expected over Indonesia. 85

LIST OF TABLES

Table 1-1 Definitions of Data Maturity based on those used by the EOS-Terra MISR Team 1

Table 1-2 Current Validation Status of TES L2 Data Products 2

Table 2-1 Description of TES Global Survey Modifications 4

Table 2-2 Description of TES Special Observation Modes 6

Table 2-3 Description of the TES L2 Data Product Version Labels 9

Table 2-4 Description of the TES L2 Data Product Files Currently Available 11

Table 4-1 The list of IRK products 23

Table 6-1 TES-MOPITT CO comparisons for Sept 20-21, 2004 48

Table 6-2 TES-MOPITT CO comparisons for June 5-6, 2009 48

Table 6-3 TES-MOPITT CO comparisons for June 6-7, 2010 49

1. Overview of TES Product Validation

This document is intended to provide our best determination of the quality of the TES data products based on detailed comparisons between TES Level 2 (L2) data products and other independent data sets. Section 2 provides an overview of the TES instrument and data products. Section 3 is an Executive Summary of the validation of each standard TES product.

Validation is defined, for purposes of this report, as comparison between quantities measured by TES and other data products that represent the state of the atmosphere. Data used in these figures come from processing at the TES Science Computing Facility and are all publicly available.

The TES L2 nadir products have undergone extensive quality control and validation testing. Table 1-1 shows the definitions of data maturity developed by the Terra-MISR (Multi-angle Imaging SpectroRadiometer) team and adopted by the TES team (<http://www-misr.jpl.nasa.gov/getData/maturityLevels/>).

Using these definitions, the current validation status of the TES L2 data products are given in Table 1-2. Currently, all the TES L2 nadir products are ready for scientific use with the exception of the emissivity reported over land surfaces. TES methane products should be used in a manner similar to that outlined in Payne et al. (2009) (see Section 11). The TES limb products are provisionally validated but should not be used without working with the TES team. Limb data was taken only for the first 9 months of the TES mission and some special observations in 2006. The TES limb data is provisionally validated, but should be used only in collaboration with the TES science team at JPL. This validation report does not include analysis of the limb data validation.

Table 1-1 Definitions of Data Maturity based on those used by the EOS-Terra MISR Team

Term	Definition
Beta	Early release products for users to gain familiarity with data formats and parameters.
Provisional	Limited comparisons with independent sources have been made and obvious artifacts fixed.
Validated Stage 1	Biases are estimated from independent measurements at selected locations and times.
Validated Stage 2	Biases are estimated from more widely distributed independent measurements.
Validated Stage 3	Biases are estimated from independent measurements representing global conditions.

Note: TES L2 retrievals include fully characterized internal error estimates and do not obtain error estimates from external sources. Uncertainty in the TES validation work describes biases when compared to other data sources.

Table 1-2 Current Validation Status of TES L2 Data Products

Species	Validation Status
Nadir Ozone (O ₃)	Validated Stage 3
Nadir Carbon Monoxide (CO)	Validated Stage 3
Nadir Temperature	Validated Stage 3
Nadir Water (Lower/Middle Troposphere)	Validated Stage 3
Nadir Water (Upper Troposphere)	Validated Stage 2
Sea Surface Temperature	Validated Stage 3
Nadir Methane (CH ₄)	Validated Stage 2
Cloud Properties	Validated Stage 2
Water Isotopologue (HDO/H ₂ O)	Validated Stage 1
Nadir Carbon Dioxide (CO ₂)	Validated Stage 2
Nadir Ammonia (NH ₃)	Validated Stage 1
Nadir Formic Acid (HCOOH)	Provisional
Nadir Methanol (CH ₃ OH)	Provisional
Nadir Peroxyacetyl Nitrate (PAN)	Provisional
Nadir Carbonyl Sulfide (OCS)	Validated Stage 1
Instantaneous Radiative Kernel (IRK)	Provisional
Nadir Hydrogen Cyanide (HCN)	Provisional
Note: TES L2 limb products (Nitric Acid, Ozone, Temperature and Water) are provisionally validated but are not included in this report.	

In order to compare TES profile data with other measurements, vertical smoothing and sensitivity must be accounted for by applying the appropriate averaging kernels (such as those supplied with the TES data products). The error estimates included in the L2 data products are meaningful based on the current validation analysis.

1.1 Applicable Documents

Note: A selection of TES documents are available online at the TES website, <http://tes.jpl.nasa.gov/data/documents> and at the NASA (National Aeronautics and Space Administration) Langley Atmospheric Science Data Center (ASDC) https://eosweb.larc.nasa.gov/project/tes/tes_table (Documentation tab). All TES related publications are available at the TES web site <http://tes.jpl.nasa.gov/documents/publications/>

- [1] Herman, Robert and Gregory Osterman (editors), Matthew Alvarado, Christopher Boxe, Kevin Bowman, Karen Cady-Pereira, Tony Clough, Annmarie Eldering, Brendan Fisher, Dejian Fu, Robert Herman, Daniel Jacob, Line Jourdain, Le Kuai, Susan Kulawik, Michael Lampel, Qinbin Li, Jennifer Logan, Ming Luo, Inna Megretskaja, Ray Nassar, Gregory Osterman, Susan Paradise, Vivienne Payne, Hank Revercomb, Nigel Richards, Mark Shephard, Dave Tobin, Solene Turquety, Felicia Vilnrotter, Kevin Wecht, Helen Worden, John Worden, Lin Zhang (2018), Earth Observing System (EOS) Tropospheric Emission Spectrometer (TES) Data Validation Report (Version F08_11 data), Version 7.0, JPL Internal Report D-33192, May 30, 2018.
- [2] Herman, Robert and Susan Kulawik (editors), Kevin Bowman, Karen Cady-Pereira, Annmarie Eldering, Brendan Fisher, Dejian Fu, Robert Herman, Daniel Jacob, Line Jourdain, Susan Kulawik, Ming Luo, Ruth Monarrez, Gregory Osterman, Susan Paradise, Vivienne Payne, Sassaneh Poosti, Nigel Richards, David Rider, Douglas Shepard, Mark Shephard, Felicia Vilnrotter, Helen Worden, John Worden, Hyejung Yun, Lin Zhang (2018), Earth Observing System (EOS) Tropospheric Emission Spectrometer (TES) Level 2 (L2) Data User's Guide (Up to & including Version 7 data), Version 7.0, JPL Internal Report D-38042, September 27, 2018.
- [3] Lewicki, S., D. Shepard, M. Madatyan, R. Morris and J. Wood (2019), TES Science Data Processing Standard and Special Observation Data Products Specifications, Version 15, JPL Internal Report D-22993, March 18, 2019, for publically released data, software release 15.

2. An Overview of the TES Instrument and Data Products

This section provides information about the TES instrument and the L2 data products. More detailed information on the TES data products is available in the TES L2 Data User's Guide (Herman et al., 2018) and the TES Data Product Specification Document (Lewicki et al., 2019).

2.1 Instrument Description

The Tropospheric Emission Spectrometer (TES) on EOS-Aura was designed to measure the global, vertical distribution of tropospheric ozone and ozone precursors such as carbon monoxide (Beer et al., 2001; Beer, 2006). From August 2004 until its decommissioning on January 31, 2018, TES took observations in the modes of Global Surveys (Section 2.2.1) and Special Observations (Section 2.2.2). TES is a nadir and limb viewing infrared Fourier transform spectrometer (FTS) (<http://tes.jpl.nasa.gov/instrument/>). The TES spectral range is from 650 to 3250 cm^{-1} . The apodized resolution for standard TES spectra is 0.10 cm^{-1} , however, finer resolution (0.025 cm^{-1}) is available for special observations. The footprint of each nadir observation is 5 km by 8 km, averaged over detectors. Limb observations (each detector) have a projection around 2.3 km x 23 km (vertical x horizontal).

TES is on the EOS-Aura platform (<http://aura.gsfc.nasa.gov/>) in a near-polar, sun-synchronous, 705 km altitude orbit. The ascending node equator crossings are near 1:45 pm local solar time.

2.2 TES Observation Modes

2.2.1 Global Surveys

TES makes routine observations in a mode referred to as the “global survey”. A global survey is run every other day on a predefined schedule and collects 16 orbits (~26 hours) of continuous data. Each orbit consists of a series of repetitive units referred to as a sequence. A sequence is further broken down into scans. Global surveys are always started at the minimum latitude of an Aura orbit. Table 2-1 provides a summary of the initial and modified versions of the TES Global Surveys from Launch to the present day.

Table 2-1 Description of TES Global Survey Modifications

Start Date/ First Run ID	Scans	Sequences	Maximum Number of TES L2 Profiles	Along-Track Distance between Successive Nadir Scan Locations	Description
August 22, 2004 / First GS Run ID 2026 (First 4 GS runs were 4 orbits only) (First full GS is Run ID 2147/Sep 20, 2004)	3 Limb/ 2 Nadir	1152 sequences (72 per orbit)	Maximum of 4608 L2 profiles (1152 sequences x (3 Limb Scans+ 1 Nadir Scan))	~544 km	<ul style="list-style-type: none"> At-launch Global Survey (Aura launched on July 15, 2004) Each sequence composed of 2 calibration scans, 2 nadir viewing scans and 3 limb scans. The two nadir scans were acquired at the same location on the spacecraft ground track. Their radiances were averaged, providing a single TES L2 profile.

Start Date/ First Run ID	Scans	Sequences	Maximum Number of TES L2 Profiles	Along-Track Distance between Successive Nadir Scan Locations	Description
May 21, 2005 / Run ID 2931	3 Nadir	1152 sequences (72 per orbit)	Maximum of 3456 L2 profiles (1152 sequences x 3 nadir scans)	~182 km	<ul style="list-style-type: none"> Global survey was modified to conserve instrument life. Three limb scans were eliminated and replaced by an additional nadir scan. The 3 Nadir scans were acquired at locations equally spaced along the spacecraft ground track. The radiances of individual scans are not averaged.
January 10, 2006 / Run ID 3239.	3 Nadir	1136 sequences (71 per orbit)	Maximum of 3408 L2 profiles (1136 sequences x 3 nadir scans)	~182 km	<ul style="list-style-type: none"> The last sequence in each orbit was replaced with an instrument maintenance operation.
June 6, 2008 / Run ID 7370.	3 Nadir	960 sequences (60 per orbit)	Maximum of 2880 L2 profiles (960 sequences x 3 nadir scans)	~182 km	<ul style="list-style-type: none"> Global survey was modified to conserve instrument life. No measurements poleward of 60°S latitude.
July 30, 2008 / Run ID 8187.	3 Nadir	768 sequences (48 per orbit)	Maximum of 2304 L2 profiles (768 sequences x 3 nadir scans)	~182 km	<ul style="list-style-type: none"> Global survey was further modified to conserve instrument life. No measurements poleward of 50°S, 70°N latitude.
April 7, 2010 / Run ID 11125	4 Nadir	512 sequences (32 per orbit)	Maximum of 2048 L2 profiles (512 sequences x 4 nadir scans)	Spacing regular, but no longer uniform (56, 195, 187, 122 km)	<ul style="list-style-type: none"> Global survey was further modified to conserve instrument life. No measurements poleward of 30°S, 50°N latitude. Blackbody calibrations reduced: no calibrations within the GS, only one pre-GS and one post-GS.

2.2.2 Special Observations

Observations are sometimes scheduled on non-global survey days. In general, these are measurements made for validation purposes or with highly focused science objectives. These non-

global survey measurements are referred to as “special observations”. Eight special observation scenarios have been used to date and are summarized in Table 2-2.

Table 2-2 Description of TES Special Observation Modes

Name	Dates	Pointing	Sequences	Scans per Sequence	Distance Between Scans	Comments
Step and Stare	March 1, 2013 - Jan 31, 2018	Nadir	1	38	146 km	Continuous along-track nadir views, 50 degrees of latitude.
Step and Stare	April 20, 2012 - Jan 31, 2018	Nadir	1	44	76 km	Continuous along-track nadir views, ~29 degrees of latitude.
Step and Stare	Sep 2004 through Aug 6, 2005	Nadir	6	25	40 km	Continuous along-track nadir views, ~45 degrees of latitude.
Step and Stare	July 1, 2007 through Dec 29, 2011	Nadir	1	165	45 km	Along track nadir observations spanning 65 degrees of latitude
Step and Stare	Jan 17, 2006 – Oct 8, 2006 and Spring 2008	Nadir	1	125	45 km	Continuous along-track nadir views, ~50 degrees of latitude.
Note: In 2008 both the 125 and 165 scan Step and Stare macros were used						
Transect	April 20, 2012 through Jan 31, 2018	Near Nadir	1	20	12 km	Hi density along-track or off nadir views.
Transect	Jan 16, 2006 through Dec 29, 2011	Near Nadir	1	40	12 km	Hi density along-track or off nadir views.
Transect	Aug 20, 2005 – Sept 2, 2005	Near Nadir	1	68	25 km	Hi density along-track or off nadir views.
Stare	April 20, 2012 through Jan 31, 2018	Near Nadir	1	14	0 km	All measurements at a single location.
Stare	Launch through Dec 29, 2011	Near Nadir	1	32	0 km	All measurements at a single location.
Limb Only	Jan 31, 2006 – May 20, 2006	Limb	1	62	45 km	Continuous along-track limb views, 25 degrees of latitude.

Name	Dates	Pointing	Sequences	Scans per Sequence	Distance Between Scans	Comments
Limb HIRDLS	Feb 13, 2006 Only	Limb	142	3	182 km	2 orbits of continuous limb measurements for HIRDLS (High Resolution Dynamics Limb Sounder) comparison

2.3 TES Scan Identification Nomenclature

Each TES scan is uniquely identified by a set of three numbers called the run ID, the sequence ID and the scan ID. Each major unit of observation is assigned a unique run ID. Run IDs increase sequentially with time. The first on-orbit run ID is 2000. The sequence ID is assigned to repetitive units of measurements within a run. They start at 1 and are automatically incremented serially by the TES flight software. The scan ID is also incremented by the flight software each time a scan is performed. Each time the sequence is set to 1, the scan ID is reset to 0.

Each time TES makes a set of measurements, that data set is assigned an identification number (referred to as a “run ID”). A calendar of the TES run IDs for global surveys and a list of all TES run IDs (including observation data, time and date) can be found at <http://tes.jpl.nasa.gov/data/datacalendar/>)

2.4 Derived Products and Data Visualization

The standard TES products are in Hierarchical Data Format (HDF), grouped based on run ID at https://eosweb.larc.nasa.gov/project/tes/tes_table. The TES “Lite” products are in netcdf format, and grouped into a monthly based file (follow the link: <https://tes.jpl.nasa.gov/data/products/lite> to “Lite Products”). The lite products are reported on the TES retrieval pressure grid which makes the products more compact, and combine datasets (e.g. H₂O (Water) and HDO (Hydrogen Deuterium Monoxide or Heavy Water) fields) and apply known bias corrections to make the data easier to use. More information can be obtained from the Lite Products user’s guide found at the same site.

2.5 Where to Obtain TES Data

There are two locations for obtaining TES data. Links to both locations are available from the TES site at the Langley Atmospheric Science Data Center (ASDC) <http://eosweb.larc.nasa.gov/>. The supporting documentation necessary to use TES data is also available at the Langley ASDC site.

- The primary location for obtaining TES data is the NASA Earthdata site <https://search.earthdata.nasa.gov/search?fi=TES>. This site makes available some earlier versions of the TES data, along with data from many other platforms and instruments.
- A secondary location for obtaining TES data is the Langley ASDC data pool. The data pool has space limitations that make it somewhat dynamic, therefore older versions of TES data may not be available there.

The TES data files are listed in different ways for the different sites. The naming convention will be described in Section 2.6.

All TES data products are in HDF-EOS 5 format and are completely documented in the TES Data Product Specification documents referenced at <https://eosweb.larc.nasa.gov/project/tes/DPS>. The site also contains links to the TES documentation mentioned in this manuscript.

Routines for reading the TES Level 2 data products, written in Interactive Data Language (IDL), are available at ASDC TES site. We expect to have IDL routines for determining “C-Curve” ozone retrievals (see section 6.2.1.2 of the TES L2 Data User’s Guide (Herman et al., 2018)) available at the ASDC as well.

2.6 File Formats and Data Versions

Information about the TES data file content and format versioning can be found in the L2 product filenames. Table 2-3 provides information for differentiating between the TES versions. When ordering the data on the EOS Data Gateway, the TES level 2 products can be initially differentiated by the TES Product (ESDT or Earth Science Data Type) version label shown in the first column of Table 2-3. Once the data is downloaded, more information can be gathered from the TES version string in the filename.

The TES L2 Data Products are provided in files separated out by the atmospheric species being measured. The parts of the product filename are:

<inst.>-<platform>_<process level>-<species>-<TES view mode>_r<run id>_<version id>.he5

The TES Version String (version id), contains the Format and content version:

F<format version>_<science content version>

A change to the format version string corresponds to minor updates to the fields available within the file or minor bug fixes. Changes to the science content string reflect major changes in the science content of certain fields in the data products.

An example file name is:

TES-Aura_L2-O3-Nadir_r000002945_F04_04.he5

This particular file contains TES nadir measurements of ozone for run ID 2945 (000002945).

In addition to the atmospheric products, there are data files with additional (ancillary) data that are important for working with TES data. These ancillary files can be used with any species data file and contain the string “Anc” in the filename.

Table 2-3 provides a way to map the TES version string information to the TES data product version. For example, version F03_03 is the first version to contain limb data and version F03_02 data was a significant upgrade to the science content in the data products and therefore is referred to as version 2 (V002) TES data. When ordering TES Level 2 data products through the EOS Data Gateway, the products will be grouped by the TES version number (ESDT) in a form that looks like:

TES/AURA L2 O3 NADIR V003.

If the TES data is ordered through the Langley ASDC Data Pool using the FTP (File Transfer Protocol) interface, the version 3 nadir ozone data will be listed in the form:

TL2O3N.003.

If the TES data is ordered through the Langley Data Pool using the Web interface, the version 3 nadir ozone data will be listed as:

TL2O3N.3.

While the data may be listed differently for the different sites for downloading the products, the filenames will be identical.

There are eight different versions of TES L2 data products. The current version is V006 (F07_10). Data from versions prior to V003 (F04_04) are no longer publicly available, but the evolution of the product versions and file formats is provided in this document back to V001 (F01_01 and F02_01).

Table 2-3 Description of the TES L2 Data Product Version Labels

TES Product (ESDT) Version	TES Version String	Format Version	Science Content Version	Description
V001	F01_01	1	1	The first publicly released L2 data
V001	F02_01	2	1	Bug fixes and additional fields
V002	F03_02	3	2	Some additional fields but major upgrade to scientific quality of data.
V002	F03_03	3	3	Limb data and some bug fixes
V003	F04_04	4	4	Improvements to nadir ozone, temperature, methane and to limb products. Fully processed from Sep 2004 through present.

TES Product (ESDT) Version	TES Version String	Format Version	Science Content Version	Description
V004	F05_05 or F05_06 F05_07 (Final V004)	5	5,6 or 7	<p>Improvements to temperature and methane retrievals.</p> <p>F05_07 is the final V004 release using retrieval software R11.3 and when available should be used over F05_05 or F05_06.</p> <p>F05_07 differentiates between GMAO* versions used in retrieval by date and TES run ID (see below)</p> <p>F05_05 refers to data processed using GMAO GEOS-5.1.0 products using TES retrieval software release R11.2</p> <p>F05_06 refers to data processed using GMAO GEOS-5.2.0 products using TES retrieval software release R11.2</p>
V005	F06_08 or F06_09	6	8 or 9	<p>F06_08 added Carbon Dioxide (CO₂) and Ammonia (NH₃) to the list of Standard Products.</p> <p>F06_09 added Nitrous Oxide (N₂O) to the list of Standard Products.</p>
V006	F07_10	7	10	<p>F07_10 added Formic Acid (HCOOH) and Methanol (CH₃OH) to the list of Standard Products.</p>
V007	F08_11	8	11	<p>F08_11 added Peroxyacetyl Nitrate (PAN), Carbonyl Sulfide (OCS) and Instantaneous Radiative Kernel (IRK) to the list of Standard Products.</p>
V008	F08_12	8	12	<p>F08_12 added Hydrogen Cyanide (HCN) to the list of Standard Products.</p>

* The TES processing software uses meteorological fields from the NASA Global Modeling and Assimilation Office (GMAO) GEOS (Goddard Earth Observing System) model as inputs to the Level 2 data retrievals.

2.7 TES Standard L2 Products

Currently the TES data products available for any given run ID are listed in Table 2-4. The products are separated by species with an ancillary file providing additional data fields applicable to all species. A description of the contents of the product files, information on the Earth Science Data Type names and file organization can be found in the TES Data Products Specification (DPS) document (Lewicki, et al., 2019).

Table 2-4 Description of the TES L2 Data Product Files Currently Available

TES L2 Standard Data Product	TES View Mode	Description
Ozone	Nadir	TES ozone profiles and some geolocation information
Temperature	Nadir	TES atmospheric temperature profiles and some geolocation information.
Water Vapor	Nadir	TES nadir water vapor profiles and some geolocation information
Carbon Monoxide	Nadir	TES nadir carbon monoxide profiles and some geolocation information
Carbon Dioxide	Nadir	TES nadir carbon dioxide profiles and some geolocation information
Ammonia	Nadir	TES nadir ammonia profiles and some geolocation information
HDO	Nadir	TES HDO (Hydrogen Deuterium Monoxide) profiles and some geolocation information
Methane	Nadir	TES nadir methane profiles and some geolocation information
Nitric Acid	Limb	TES limb nitric acid profiles and some geolocation information
Formic Acid	Nadir	TES nadir formic acid profiles and some geolocation information
Methanol	Nadir	TES nadir methanol profiles and some geolocation information
Peroxyacetyl Nitrate (PAN)	Nadir	TES nadir PAN profiles and some geolocation information

TES L2 Standard Data Product	TES View Mode	Description
Carbonyl Sulfide (OCS)	Nadir	TES nadir OCS profiles and some geolocation information
Hydrogen Cyanide (HCN)	Nadir	TES nadir HCN profiles and some geolocation information
Instantaneous Radiative Kernel (IRK)	Nadir	TES nadir IRK profiles and some geolocation information
Ancillary	Nadir	Additional data fields necessary for using retrieved profiles.
Summary	Nadir	Provides information on retrieved volume mixing ratios/temperatures without averaging kernel, error matrices.
Supplemental	Nadir and Limb	Provides information on non-retrieved species that are used in the Level 2 retrievals (climatologies, covariance matrices, etc.)

TES retrieves surface temperature and it is reported in each nadir species file, however the value in the atmospheric temperature file is the one that should be used for scientific analysis.

2.8 References

2.8.1 TES References

- [1] Beer, R., T. A. Glavich, and D. M. Rider (2001), Tropospheric emission spectrometer for the Earth Observing System's Aura satellite, *Applied Optics*, 40 (15), 2356-2367, May 20, 2001.
- [2] Beer, R. (2006), TES on the Aura Mission: Scientific Objectives, Measurements and Analysis Overview, *IEEE Transactions on Geoscience and Remote Sensing*, 44 (No.5), Special Issue on Aura, 1102-1105, May 2006.
- [3] Lewicki, S., D. Shepard, M. Madatyan, R. Morris and J. Wood (2019), TES Science Data Processing Standard and Special Observation Data Products Specifications, Version 15, JPL Internal Report D-22993, March 18, 2019, for publically released data, software release 15.
- [4] Herman, Robert and Susan Kulawik (editors), Kevin Bowman, Karen Cady-Pereira, Annmarie Eldering, Brendan Fisher, Dejian Fu, Robert Herman, Daniel Jacob, Line Jourdain, Susan Kulawik, Ming Luo, Ruth Monarrez, Gregory Osterman, Susan

Paradise, Vivienne Payne, Sassaneh Poosti, Nigel Richards, David Rider, Douglas Shepard, Mark Shephard, Felicia Vilnrotter, Helen Worden, John Worden, Hyejung Yun, Lin Zhang (2018), Earth Observing System (EOS) Tropospheric Emission Spectrometer (TES) Level 2 (L2) Data User's Guide (Up to & including Version 7 data), Version 7.0, JPL Internal Report D-38042, September 27, 2018.

3. Executive Summary

This is the Executive Summary of validation of TES Version 8 data (Version 8, files ending in F08_12). Version 8 (V008) has the same standard TES products as Version 6, including TES Level 1B (L1B) radiances, ozone, carbon monoxide, atmospheric temperature, water vapor, HDO, methane, surface temperature, cloud properties, carbon dioxide, formic acid (HCOOH), methanol (CH₃OH), ammonia, and the ozone band Instantaneous Radiative Kernel (IRK). For water vapor and atmospheric temperature initial guess and constraint, the Global Modeling and Data Assimilation Office (GMAO) GEOS-5.12.4 model is used. Version 8 Level 2 data nadir products ozone, carbon monoxide, carbon dioxide, water vapor, temperature, HDO, sea surface temperature, methane, formic acid (HCOOH), methanol (CH₃OH), ammonia, peroxyacetyl nitrate (PAN) and carbonyl sulfide (OCS) have undergone validation and are usable in scientific analyses. What's new in TES V008 is hydrogen cyanide (HCN). Below is a summary of each data validation section.

- **Section 4 – L1B Radiance and Level 2 Instantaneous Radiative Kernel (IRK):**

Though this report is focused primarily on the TES Level 2 data products, it is important to understand that the L1B radiance products have also undergone a rigorous validation as reported in Shephard et al. (2008) and in the TES Validation Report V003 (Osterman et al., 2007). The fundamental measurement of the Tropospheric Emission Spectrometer (TES) on board the Aura spacecraft is upwelling infrared spectral radiances. Accurate radiances are critical for trace gas profile retrievals for air quality as well as sensitivity to climate processes. For example, any radiometric systematic errors (*e.g.* calibration) not addressed in the L1B radiances will propagate as errors into the retrieved atmospheric parameters (Bowman et al., 2006; Worden et al., 2004). Connor et al. (2011) showed that the TES relative radiometric calibration was extremely stable over the time period used in their analysis: 2005 to 2009.

Level 2 TES Instantaneous Radiative Kernel (IRK) just for ozone over 9.6-micron ozone band was a standard product in TES Version 6 using a 3-point Gaussian integration method. In TES Versions 7 and 8, we use a 5-point Gaussian integration, a computationally more expensive but more accurate method, to compute IRK and expand the IRK products to include 1) 9.6-micron band TOA flux (980 – 1020.2 /cm), 2) both IRK and LIRK (logarithm IRK) for O₃ and water vapor (H₂O), 3) LIRK for cloud optical depth (COD), cloud top pressure (CTP), and emissivity (EMIS), and 4) IRK for atmospheric temperature (TATM) and surface temperature (TSUR) (see Table 1-1). These products have been validated individually with prototype (IDL) code calculations (Kuai et al., 2017) using one global survey observations.

The statistics (the mean and one standard deviation) for the fractional differences between Product Generation Executive (PGE) and prototype of all IRK products' calculated using the same Jacobians for integration are showed to have negligible differences (1E-06% ± 3E-06%). The global pattern for all products are well replicated by PGE algorithm.

In April 2010, TES implemented a new strategy for observing and processing calibration measurements (see Section 4 of the Version 5 Data Validation Report (Herman et al., 2012)). In order to validate TES spectra processed with the new calibration strategy, and to check comparisons of TES with Atmospheric Infrared Sounder (AIRS) over the entire TES data record from 2004 to present, we developed a more automated comparison tool based on the methods used

for TES/AIRS comparisons in Shephard et al. (2008). Given the differences in ground footprints for TES and AIRS, comparisons are only meaningful for clear-sky, ocean scenes. Results for April 2009 (old calibration approach) compared to April 2010 (new calibration approach) are not significantly different, which suggests the new approach provides the same radiance accuracy as before.

- **Section 5 – Nadir Ozone:**

The retrieval algorithm for TES Version 8 (Release 15) is largely the same as that utilized for the Version 6 data set. There were few changes in the retrieval code for this latest version of the TES that affect the ozone retrievals and the comparisons to ozonesondes support that conclusion. The changes to the retrieval system are mostly in the Level 1B steps, including updates to radiance spike detection and path difference thresholds. Previous versions of the TES Validation Report have shown the consistency in the ozone retrievals as the retrieval system has evolved.

TES Version 8 nadir ozone profiles have been compared with ozonesonde measurements archived in the World Ozone and Ultraviolet Radiation Data Center (The Global Atmosphere Watch Programme (GAW) of the World Meteorological Organization (WMO), 2017). As of the writing of this document, the TES ozone retrievals have been matched with ozonesonde data with coincidence criteria of ± 9 hours and 300 km distance and a limit on the cloud optical depth of a value less than 2.0. The comparison of the differences between the Version 8 ozone retrievals with the sondes and corresponding Version 7 data show very consistent results. Looking at the mean values for 2005-2010, the Version 8 data agreed slightly better with the sondes in the troposphere by about 4-6 percent. The bias and error statistics generally show an improvement when compared to earlier ozonesonde comparisons published by Nassar et al. (2008) and Boxe et al. (2010).

- **Section 6 – Carbon Monoxide:**

Comparisons have been carried out between TES carbon monoxide retrievals and those from a variety of satellite and aircraft instruments. Global patterns of carbon monoxide as measured by TES are in good qualitative agreement with those seen by MOPITT (Measurement Of Pollution In The Troposphere) on the NASA Terra satellite. Comparisons of profiles of CO between TES and MOPITT show better agreement when a priori information is accounted for correctly. TES carbon monoxide agrees to within the estimated uncertainty of the aircraft instruments, including both errors and the variability of CO itself.

- **Section 7 – Nadir Temperature:**

TES V008 nadir temperature (TATM) retrievals have been compared with nearly coincident radiosonde measurements from the National Oceanic and Atmospheric Administration (NOAA) Earth Science Research Laboratory (ESRL) global radiosonde database. Generally, V008 TATM is very similar to the previous V007 data.

To evaluate the retrieval stability the monthly mean and standard deviation of the TATM residual between TES V005 and the Global Modeling and Data Assimilation Office (GMAO) GEOS-5.2 model, which provides the first guess and a priori for the TATM retrieval, were calculated. The statistics for both Tropical Pacific and Northern Atlantic Ocean regions indicate only minor month-to-month variability and no substantial trends over a five-and-a-half year period of 2006 through 2011. The standard deviation of the residual was generally smaller than the standard deviation of the GMAO GEOS-5.2 but larger than the TES estimated measurement error. Overall, based on

this analysis it appears that the TES retrieval quality has remained stable over the years inspected, 2006 through 2011.

- **Section 8 – Sea Surface Temperature:**

TES retrievals of sea surface temperature rely on validation of previous data versions, as described in detail in the TES Validation Report V003 (Osterman et al., 2007).

- **Section 9 – Water Vapor:**

TES V008 H₂O has been compared to V006 H₂O. On average, the mean differences between V008 and V007 are insignificant. The user should select data using the master data quality flag ("speciesretrievalquality") and filter by degree of freedom for signal (DOFS).

- **Section 10 – HDO/H₂O:**

TES V008 estimates of HDO/H₂O have been compared to V007. There is essentially a zero-mean difference between the versions and the uncertainty calculation between versions are consistent. V008 HDO/H₂O shows considerable sensitivity to the isotopic composition of water vapor with typically DOFS~2 in the tropics and DOFS~1 at high latitudes. This increased sensitivity allows the TES estimates to resolve lower tropospheric and mid-tropospheric variability of the HDO/H₂O vapor ratio (see Worden et al. (2012)) with the expense of increased uncertainty over tropical oceans.

- **Section 11 – Methane:**

Here, we reference the V008 (R15) results to the V006 (R13) results that were validated against HIPPO. Using 37 TES global surveys from the time periods of the HIPPO campaign, we find that the mean difference between V006 and V007 is less than 4 ppbv at all altitudes for both uncorrected and N₂O-corrected profiles, with standard deviation less than 37 ppbv at all altitudes. Therefore, the biases between V008 and V006 are relatively small compared to the biases with respect to the HIPPO aircraft profiles.

- **Section 12 – Cloud Products:**

TES retrievals of cloud products rely on validation of previous data versions, as described in detail in the TES Validation Report V004 (Herman et al., 2011).

- **Section 13 – Carbon Dioxide:**

TES CO₂ is retrieved between 40S and 45N, with average cloud optical depth < 0.5, among other tests, for good quality. Errors tend to be correlated for close locations and times, and it is recommended to use TES data averaged in 10 degree by 10 degree by 1 month averages, both to mitigate correlated errors and reduce errors to useful levels. On average, TES CO₂ has an average of 0.65 degree of freedom for signal (DOFS) – with the most DOFS for daytime land cases (which can be on the order of 1 DOFS) and the least for nighttime or winter land cases (which can be on the order of 0.3 DOFS). Ocean targets (day or night) have intermediate DOFS with about 0.8 DOFS. The averaging kernel indicates sensitivity between the surface to above 100 hPa, with the most sensitivity between about 700 and 300 hPa, peaking at about 650 hPa. Although a profile is

retrieved, there is very little independent information at the different profile levels and it is necessary to utilize the provided averaging kernel when using TES data. Most of the validation has been performed at the 510 hPa pressure level. TES V008 CO₂ is compared with aircraft vertical profiles over the Pacific from the High-Performance Instrumented Airborne Platform for Environmental Research (HIAPER) Pole-to-Pole Observation (HIPPO) program (Wofsy, 2011). The error assessment follows Kulawik et al. (2019), which estimates systematic and random errors, such that the error for an average of n observations equals $\sqrt{\text{systematic}^2 + \text{random}^2/n}$. The TES observations have an overall bias of -1.1 ppm versus HIPPO, a systematic error of 1.4 ppm, and random error of 7.3 ppm. This is similar to the previous V007 errors, which were estimated to be a random error of 6 ppm, and a correlated error of 1.7 ppm.

- **Section 14 – Ammonia, Formic Acid (HCOOH), Methanol (CH₃OH):**

Ammonia (NH₃) is a standard product in TES V008. The V008 algorithm update had little impact on the retrieved profiles, with insignificant bias between versions V008 and V006. TES NH₃ provides useful information over regions with moderate to strong NH₃ sources. Due to the sparse TES coverage and the weak signal from NH₃, single TES observations have large uncertainties, except over regions with very high NH₃ concentrations. However, spatial and temporal averages show good correlation with chemical transport model (CTM) output and with in situ measurements. Since there is insignificant change from V006 to V008 NH₃, we rely on validation of previous data versions, as described in detail in the TES Validation Report V007 (Herman et al., 2018).

TES V008 formic acid (HCOOH) provides useful information over regions with strong HCOOH sources, e.g. biomass burning events. Due to the sparse TES coverage and the weak signal from HCOOH, single TES observations have large uncertainties. However, spatial and temporal averages show good correlation with CTM output and with the very limited set of co-located in situ measurements. For formic acid, we rely on validation of previous data versions, as described in detail in the TES Validation Report V007 (Herman et al., 2018).

TES methanol (CH₃OH) has a weak signal and an a priori distribution chosen as a function of location and date. The information content of the retrieval is quite low, but seasonal averages over large regions do provide useful information for evaluating CTMs. For CH₃OH, we rely on validation of previous data versions, as described in detail in the TES Validation Report V007 (Herman et al., 2018).

- **Section 15 – Peroxyacetyl Nitrate (PAN):**

The V007 retrievals (as well as prototype results that preceded V007) have been extensively utilized in peer-reviewed publications. Therefore, we have performed a preliminary assessment of the V008 (R15) PAN product by (1) comparing to TES observations/time periods that have previously been utilized in publications and (2) checking consistency between V007 and V008.

The PAN algorithm has not changed between V007 and V008, but there have been updates to the spectroscopy of interfering species that could cause minor changes to the retrieved PAN. Payne et al. (2014) showed that the dominant sources of error in the TES PAN retrievals are instrument noise, water vapor and ozone. V007 uses the ABSCO v2.5 tables, while V008 uses ABSCO v3.0.

- **Section 16 – Carbonyl Sulfide (OCS):**

The data quality of TES OCS product has been assessed through comparisons between TES OCS and aircraft measurements collected during five HIAPER Pole-to-Pole (HIPPO) campaigns during months of January, March to April, June to July, August to September, and November.

The latitudinal distribution in TES OCS is consistently varying with HIPPO observations with root-mean-square of the differences for individual comparison range from 3 to 7 ppt. The global bias is approximately 1.46 ppt with an error standard deviation of about 5.97 ppt. The correlation coefficients between TES OCS and HIPPO for five campaigns are on average of 0.8.

- **Section 17 – Hydrogen Cyanide (HCN) - New**

Hydrogen cyanide (HCN) is a new product in TES V008. TES is sensitive to HCN in the upper troposphere (e.g. 200 hPa) and therefore will primarily observe fire signatures with high injection heights. TES HCN is the first product to be retrieved in linear volume mixing ratio (VMR). This has the advantage of resulting in very consistent sensitivity over the large range of retrieved HCN, but also may result in negative HCN values. The initial guess and a priori for HCN are set to a constant value of 100 parts per trillion.

Validation of HCN is from the global distribution of HCN for October, 2006. The large Indonesian fires of that month have a verified large HCN signal in the TES V008 data.

3.1 References

3.1.1 TES References

- [1] Alvarado, M.J., J. A. Logan, J. Mao, E. Apel, D. Riemer, D. Blake, R. C. Cohen, K.-E. Min, A. E. Perring, E. C. Browne, P. J. Wooldridge, G. S. Diskin, G. W. Sachse, H. Fuelberg, W. R. Sessions, D. L. Harrigan, G. Huey, J. Liao, A. Case-Hanks, J. L. Jimenez, M. J. Cubison, S. A. Vay, A. J. Weinheimer, D. J. Knapp, D. D. Montzka, F. M. Flocke, I. B. Pollack, P. O. Wennberg, A. Kurten, J. Crouse, J. M. St. Clair, A. Wisthaler, T. Mikoviny, R. M. Yantosca, C. C. Carouge, and P. Le Sager (2010), Nitrogen oxides and PAN in plumes from boreal fires during ARCTAS-B and their impact on ozone: an integrated analysis of aircraft and satellite observations, *Atmospheric Chemistry and Physics*, 10, doi:10.5194/acp-10-9739-2010, 2010
- [2] Alvarado, M. J., V. H. Payne, K. E. Cady-Pereira, J. D. Hegarty, S. S. Kulawik, K. J. Wecht, J. R. Worden, V. Pittman and S. C. Wofsy (2015), Impacts of updated spectroscopy on thermal infrared retrievals of methane evaluated with HIPPO data, *Atmos. Meas. Tech.*, 8, pp. 965-985, 2015.
- [3] Bowman K.W., C.D. Rodgers, S.S. Kulawik, J. Worden, E. Sarkissian, G. Osterman, T. Steck, M. Lou, A. Eldering, M. Shephard, H. Worden, M. Lampel, S.A. Clough, P.D. Brown, C.P. Rinsland, M. Gunson, and R. Beer (2006), Tropospheric emission spectrometer: Retrieval method and error analysis, *IEEE Trans. Geosci. Remote Sens.*, 44(5), pp. 1297-1307, May 2006.
- [4] Boxe, C.S., J.R. Worden, K.W. Bowman, S.S. Kulawik, J.L. Neu, W.C. Ford, G.B. Osterman, R.L. Herman, A. Eldering, D.W. Tarasick, A.M. Thompson, D.C. Doughty, M.R. Hoffmann, S.J. Oltmans (2010), Validation of northern latitude Tropospheric

Emission Spectrometer stare ozone profiles with ARC-IONS sondes during ARCTAS: sensitivity, bias and error analysis, *Atmospheric Chemistry and Physics*, doi:10.5194/acp-10-9901-2010, October 20, 2010.

- [5] Connor, T.C., M. W. Shephard, V. H. Payne, K. E. Cady-Pereira, S. S. Kulawik, M. Luo, G. Osterman, and M. Lampel (2011), Long-term stability of TES satellite radiance measurements, *Atmospheric Measurement Techniques*, 4, doi:10.5194/amt-4-1481-2011, 1481–1490, July 25, 2011.
- [6] Herman, Robert and Gregory Osterman (editors), Christopher Boxe, Kevin Bowman, Karen Cady-Pereira, Tony Clough, Annmarie Eldering, Brendan Fisher, Dejian Fu, Robert Herman, Daniel Jacob, Line Jourdain, Susan Kulawik, Michael Lampel, Qinbin Li, Jennifer Logan, Ming Luo, Inna Megretskaya, Ray Nassar, Gregory Osterman, Susan Paradise, Vivienne Payne, Hank Revercomb, Nigel Richards, Mark Shephard, Dave Tobin, Solene Turquety, Felicia Vilnrotter, Helen Worden, John Worden, Lin Zhang (2011), Earth Observing System (EOS) Tropospheric Emission Spectrometer (TES) Data Validation Report (Version F05_05, F05_06, F05_07 data), Version 4.0, JPL Internal Report D-33192, November 23, 2011. Available online at: <https://eosweb.larc.nasa.gov/project/tes/validation>.
- [7] Herman, Robert and Gregory Osterman (editors), Christopher Boxe, Kevin Bowman, Karen Cady-Pereira, Tony Clough, Annmarie Eldering, Brendan Fisher, Dejian Fu, Robert Herman, Daniel Jacob, Line Jourdain, Susan Kulawik, Michael Lampel, Qinbin Li, Jennifer Logan, Ming Luo, Inna Megretskaya, Ray Nassar, Gregory Osterman, Susan Paradise, Vivienne Payne, Hank Revercomb, Nigel Richards, Mark Shephard, Dave Tobin, Solene Turquety, Felicia Vilnrotter, Kevin Wecht, Helen Worden, John Worden, Lin Zhang (2012), Earth Observing System (EOS) Tropospheric Emission Spectrometer (TES) Data Validation Report (Version F06_08, F06_09 data), Version 5.0, JPL Internal Report D-33192, April 8, 2012. Available online at: <https://eosweb.larc.nasa.gov/project/tes/validation>.
- [8] Herman, Robert and Gregory Osterman (editors), Matthew Alvarado, Christopher Boxe, Kevin Bowman, Karen Cady-Pereira, Tony Clough, Annmarie Eldering, Brendan Fisher, Dejian Fu, Robert Herman, Daniel Jacob, Line Jourdain, Susan Kulawik, Michael Lampel, Qinbin Li, Jennifer Logan, Ming Luo, Inna Megretskaya, Ray Nassar, Gregory Osterman, Susan Paradise, Vivienne Payne, Hank Revercomb, Nigel Richards, Mark Shephard, Dave Tobin, Solene Turquety, Felicia Vilnrotter, Kevin Wecht, Helen Worden, John Worden, Lin Zhang (2014a), Earth Observing System (EOS) Tropospheric Emission Spectrometer (TES) Data Validation Report (Version F07_10 data), Version 6.0, JPL Internal Report D-33192, June 20, 2014. Available online at: <https://eosweb.larc.nasa.gov/project/tes/validation>.
- [9] Herman, R. L., J. E. Cherry, J. Young, J. M. Welker, D. Noone, S. S. Kulawik, and J. Worden (2014b), Aircraft validation of Aura Tropospheric Emission Spectrometer retrievals of HDO / H₂O, *Atmos. Meas. Tech. Discuss.*, 7, 3127-3138, 2014, <https://doi.org/10.5194/amt-7-3127-2014>.

- [10] Herman, Robert and Gregory Osterman (editors), Matthew Alvarado, Christopher Boxe, Kevin Bowman, Karen Cady-Pereira, Tony Clough, Annmarie Eldering, Brendan Fisher, Dejian Fu, Robert Herman, Daniel Jacob, Line Jourdain, Le Kuai, Susan Kulawik, Michael Lampel, Qinbin Li, Jennifer Logan, Ming Luo, Inna Megretskaya, Ray Nassar, Gregory Osterman, Susan Paradise, Vivienne Payne, Hank Revercomb, Nigel Richards, Mark Shephard, Dave Tobin, Solene Turquety, Felicia Vlnrotter, Kevin Wecht, Helen Worden, John Worden, Lin Zhang (2018), Earth Observing System (EOS) Tropospheric Emission Spectrometer (TES) Data Validation Report (Version F08_11 data), Version 7.0, JPL Internal Report D-33192, May 30, 2018. Available online at: <https://eosweb.larc.nasa.gov/project/tes/validation>.
- [11] Kuai, L., K. W. Bowman, H. M. Worden, R. L. Herman, and S.S. Kulawik (2017), Hydrological controls on the tropospheric ozone greenhouse gas effect, *Elem. Sci. Anth.*, 2017; 5:10. DOI: <http://doi.org/10.1525/elementa.208>.
- [12] Kulawik, S.S., J.R. Worden, S.C. Wofsy, S.C. Biraud, R. Nassar, D.B.A. Jones, E.T. Olsen, G.B. Osterman, (2012), Comparison of improved Aura Tropospheric Emission Spectrometer (TES) CO₂ with HIPPO and SGP aircraft profile measurements, *Atmospheric Chemistry and Physics Discussions*, 12, 6283 – 6329, February 29, 2012.
- [13] Nassar, R., J.A. Logan, H.M. Worden, I.A. Megretskaya, K.W. Bowman, G.B. Osterman, A.M. Thompson, D.W. Tarasick, S. Austin, H. Claude, M.K. Dubey, W.K. Hocking, B.J. Johnson, E. Joseph, J. Merrill, G.A. Morris, M. Newchurch, S.J. Oltmans, F. Posny, F.J. Schmidlin, H. Vömel, D.N. Whiteman, and J.C. Witte (2008), Validation of Tropospheric Emission Spectrometer (TES) Nadir Ozone Profiles Using Ozone Sonde Measurements, *Journal of Geophysical Research* Vol. 113, D15S17, (doi:10.1029/2007JD008819), May 7, 2008.
- [14] Nassar, R., D.B.A. Jones, S.S. Kulawik, J.R. Worden, K.W. Bowman, R.J. Andres, P. Suntharalingam, J.M. Chen, C.A.M. Brenninkmeijer, T.J. Schuck, T.J. Conway, D.E. Worthy (2011), Inverse modeling of CO₂ sources and sinks using satellite observations of CO₂ from TES and surface flask measurements, *Atmos. Chem. Phys.*, **11**, (12), 6029-6047, June 24, 2011.
- [15] Nowak, J. B., J.A. Neuman, R. Bahreini, R., A.M. Middlebrook, J.S. Holloway, S.A. McKeen, D.D. Parrish, T.B. Ryerson, and M. Trainer (2012), Ammonia sources in the California South Coast Air Basin and their impact on ammonium nitrate formation, *Geophysical Research Letters*, Vol. 39, Issue 7, L07804, doi: 10.1029/2012GL051197.
- [16] Osterman, G., (editor), K. Bowman, K. Cady-Pereira, T. Clough, A. Eldering, B. Fisher, R. Herman, D. Jacob, L. Jourdain, S. Kulawik, M. Lampel, Q. Li, J. Logan, M. Luo, I. Megretskaya, R. Nassar, G. Osterman, S. Paradise, V. Payne, H. Revercomb., N. Richards, M. Shephard, D. Tobin, S. Turquety, F. Vlnrotter, H. Worden, J. Worden, and L. Zhang (2007), Earth Observing System (EOS) Tropospheric Emission Spectrometer (TES) Data Validation Report (Version F04_04 data), Version 3.0, JPL Internal Report D-33192, November 5, 2007.

- [17] Payne, V.H., S.A. Clough, M.W. Shephard, R. Nassar and J.A. Logan (2009), Information-centered representation of retrievals with limited degrees of freedom for signal: Application to methane from the Tropospheric Emission Spectrometer, *Journal of Geophysical Research: Atmospheres*, Vol. 114 Issue D10, May 27, 2009, D10307, (doi:10.1029/2008JD010155).
- [18] Payne, V. H., M. J. Alvarado, K. E. Cady-Pereira, J. R. Worden, S. S. Kulawik, and E. V. Fischer (2014), Satellite observations of peroxyacetyl nitrate from the Aura Tropospheric Emission Spectrometer, *Atmospheric Measurement Techniques*, 7/3737/2014/, doi:10.5194/amt-7-3737-2014, November 12, 2014
- [19] Payne, V. H., E.V. Fischer, J.R. Worden, Z. Jiang, L. Zhu, Thomas P. Kurosu, and S.S. Kulawik (2017), Spatial variability in tropospheric peroxyacetyl nitrate in the tropics from infrared satellite observations in 2005 and 2006, *Atmospheric Chemistry and Physics*, 17, 6341-6351, <https://doi.org/10.5194/acp-17-6341-2017>, 2017.
- [20] Roberts, J. M., J. Neuman, J. B. Nowak, T. B., Ryerson, J. W. Peischl, J. Holloway, C. Warneke, and J. A. de Gouw, (2009), Measurements of Acylperoxynitrates (PANs) in Biomass Burning Plumes over the Arctic in Spring 2008, *Eos Trans. AGU*, 90(52), American Geophysical Union, Fall Meeting Suppl., Abstract A43A-0231, 2009
- [21] Shephard, M. W., H. M. Worden, K. E. Cady-Pereira, M. Lampel, M. Luo, K. W. Bowman, E. Sarkissian, R. Beer, D. M. Rider, D. C. Tobin, H. E. Revercomb, B. M. Fisher, D. Tremblay, S. A. Clough, G. B. Osterman, and M. Gunson (2008), Tropospheric Emission Spectrometer Nadir Spectral Radiance Comparisons, *Journal of Geophysical Research: Atmospheres*, Vol. 113, Issue D15, D15S05, (doi:10.1029/2007JD008856), April 22, 2008.
- [22] Worden, J., S. S. Kulawik, M. W. Shephard, S. A. Clough, H. Worden, K. Bowman, and A. Goldman (2004), Predicted errors of tropospheric emission spectrometer nadir retrievals from spectral window selection, *Journal of Geophysical Research*, 109, D09308, May 15, 2004.
- [23] Worden, J., D. Noone, J. Galewsky, A. Bailey, K. Bowman, D. Brown, J. Hurley, S. Kulawik, J. Lee, and M. Strong (2011), Estimate of bias in Aura TES HDO/H₂O profiles from comparison of TES and in situ HDO/H₂O measurements at the Mauna Loa observatory, *Atmospheric Chemistry and Physics*, 11, 4491–4503, 2011, doi:10.5194/acp-11-4491-2011, May 12, 2011.
- [24] Worden, J., S. Kulawik, C. Frankenberg, V. Payne, K. Bowman, K. Cady-Peirara, K. Wecht, J.-E. Lee, D. Noone (2012), Profiles of CH₄, HDO, H₂O, and N₂O with improved lower tropospheric vertical resolution from Aura TES radiances, *Atmospheric Measurement Techniques*, 5, 397–411, 2012, doi:10.5194/amt-5-397-2012, February 20, 2012.

3.1.2 General References

- [25] Riley, W.J., S.C. Biraud, M.S. Torn, M.L. Fischer, D. P. Billesbach, J.A. Berry (2009), Regional CO₂ and latent heat surface fluxes in the Southern Great Plains: Measurements,

modeling, and scaling, *Journal of Geophysical Research-Biogeosciences*, 114, G04009, DOI: 10.1029/2009JG001003, 2009.

- [26] Wofsy, S.C., the HIPPO Science Team and Cooperating Modellers and Satellite Teams (2011), HIAPER Pole-to-Pole Observations (HIPPO): Fine grained, global scale measurements for determining rates for transport, surface emissions, and removal of climatically important atmospheric gases and aerosols, *Phil. Trans. of the Royal Society A*, vol. 369 (no. 1943), 2073-2086, May 28, 2011.

4. TES Level 1B Radiance Data Products and Level 2 IRK

Though this report is focused primarily on the TES Level 2 data products, it is important to understand that the L1B radiance products have also undergone a rigorous validation as reported in Shephard et al. (2008) and in the TES Validation Report V003 (Osterman et al., 2007). The fundamental measurement of the Tropospheric Emission Spectrometer (TES) on board the Aura spacecraft is upwelling infrared spectral radiances. Accurate radiances are critical for trace gas profile retrievals for air quality as well as sensitivity to climate processes. For example, any radiometric systematic errors (e.g. calibration) not addressed in the L1B radiances will propagate as errors into the retrieved atmospheric parameters (Bowman et al., 2006; Worden et al., 2004). Connor et al. (2011) showed that the TES relative radiometric calibration was extremely stable over the time period used in their analysis: 2005 to 2009.

In April 2010, TES implemented a new strategy for observing and processing calibration measurements (see Section 4 of the Version 5 Data Validation Report (Herman et al., 2012)). In order to validate TES spectra processed with the new calibration strategy, and to check comparisons of TES with AIRS over the entire TES data record from 2004 to present, we developed a more automated comparison tool based on the methods used for TES/AIRS comparisons in Shephard et al. (2008). Given the differences in ground footprints for TES and AIRS, comparisons are only meaningful for clear-sky, ocean scenes. Results for April 2009 (old calibration approach) compared to April 2010 (new calibration approach) are not significantly different, which suggests the new approach provides the same radiance accuracy as before.

4.1 Level 2 Product: Ozone Band Instantaneous Radiative Kernel (IRK)

Similar to TES V007, the IRK product for TES V008 include 1) 9.6-micron band Top of Atmosphere (TOA) flux (narrow band: $980 - 1020.2 \text{ cm}^{-1}$ for band flux; Wide band: $970 - 1120 \text{ cm}^{-1}$ for flux Segments), 2) both IRK and LIRK (logarithm IRK) profiles for Ozone (O_3) and water vapor (H_2O), 3) LIRK for cloud effective optical depth (COD), cloud top pressure (CTP), and emissivity (EMIS), and 4) IRK for atmospheric temperature (TATM) and surface temperature (TSUR) (see Table 4-1).

Table 4-1 The list of IRK products

Variable name	Description	Dimension	Window
FmBandFlux	Forward model band flux	[nrun#]	Narrow*
FmFluxSegs	Forward model flux segments over ozone band	[nrun×nfreq ^s]	Wide**
L1bBandFlux	Measured band flux from L1b data	[nrun]	Narrow
L1bFluxSegs	Measured flux segments over ozone band	[nrun × nfreq]	Wide
Frequency_FluxSegs	Frequency for flux segments	[nfreq]	Wide

Variable name	Description	Dimension	Window
O3IRK	Ozone Instantaneous Radiative Kernel	[nrun × nlev ^{&}]	Narrow
O3IRKSegs	Ozone Instantaneous Radiative Kernel segments	[nrun × nlev]	Narrow
O3LIRK	Ozone Logarithm Instantaneous Radiative Kernel	[nrun × nlev]	Narrow
H2OLIRK	Water vapor Logarithm Instantaneous Radiative Kernel	[nrun × nlev]	Narrow
TATMIRK	Atmospheric temperature Instantaneous Radiative Kernel	[nrun × nlev]	Narrow
SurfaceTemperatureIRK	Surface temperature Instantaneous Radiative Kernel	[nrun]	Narrow
CloudTopPressureLIRK	Cloud top pressure logarithm Instantaneous Radiative Kernel	[nrun]	Narrow
SurfaceEmissivityIRK	Surface emissivity Logarithm Instantaneous Radiative Kernel	[nrun × 10]	Narrow
CloudEffectiveOpticalDepthLIRK	Cloud effective optical depth Logarithm Instantaneous Radiative Kernel	[nrun × 6]	Narrow

* Narrow band: 980 – 1080.2 cm⁻¹

** Wide band: 970 – 1120 cm⁻¹

nrun = 1118 runs for GS 2147

& nlev =< 67 levels depending on surface pressure

\$ nfreq = 50 frequencies

There is no algorithm update for IRK but the data processed (as of October 2019) for validation is incomplete for V008 (especially at high latitudes). In general, the seasonal distributions over four seasons in O₃ and H₂O longwave radiative effect (LWRE), and TSUR IRK all stay highly consistent with V007. This suggests the IRK data of V008 are all reasonable except the hotspot region in V008 is slightly smaller and less intense. This difference is believed to be lower sampling density in new version data.

Figure 4-1 to Figure 4-3 are the global distributions averaged seasonally for O₃ LWRE, H₂O LWRE and TSUR IRK respectively. O₃ LWRE (Figure 4-1) show the two belts with high values over both subtropical regions and the notable hot spot at Middle East, especially during summer (JJA). The same regions with V007 product have seasonal high, such as India, Africa Savona, and Australia when there is hot and dry.

Water vapor LWRE in Figure 4-2 is highest at tropics and decrease with latitude as expected. The tropical high H₂O LWRE region migrates seasonally with the Intertropical Convergence Zone (ITCZ) due to the Hadley cell upwelling branch shift north and south, which is consistent with the pattern in V007.

TSUR IRK is known to be linear with TSUR and therefore has the similar pattern with TSUR distributions. As expected, the high IRK regions are found over subtropical major desert areas (e.g. Australia, Sahara, and Middle East) as well as west coast continental region, such as California and Chile. Again, the distributions are very consistent with V007.

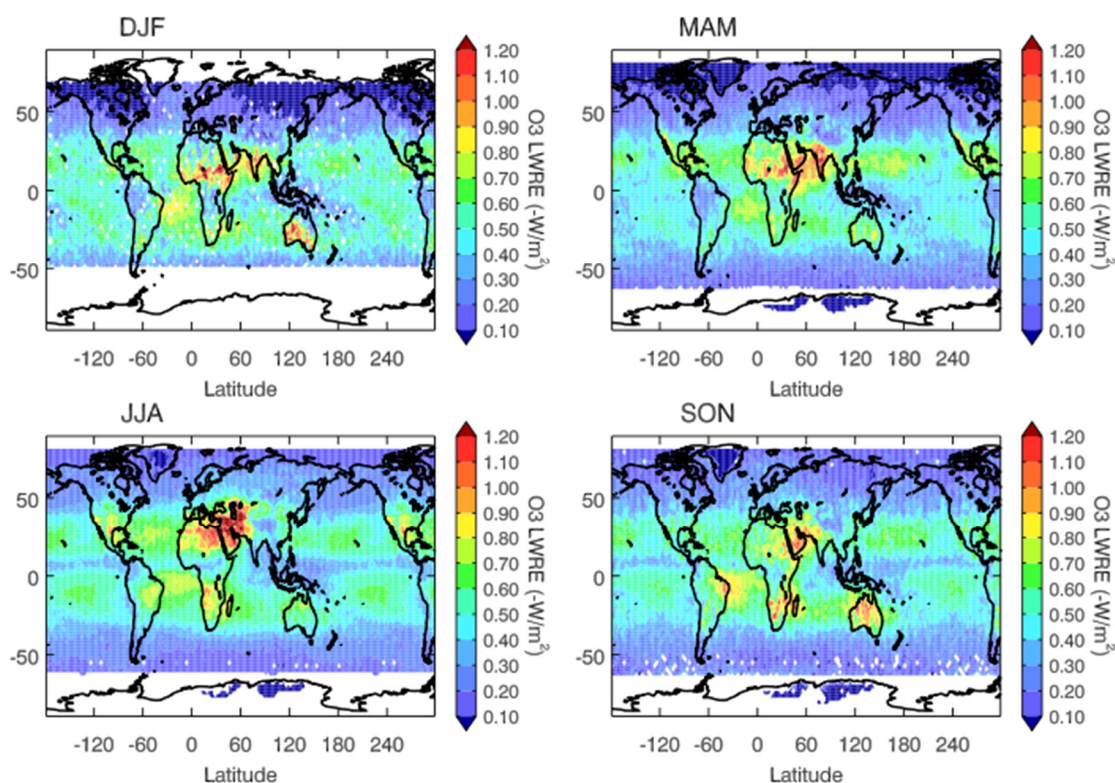


Figure 4-1 O₃ LWRE global pattern averaged seasonally.

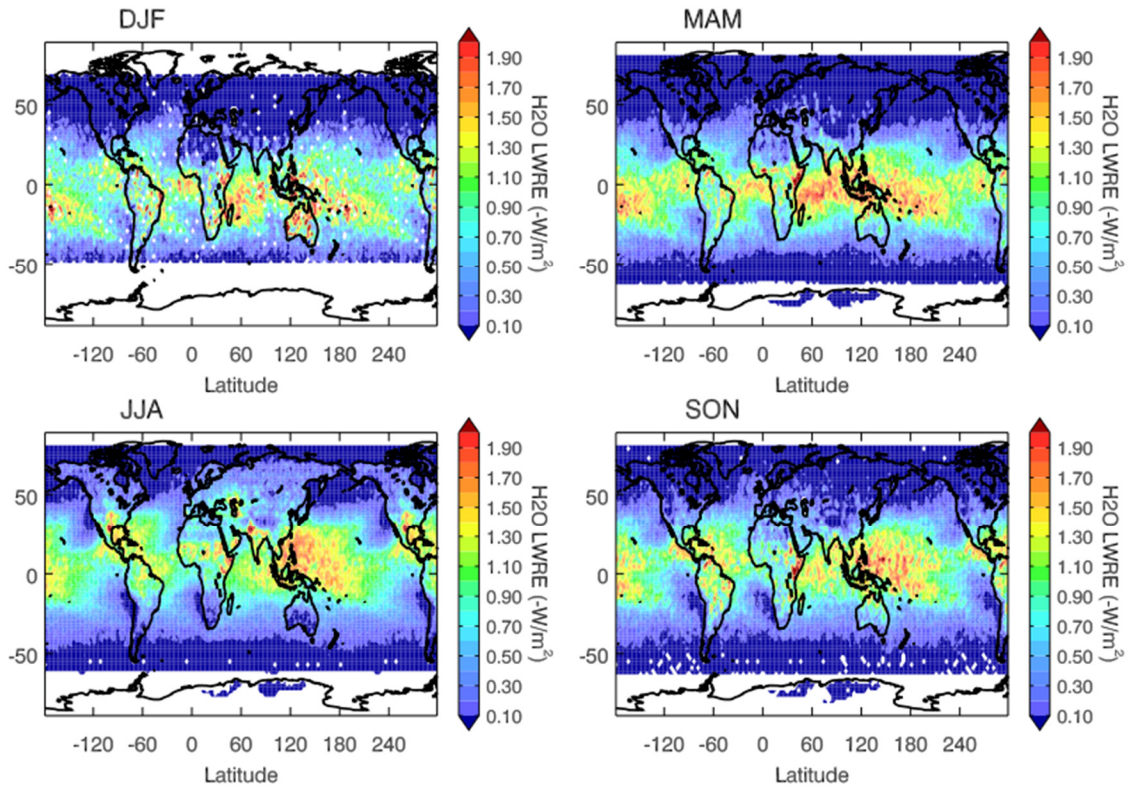


Figure 4-2 The same as Figure 4-1 but global pattern averaged seasonally for H₂O LWRE.

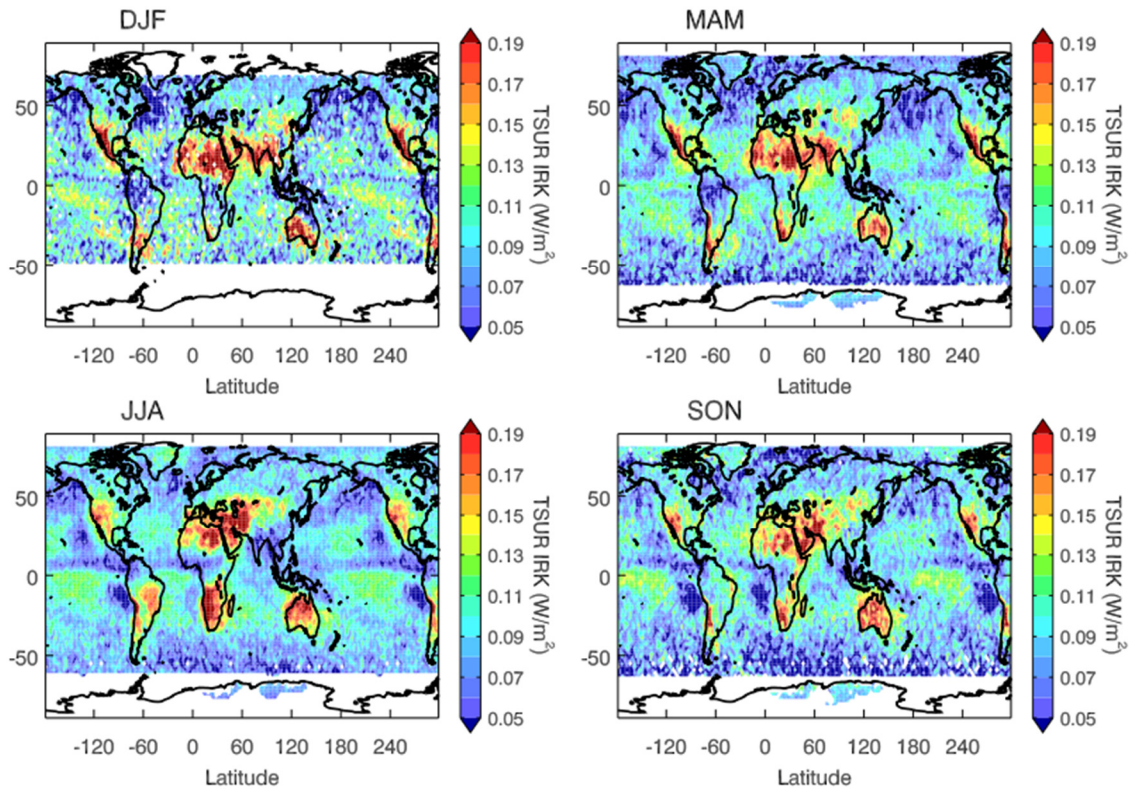


Figure 4-3 The same as Figure 4-1 and Figure 4-2 but global pattern averaged seasonally for TSUR IRK.

4.2 Single Sounding Comparison between V008 and V007

The following analysis shows the comparison of the IRK products for sounding ID: 2173_0171_02 between V008 and V007. The band flux within V008 is 33.03 W/m^2 , summed up from its segments calculation, which are self-consistent between forward model and L1b data calculation (Figure 4-4). But this band flux in V008 (33.03 W/m^2) is 0.1 W/m^2 lower than V007 (33.13 W/m^2) for the wide window ($970\text{-}1120 \text{ cm}^{-1}$). While, the flux for ozone band ($980\text{-}1079 \text{ cm}^{-1}$) is 0.05 lower in V008 (20.59 W/m^2) than V007 (20.64 W/m^2).

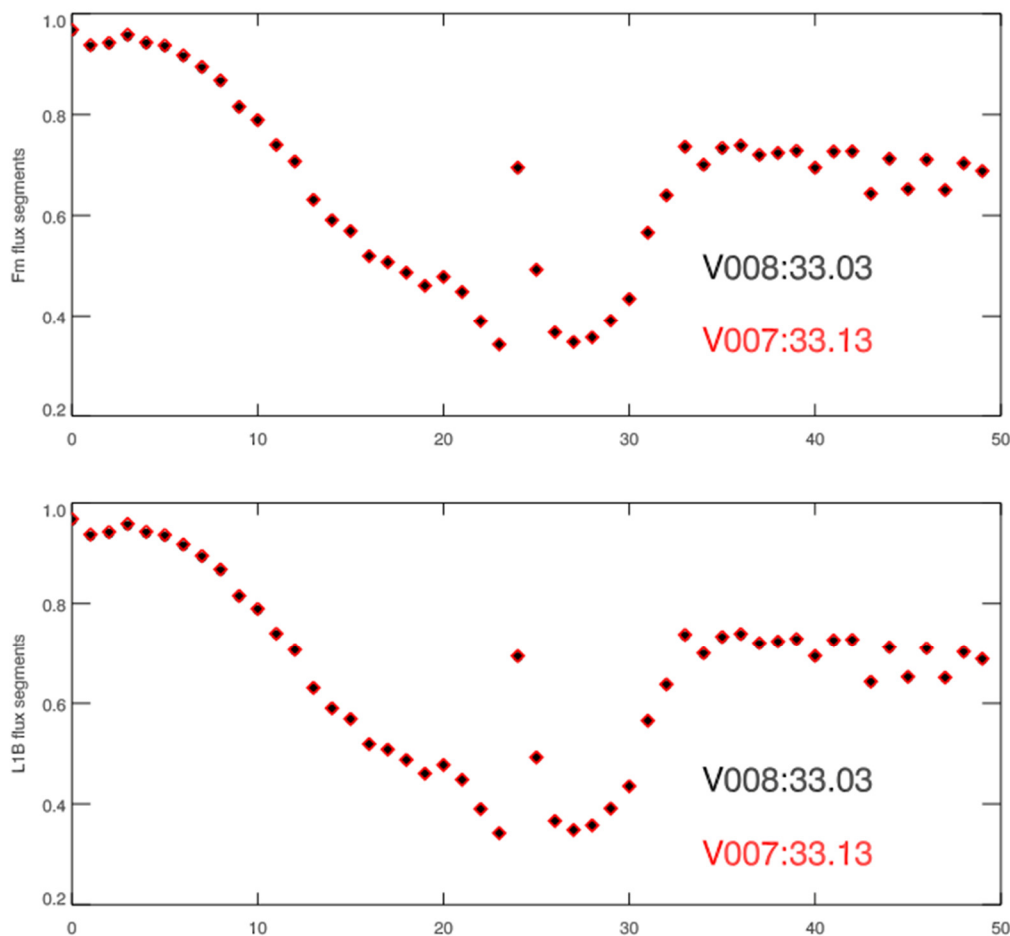


Figure 4-4 Top: forward model flux segments (every 3 cm^{-1}) for $970\text{-}1120 \text{ cm}^{-1}$. Red for V007 and black for V008. Bottom: the same as top but for L1B data.

The V008 O_3 LIRK, H_2O LIRK, and TATM IRK profiles all look reasonable but have slightly difference from V007 (Figure 4-5). This must because of the change of the retrieved O_3 , H_2O , and TATM profiles (Figure 4-6).

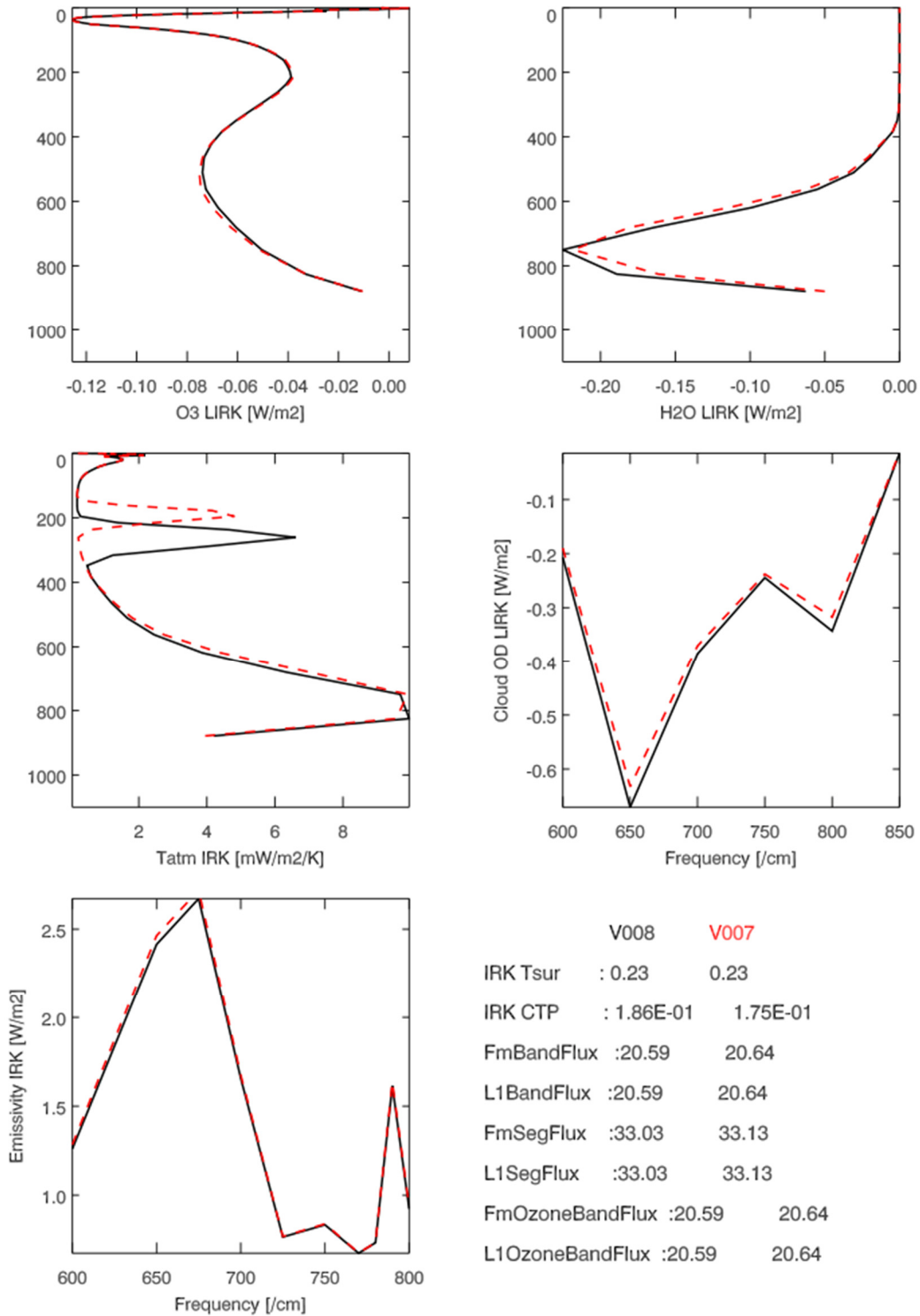


Figure 4-5 O₃ LIRK, H₂O LIRK, TATM IRK, Cloud OD LIRK, and Emissivity IRK comparisons between V008 and V007.

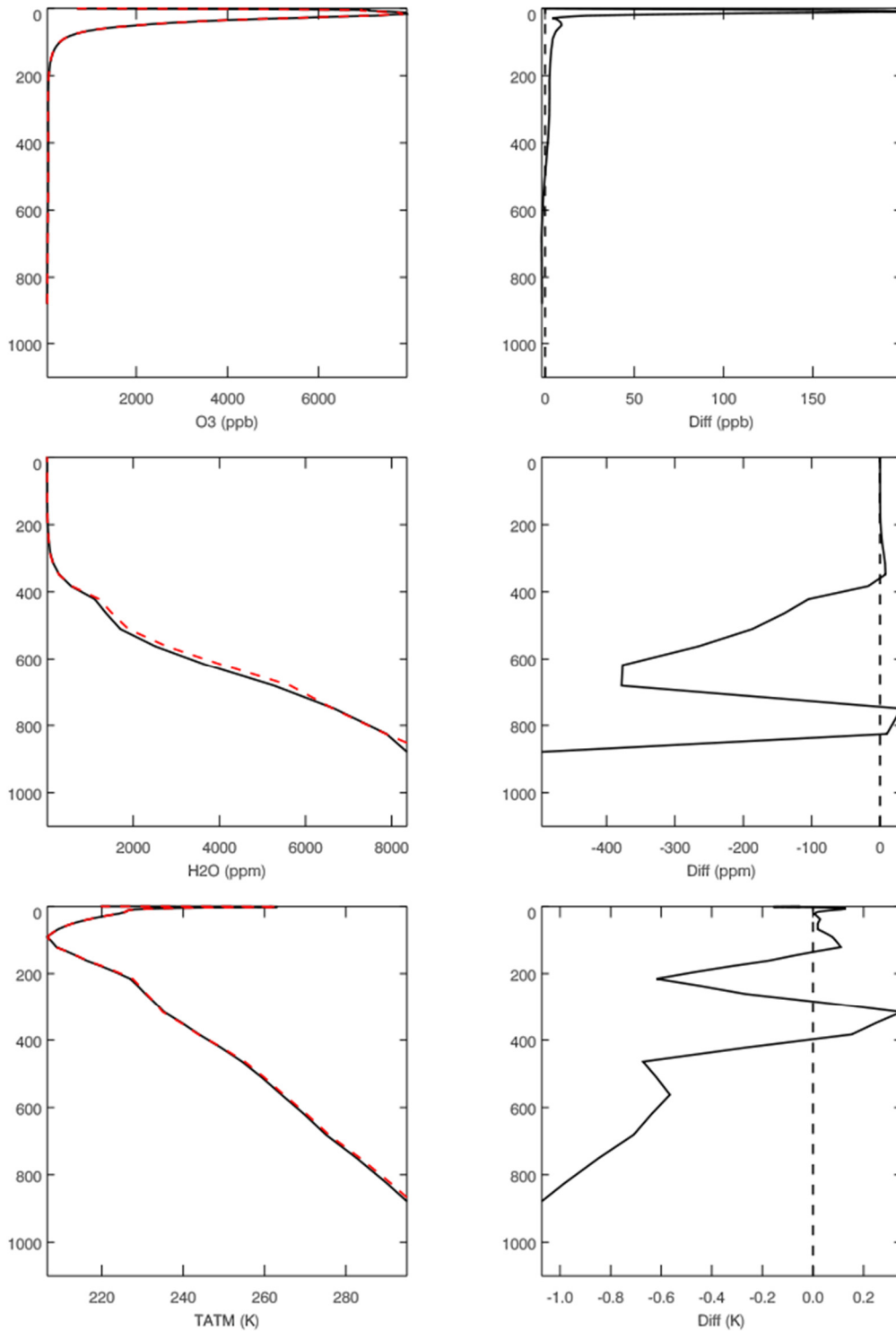


Figure 4-6 The comparisons of V007 (red) and V008 (black) O₃, H₂O, TATM profiles in the left column. Their differences in the right column.



4.3 References

4.3.1 TES L1B Radiance Validation References

- [1] Connor, T.C., M. W. Shephard, V. H. Payne, K. E. Cady-Pereira, S. S. Kulawik, M. Luo, G. Osterman, and M. Lampel (2011), Long-term stability of TES satellite radiance measurements, *Atmospheric Measurement Techniques*, Volume 4, Issue 7, doi:10.5194/amt-4-1481-2011, 1481–1490, July 25, 2011.
- [2] Osterman, G., (editor), K. Bowman, K. Cady-Pereira, T. Clough, A. Eldering, B. Fisher, R. Herman, D. Jacob, L. Jourdain, S. Kulawik, M. Lampel, Q. Li, J. Logan, M. Luo, I. Megretskaia, R. Nassar, G. Osterman, S. Paradise, V. Payne, H. Revercomb., N. Richards, M. Shephard, D. Tobin, S. Turquety, F. Vilnrotter, H. Worden, J. Worden, and L. Zhang (2007), Earth Observing System (EOS) Tropospheric Emission Spectrometer (TES) Data Validation Report (Version F04_04 data), Version 3.0, JPL Internal Report D-33192, November 5, 2007.
- [3] Shephard, M. W., H. M. Worden, K. E. Cady-Pereira, M. Lampel, M. Luo, K. W. Bowman, E. Sarkissian, R. Beer, D. M. Rider, D. C. Tobin, H. E. Revercomb, B. M. Fisher, D. Tremblay, S. A. Clough, G. B. Osterman, and M. Gunson (2008), Tropospheric Emission Spectrometer nadir spectral radiance comparisons, *J. Geophys. Res.*, 113, D15S05, (doi:10.1029/2007JD008856), April 22, 2008.

4.3.2 TES Level 2 IRK References

- [4] Kuai, L., K. W. Bowman, H. M. Worden, R. L. Herman, and S.S. Kulawik (2017), Hydrological controls on the tropospheric ozone greenhouse gas effect, *Elem. Sci. Anth.*, 2017; 5:10. DOI: <http://doi.org/10.1525/elementa.208>.

4.3.3 TES References

- [5] Bowman K. W., C. D. Rodgers, S. S. Kulawik, J. Worden, E. Sarkissian, G. Osterman, T. Steck, M. Lou, A. Eldering, M. Shephard, H. Worden, M. Lampel, S. A. Clough, P. D. Brown, C. P. Rinsland, M. Gunson, and R. Beer (2006), Tropospheric emission spectrometer: Retrieval method and error analysis, *IEEE Trans. Geosci. Remote Sens.*, 44(5), 1297-1307, May 2006.
- [6] Herman, R. and G. Osterman, (editors), C. Boxe, K. Bowman, K. Cady-Pereira, T. Clough, A. Eldering, B. Fisher, D. Fu, R. Herman, D. Jacob, L. Jourdain, S. Kulawik, M. Lampel, Q. Li, J. Logan, M. Luo, I. Megretskaia, R. Nassar, G. Osterman, S. Paradise, V. Payne, H. Revercomb, N. Richards, M. Shephard, D. Tobin, S. Turquety, F. Vilnrotter, K. Wecht, H. Worden, J. Worden, L. Zhang (2012), Earth Observing System (EOS) Tropospheric Emission Spectrometer (TES) Data Validation Report (Version F06_08, F06_09 data), Version 5.0, JPL Internal Report D-33192, April 8, 2012.
- [7] Worden, J., S. S. Kulawik, M. W. Shephard, S. A. Clough, H. Worden, K. Bowman, and A. Goldman (2004), Predicted errors of tropospheric emission spectrometer nadir retrievals from spectral window selection, *J. Geophys. Res.*, 109, D09308, May 15, 2004.

5. Nadir Ozone Validation

5.1 Overview

The changes to the TES retrieval algorithm for TES V007 did not have a strong impact on ozone retrievals, though some of the changes to the retrieval could have had effects on ozone. V007 has the following retrieval algorithm updates: (1) Updated L1B spike detection; (2) Updated thresholds for L1B zero path difference thresholds; Updated analytic surface temperature Jacobian computations.

Previous versions of the TES Validation Report have shown consistency in the ozone retrievals and in comparisons of TES retrievals to ozonesondes. Most recent updates to the ozone product showed minimal changes in ozone biases with respect to ozonesondes (V007 comparisons to V006, etc.) Hence, comparisons between the percent biases and random error of differences between TES V008 and ozonesondes and similar calculations using TES V007 ozone are sufficient to validate TES V008 nadir ozone profile. TES V008 nadir ozone profiles provide data that were measured in the TES global survey, step-and-stare, transect, and stare observation modes. The TES ozone data have been compared with ozonesonde measurements archived in the World Ozone and Ultraviolet Radiation Data Center (WOUDC: <http://www.woudc.org>). In past versions, percent differences between TES and ozonesonde were investigated in six latitude zones. The seasonal variability of ozone was investigated by using matches between coincident TES and ozonesonde observations in the 35°N to 56°N latitude zone.

The criteria of ± 9 hours, a 300 km radius and a cloud optical depth less than 2.0 were applied to search for the TES-ozonesonde coincidence measurements. TES data flagged as poor quality have been filtered out of the comparisons. In this comparison matches from 2005 through 2010 were used out of all TES measurements that have been processed for V008. The ozonesonde comparisons span a latitude range is from 73.26°S to 81.82°N (Figure 5-1) and time spans from 2005 to 2010.

Sonde and TES geolocations, 2005–2010

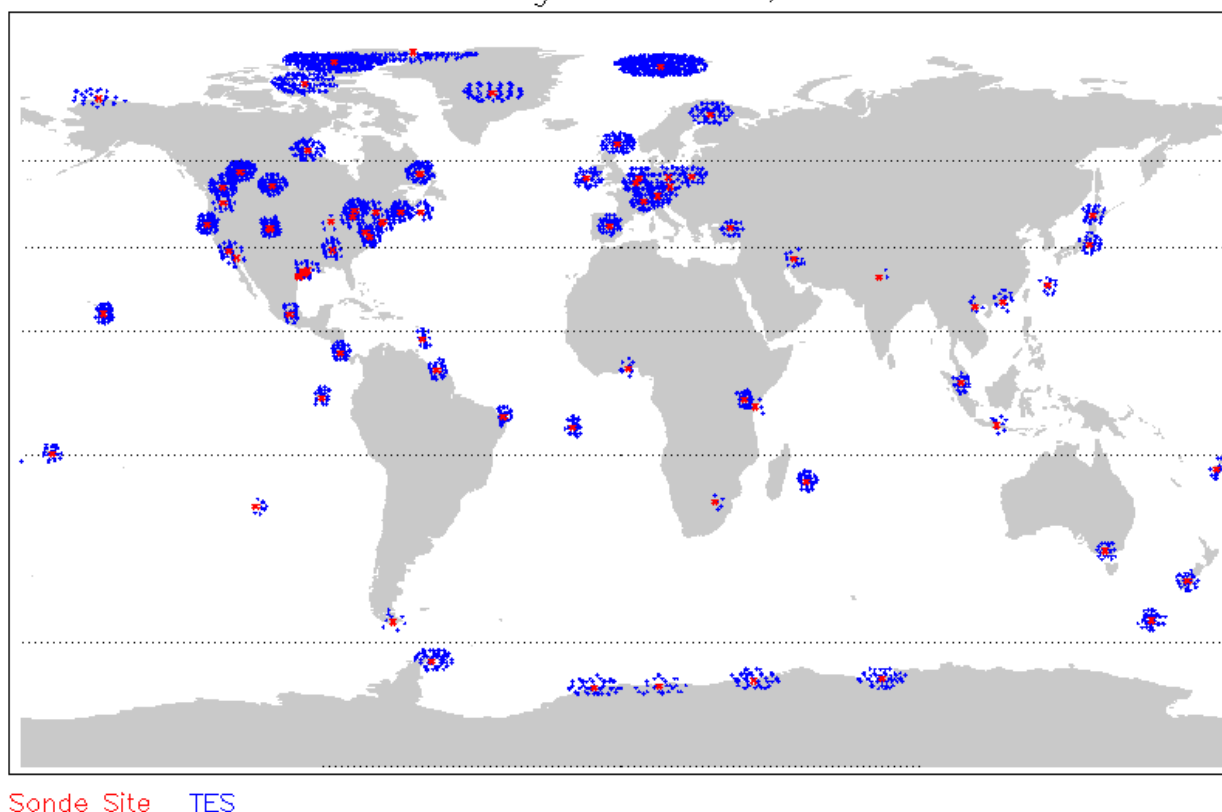


Figure 5-1 The global distribution of coincident TES (black plus) and WOUDC ozonesonde (blue diamond) measurements. Their latitude range is from 73.26°S to 81.82°N and time spans from 2004 to 2016, though only years 2005-20010 are used in this analysis.

The TES averaging kernel and a priori constraint were applied to the ozonesonde data in order to: (1) compare the TES ozone profiles and ozonesonde data in an unbiased quantifiable manner (i.e., not biased by the TES a priori); (2) take TES measurement sensitivity and vertical resolution into account.

In general, TES V008 ozone profiles are positively biased (by 0-10%) from the surface to 5 hPa relative to ozonesondes (Figure 5-2 (right panel)). Figure 5-2 (left panel) shows the same results for V007. In the altitude range from surface to 100 hPa (approximately the troposphere), both V008 and V007 TES data have a mean bias of approximately 5-10% and rms ranging from 10 to 25%. In the altitude range from 300 to 20 hPa, V008 and V007 are quite consistent with each other for bias relative to the ozonesondes, less than 10% differences in bias and less than 3% difference in rms (with V007 performing slightly better in the upper troposphere/lower stratosphere). In the altitude range above 20 hPa, both the mean and rms of differences between V008 and ozonesondes are roughly the same for V008 when compared to those of V007. Overall the differences when compared to ozonesondes are smaller (improved) for mid-to-lower tropospheric ozone when compared to the published comparisons of Nassar et al. (2008) and Boxe et al. (2010). Full details of the methodology of the comparing ozonesondes to TES data are provided in those published papers.

5.2 TES Ozonesonde Comparisons

TES nadir ozone profiles were retrieved using the optimal estimation method (OEM). The OEM combines TES measurements and a priori into the retrieved ozone profiles. An unbiased and quantitative TES-ozonesonde comparison method, which has been applied in the validation for all versions of TES products (V001 – V008), takes the impacts of a priori into account. The method applies the TES operator (i.e., averaging kernel and a priori constraint) to ozonesonde profiles. This approach generated ozonesonde profiles for the TES-ozonesonde comparisons by smoothing the high vertical resolution ozonesonde data with the TES averaging kernels and adding a priori information into the ozonesonde data. TES-ozonesonde percent differences were calculated using TES nadir ozone profiles and the ozonesonde profiles whose vertical resolution and impacts of a priori profiles are consistent to those TES nadir ozone profiles.

The number of matches from TES V008 is slightly higher than for TES V007 with nearly the full 2005-2010 data record processed in both versions for these comparisons.

2005-2010: V007	2005-2010: V008
# Pairs = 18462	# Pairs = 18916
Coincidence Distance < 300 km	Coincidence Distance < 300 km
Time Difference < 9 hours	Time Difference < 9 hours

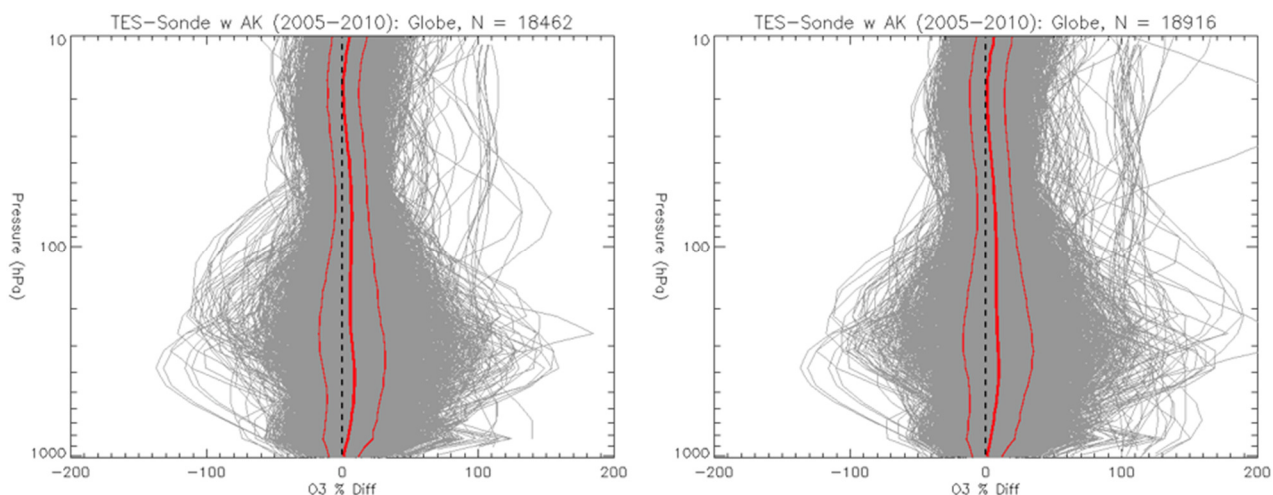


Figure 5-2 TES-ozonesonde percent differences. (Left) Individual profile of differences between TES V007 and ozonesonde for 2005-2010 are shown in grey, mean and one standard deviation ranges are overlaid in solid red and dash red lines, respectively. (Right) The same plot for the new version of TES data (V008).

Individual years show similar results for the comparison between TES ozone retrievals and ozonesondes as seen in the 2005-2010 aggregate comparisons. Comparisons for specific latitude bands are also consistent between the two versions.

5.3 References

5.3.1 Primary TES Nadir Ozone References

- [1] Boxe, C.S., J.R. Worden, K.W. Bowman, S.S. Kulawik, J.L. Neu, W.C. Ford, G.B. Osterman, R.L. Herman, A. Eldering, D.W. Tarasick, A.M. Thompson, D.C. Doughty, M.R. Hoffmann, S.J. Oltmans (2010), Validation of northern latitude Tropospheric Emission Spectrometer stare ozone profiles with ARC-IONS sondes during ARCTAS: sensitivity, bias and error analysis, *Atmospheric Chemistry and Physics*, doi:10.5194/acp-10-9901-2010, October 20, 2010.
- [2] Nassar, R., J.A. Logan, H.M. Worden, I.A. Megretskaia, K.W. Bowman, G.B. Osterman, A.M. Thompson, D.W. Tarasick, S. Austin, H. Claude, M.K. Dubey, W.K. Hocking, B.J. Johnson, E. Joseph, J. Merrill, G.A. Morris, M. Newchurch, S.J. Oltmans, F. Posny, F.J. Schmidlin, H. Vömel, D.N. Whiteman, J.C. Witte (2008), Validation of Tropospheric Emission Spectrometer (TES) Nadir Ozone Profiles Using Ozone Sonde Measurements, *J. Geophys. Res.* *113*, D15S17, (doi:10.1029/2007JD008819), May 7, 2008.
- [3] Osterman, G., S. S. Kulawik, H. M. Worden, N. A. D. Richards, B. M. Fisher, A. Eldering, M. W. Shephard, L. Froidevaux, G. Labow, M. Luo, R. L. Herman, K. W. Bowman, and A. M. Thompson, Validation of Tropospheric Emission Spectrometer (TES) Measurements of the Total, Stratospheric and Tropospheric Column Abundance of Ozone, *J. Geophys. Res.*, *113*, D15S16, (doi:10.1029/2007JD008801) May 7, 2008.
- [4] Richards, N. A. D., G. B. Osterman, E. V. Browell, J. W. Hair, M. Avery and Q. Li, Validation of Tropospheric Emission Spectrometer ozone profiles with aircraft observations during the Intercontinental Chemical Transport Experiment–B, *J. Geophys. Res.*, *113*, D16S29, (doi:10.1029/2007JD008815) May 23, 2008.
- [5] Worden, H. M., J. Logan, J. R. Worden, R. Beer, K. Bowman, S. A. Clough, A. Eldering, B. M. Fisher, M. R. Gunson, R. L. Herman, S. S. Kulawik, M. C. Lampel, M. Luo, I. A. Megretskaia, G. B. Osterman, and M. W. Shephard (2007), Comparisons of Tropospheric Emission Spectrometer (TES) ozone profiles to ozonesondes: Methods and initial results, *J. Geophys. Res.*, *112*, D03309, (doi:10.1029/2006JD007258), February 15, 2007.
- [6] Worden, J., X. Liu, K. Bowman, K. Chance, R. Beer, A. Eldering, M. Gunson, and H. Worden, (2007), Improved Tropospheric Ozone Profile Retrievals Using OMI and TES Radiances, *Geophys. Res. Lett.*, *34*, L01809, (doi:10.1029/2006GL027806) January 10, 2007.

5.3.2 TES References

- [7] Beer, R., T. A. Glavich, D. M. Rider (2001), Tropospheric Emission Spectrometer for the Earth Observing System's Aura satellite, *Applied Optics*, *40* (15), 2356-2367, May 20, 2001.

- [8] Beer, R. (2006), TES on the Aura Mission: Scientific Objectives, Measurements and Analysis Overview, *IEEE Transactions on Geoscience and Remote Sensing*, 44 (No.5), 1102-1105, May 2006.
- [9] Bowman K.W., C. D. Rodgers, S. S. Kulawik, J. Worden, E. Sarkissian, G. Osterman, T. Steck, M. Lou, A. Eldering, M. Shepherd, H. Worden, M. Lampel, S. Clough, P. Brown, C. Rinsland, M. Gunson, R. Beer, “Tropospheric Emission Spectrometer: Retrieval Method and Error Analysis”, *IEEE Trans. Geoscience and Remote Sensing*, 44, (No.5), 1297-1307. May 2006.
- [10] Eldering, A., S. S. Kulawik, J. Worden, K. Bowman, G. Osterman (2008), Implementation of cloud retrievals for TES Atmospheric retrievals: 2. Characterization of cloud top pressure and effective optical depth retrievals, *Journal of Geophysical Research*, Vol. 113, D16S37, (doi:10.1029/2007JD008858) June 10, 2008.
- [11] Herman, R., and S. Kulawik, (editors), K. Bowman, K. Cady-Pereira, A. Eldering, B. Fisher, D. Fu, R. Herman, D. Jacob, L. Jourdain, S. Kulawik, M. Luo, R. Monarrez, G. Osterman, S. Paradise, V. Payne, S. Poosti, N. Richards, D. Rider, D. Shepard, M. Shephard, F. Vilnrotter, H. Worden, J. Worden, H. Yun and L. Zhang (2018), Earth Observing System (EOS) Tropospheric Emission Spectrometer (TES) Level 2 (L2) Data User’s Guide (Up to & including Version 7 data), Version 7.0, JPL Internal Report D-38042, September 27, 2018.
- [12] Herman, Robert and Gregory Osterman (editors), Christopher Boxe, Kevin Bowman, Karen Cady-Pereira, Tony Clough, Annmarie Eldering, Brendan Fisher, Dejian Fu, Robert Herman, Daniel Jacob, Line Jourdain, Susan Kulawik, Michael Lampel, Qinbin Li, Jennifer Logan, Ming Luo, Inna Megretskaja, Ray Nassar, Gregory Osterman, Susan Paradise, Vivienne Payne, Hank Revercomb, Nigel Richards, Mark Shephard, Dave Tobin, Solene Turquety, Felicia Vilnrotter, Kevin Wecht, Helen Worden, John Worden, Lin Zhang (2012), Earth Observing System (EOS) Tropospheric Emission Spectrometer (TES) Data Validation Report (Version F06_08, F06_09 data), Version 5.0, JPL Internal Report D-33192, April 8, 2012.
- [13] Jourdain, L., H. M. Worden, J. R. Worden, K. Bowman, Q. Li, A. Eldering, S. S. Kulawik, G. Osterman, K. F. Boersma, B. Fisher, C. P. Rinsland, R. Beer, M. Gunson., (2007), Tropospheric vertical distribution of tropical Atlantic ozone observed by TES during the northern African biomass burning season, *Geophysical Research Letters*, 34, L04810, (doi:10.1029/2006GL028284) February 23, 2007.
- [14] Kulawik, S. S., J. Worden, A. Eldering, K. Bowman, M. Gunson, G. B. Osterman, L. Zhang, S. Clough, M. W. Shephard, R. Beer (2006), Implementation of cloud retrievals for Tropospheric Emission Spectrometer (TES) atmospheric retrievals: part 1. Description and characterization of errors on trace gas retrievals, *J. Geophys. Res.*, 111, D24204, (doi:10.1029/2005JD006733), December 22, 2006.
- [15] Luo M., C. P. Rinsland, C. D. Rodgers, J. A. Logan, H. Worden, S. Kulawik, A. Eldering, A. Goldman, M. W. Shephard, M. Gunson, and M. Lampel (2007) Comparison of carbon monoxide measurements by TES and MOPITT: Influence of a priori data and instrument characteristics on nadir atmospheric species retrievals, *Journal of Geophysical Research*, Vol. 112, D09303, (doi:101029/2006JD007663) May 3, 2007.

- [16] Worden, J., S. S. Kulawik, M. W. Shephard, S. A. Clough, H. Worden, K. Bowman, and A. Goldman (2004), Predicted errors of tropospheric emission spectrometer nadir retrievals from spectral window selection, *J. Geophys. Res.*, *109*, D09308, May 15, 2004.

5.3.3 General References

- [17] Bloom, S., A. da Silva, D. Dee, M. Bosilovich, J.-D. Chern, S. Pawson, S. Schubert, M. Sienkiewicz, I. Stajner, W.-W. Tan, M.-L. Wu (2005). Documentation and Validation of the Goddard Earth Observing System (GEOS) Data Assimilation System - Version 4. *Technical Report Series on Global Modeling and Data Assimilation 104606, Vol. 26*, 187 pages, April 2005. Available from (paste entire link including pdf into browser):
http://ntrs.nasa.gov/archive/nasa/casi.ntrs.nasa.gov/20050175690_2005173043.pdf
- [18] Brasseur, G. P., D. A. Hauglustaine, S. Walters, R. J. Rasch, J.-F. Müller, C. Granier, and X. X. Tie (1998), MOZART, a global chemical transport model for ozone and related chemical tracers 1. Model description, *J. Geophys. Res.*, *103* (D21), 28, 265–28, 289 (1998).
- [19] Draxler, R.R. and Rolph, G.D. (2003), HYSPLIT (HYbrid Single-Particle Lagrangian Integrated Trajectory) Model access via NOAA ARL READY Website (<http://www.arl.noaa.gov/ready/hysplit4.html>). NOAA Air Resources Laboratory, Silver Spring, MD (2003).
- [20] Froidevaux, L., Y.B. Jiang, A. Lambert, N.J. Livesey, W.G. Read, J.W. Waters, E.V. Browell, J.W. Hair, M.A. Avery, T.J. McGee, L.W. Twigg, G.K. Sumnicht, K.W. Jucks, J.J. Margitan, B. Sen, R.A. Stachnik, G.C. Toon, P.F. Bernath, C.D. Boone, K.A. Walker, M.J. Filipiak, R.S. Harwood, R.A. Fuller, G.L. Manney, M.J. Schwartz, W.H. Daffer, B.J. Drouin, R.E. Cofield, D.T. Cuddy, R.F. Jarnot, B.W. Knosp, V.S. Perun, W.V. Snyder, P.C. Stek, R.P. Thurstans, P.A. Wagner (2008), Validation of Aura Microwave Limb Sounder stratospheric ozone measurements, *J. Geophys. Res.*, *113*, D15S20, (doi:10.1029/2007JD008771) 2008.
- [21] Jiang, Y. B., L. Froidevaux, A. Lambert, N.J. Livesey, W.G. Read, J.W. Waters, B. Bojkov, T. Leblanc, I.S. McDermid, S. Godin-Beekmann, M.J. Filipiak, R.S. Harwood, R.A. Fuller, W.H. Daffer, B.J. Drouin, R.E. Cofield, D.T. Cuddy, R.F. Jarnot, B.W. Knosp, V.S. Perun, M.J. Schwartz, W.V. Snyder, P.C. Stek, R.P. Thurstans, P.A. Wagner, M. Allaart, S.B. Andersen, G. Bodeker, B. Calpini, H. Claude, G. Coetzee, J. Davies, H. De Backer, H. Dier, M. Fujiwara, B. Johnson, H. Kelder, N.P. Leme, G. König-Langlo, E. Kyro, G. Laneve, L.S. Fook, J. Merrill, G. Morris, M. Newchurch, S. Oltmans, M.C. Parrondos, F. Posny, F. Schmidlin, P. Skrivankova, R. Stubi, D. Tarasick, A. Thompson, V. Thouret, P. Viatte, H. Vomel, P. von der Gathen, M. Yela, G. Zablocki (2007), Validation of Aura Microwave Limb Sounder Ozone by Ozone sonde and Lidar Measurements, *Journal of Geophysical Research*, *112*, D24S34, (doi:10.1029/2007JD008776) 2007.

- [22] Levelt, P. F., G.H.J. van den Oord, M.R. Dobber, A. Mälkki, H. Visser, J. de Vries, P. Stammes, J. Lundell and H. Saari (2006a), The Ozone Monitoring Instrument, *IEEE Trans. Geoscience and Remote Sensing*, *44*, (No.5), 1093-1101, May 2006.
- [23] Levelt, P. F., E. Hilsenrath, G.W. Leppelmeier, G.H.J. van den Oord, P.K. Bhartia, J. Tamminen, J.F. de Haan en J.P. Veefkind (2006b), Science objectives of the Ozone monitoring instrument, *IEEE Trans. Geoscience and Remote Sensing*, *44*, (No.5), 1199-1208, May 2006.
- [24] Livesey, N. J., W.G. Read, A. Lambert, R.E. Cofield, D. T. Cuddy, L. Froidevaux, R. A. Fuller, R. F. Jarnot, J. H. Jiang, Y. B. Jiang, B. W. Knosp, L. J. Kovalenko, H. M. Pickett, H. C. Pumphrey, M. L. Santee, M. J. Schwartz, P. C. Stek, P. A. Wagner, J. W. Waters, and D. L. Wu (2007), EOS MLS Version 2.2 Level 2 data quality and description document, Version 2.2x-1.0a Jet Propulsion Laboratory Internal Report D-33509, May 22, 2007.
- [25] Livesey N.J., M.J. Filipiak, L. Froidevaux, W.G. Read, A. Lambert, M.L. Santee, J.H. Jiang, H.C. Pumphrey, J.W. Waters, R.E. Cofield, D.T. Cuddy, W.H. Daffer, B.J. Drouin, R.A. Fuller, R.F. Jarnot, Y.B. Jiang, B.W. Knosp, Q.B. Li, V.S. Perun, M.J. Schwartz, W.V. Snyder, P.C. Stek, R.P. Thurstans, P.A. Wagner, M. Avery, E.V. Browell, J-P. Cammas, L.E. Christensen, G.S. Diskin, R-S. Gao, H-J. Jost, M. Loewenstein, J.D. Lopez, P. Nedelec, G.B. Osterman, G.W. Sachse, and C.R. Webster (2008), Validation of Aura Microwave Limb Sounder O₃ and CO observations in the upper troposphere and lower stratosphere, *J. Geophys. Res.*, *113*, D15S02, (doi:10.1029/2007JD008805) March 27, 2008.
- [26] Logan, J.A., An analysis of ozonesonde data for the troposphere: Recommendations for testing 3-D models, and development of a gridded climatology for tropospheric ozone, *J. Geophys. Res.*, *104*, 16115-16149, 1999.
- [27] Rodgers, C. D. (2000), *Inverse Methods for Atmospheric Sounding: Theory and Practice*. World Scientific Publishing Co. Ltd., 2000.
- [28] Rodgers, C. D. and B. J. Conners (2003), Intercomparison of remote sounding instruments, *J. Geophys. Res.*, *108*,(D3), 4116, (doi:10.1029/2002JD002299) 2003.
- [29] Schoeberl, M.R., J.R. Ziemke, B. Bojkov, N. Livesey, B. Duncan, S. Strahan, L. Froidevaux, S. Kulawik, P.K. Bhartia, S. Chandra, P.F. Levelt, J.C. Witte, A.M. Thompson, E. Cuevas, A. Redondas, D.W. Tarasick, J. Davies, G. Bodeker, G. Hansen, B.J. Johnson, S.J. Oltmans, H. Vomel, M. Allaart, H. Kelder, M. Newchurch, S. Godin-Beekmann, G. Ancellet, H. Claude, S.B. Andersen, E. Kyro, M. Parrondos, M. Yela, G. Zablocki, D. Moore, H. Dier, P. von der Gathen, P. Viatte, R. Stubi, B. Calpini, P. Skrivankova, V. Dorokhov, H. De Backer, F.J. Schmidlin, G. Coetzee, M. Fujiwara, V. Thouret, F. Posny, G. Morris, J. Merrill, C.P. Leong, G. Koenig-Langlo, and E. Joseph. (2007), A trajectory-based estimate of the tropospheric ozone column using the residual method, *J. Geophys. Res.* *112*, D24S49, (doi:10.1029/2007JD008773) December 19, 2007.
- [30] Waters, J.W., L. Froidevaux, R.S. Harwood, R.F. Jarnot, H.M. Pickett, W.G. Read, P.H. Siegel, R.E. Cofield, M.J. Filipiak, D.A. Flower, J.R. Holden, G.K. Lau, N.J. Livesey, G.L. Manney, H.C. Pumphrey, M.L. Santee, D.L. Wu, D.T. Cuddy, R.R. Lay, M.S. Loo,

V.S. Perun, M.J. Schwartz, P.C. Stek, R.P. Thurstans, M.A. Boyles, S. Chandra, M.C. Chavez, G-S. Chen, B.V. Chudasama, R. Dodge, R.A. Fuller, M.A. Girard, J.H. Jiang, Y. Jiang, B.W. Knosp, R.C. LaBelle, J.C. Lam, K.A. Lee, D. Miller, J.E. Oswald, N.C. Patel, D.M. Pukala, O. Quintero, D.M. Scaff, W.V. Snyder, M.C. Tope, P.A. Wagner, and M.J. Walch, (2006), The Earth Observing System Microwave Limb Sounder (EOS MLS) on the Aura satellite, *IEEE Trans. Geoscience and Remote Sensing*, 44, (No.5), 1075-1092, May 2006.

- [31] Ziemke, J.R., S. Chandra, B.N. Duncan, L. Froidevaux, P.K. Bhartia, P.F. Levelt, and J.W. Waters, (2006), Tropospheric ozone determined from Aura OMI and MLS: Evaluation of measurements and comparison with the Global Modeling Initiative's Chemical Transport Model, *J. Geophys. Res.*, 111, D19303 (doi:10.1029/2006JD007089) October 5, 2006.

6. Validation of TES Retrievals of Carbon Monoxide

6.1 Overview

TES CO and other species retrievals are currently being processed in version V008 as the final version of the mission. All the original TES CO data validation activities, including comparisons with in-situ aircraft data, and with MOPITT data and other satellite data, have been carried out for TES V003 or V002 data. The TES CO V004 data have no systematic changes from previous versions. In TES CO V005, two major changes were made: we adopted CO a priori data from MOZART-4 model results (eight-year monthly averages) and the new constraint matrix used in retrievals that was derived from the same algorithm used in MOPITT CO retrievals. In TES V006/V007/V008 CO retrievals, there were no changes made in retrieval algorithms or the a priori climatology. In V007, L1B process adopted an algorithm in screening the good quality pixels (total of 16 pixels) instead of using the L1A per-scan quality flag which flags the scan bad even if only a single pixel is bad. There is no updates in L1B for the V008 CO related processing.

We briefly describe the TES instrument performance over ten years on orbit, the positive effect of the optical bench warm-up conducted early Dec 2005 on filter 1A1 and the CO retrievals, and the post April 2011 worsening throughputs in CO data due to instrument control system degradation. We give an overview of the characterization of TES CO retrievals, including the roles of the a priori profiles and the averaging kernels. A brief overview of the global distributions of TES CO measurements is given for different seasons. For previous versions of CO data, we present comparisons of TES CO profiles with in situ measurements from several aircraft campaigns, including INTEX-B (Intercontinental Transport Experiment-Phase B), AVE (Aura Validation Experiment), and CR-AVE (Costa Rica Aura Validation Experiment). Since there are no algorithm updates to CO retrieval, in this validation report, we made TES CO V007 and V008 comparisons and updated TES V008 - MOPITT new CO V8 comparisons for several Global Survey runs. These comparisons not only offer good qualitative checks for TES data, e.g., the characteristics of the CO global distribution or the shapes of their vertical profiles, but also offer quantitative validations of TES CO retrievals.

6.2 Instrument performance before and after optical bench warm-up

For constant emission source, e.g., on-board black body, the signal strength in TES 1A1 filter (1900-2300 cm⁻¹) is not constant over time and the variation of the signal strength is reflected in the CO retrievals. Figure 6-1 displays the normalized integrated spectral magnitude (ISM) (top panel), beam splitter temperature (middle panel), and degrees of freedom for signal (DOFS) for latitudes of 30°N-30°S as a function of time (Rinsland et al., 2006). Data after the middle of 2006 stays about the same level. The ISM is a sensitive indicator of the signal levels of the TES detectors and is calculated by integrating a spectrum over wavenumber. It is the primary quantity used to quantify and detect trends in the TES instrument alignment and performance. An overall trend of declining ISM with time and the measured beamsplitter temperature is apparent, with increases in beamsplitter temperatures when the detectors are de-iced periodically. The warming of the TES optical bench on Nov 29-Dec 2, 2005 improved the TES beamsplitter alignment, with an integrated spectral magnitude increase for the 1A1 filter by a factor of 3.4 as compared to the pre-warm up value.

The TES CO retrieval ‘sensitivity’, or the parameters describing the retrieval vertical information in the troposphere, e.g., the Degrees of Freedom for signal (DOFS) and the retrieval errors, are

much improved after the optical bench warm up in early December 2005 as a result of the better alignment of the instrument and increased signal to noise.

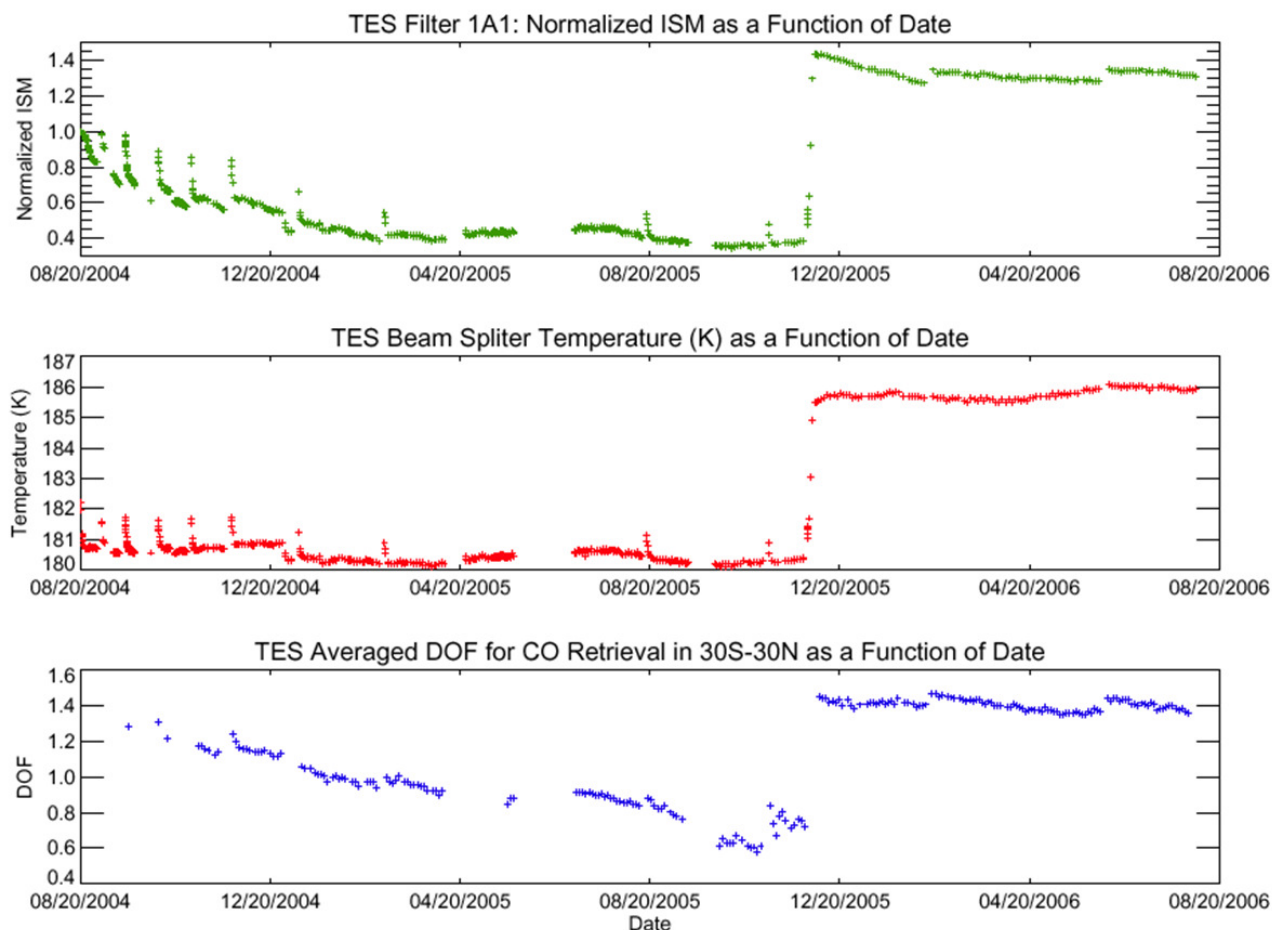


Figure 6-1 Time series of measured normalized Integrated Spectral Magnitude (ISM) (top panel), beamsplitter temperature (middle panel), and average DOFS for 30°N-30°S latitude. The ISM is normalized to 1.0 at the beginning of the time series.

6.3 Problems in filter 1A1 signal used for CO retrieval since 2011

The aging of TES mechanically moving components, e.g., Interferometer Control System (ICS) started to affect TES measured signals since early 2011. The majority of the problematic scans show ‘over/underflows’ or ‘spikes’ in the interferogram DNs (Data Number). TES Level 1A software detects and flags these scans and removes them from the L1B and L2 processing. Compared to 2004-2010 data we therefore see drop-offs in valid number of CO retrievals in the TES product since early 2011.

TES has a 16-pixel detector. The scan-removing decision described above removes the entire scan even if there are a number of good signal pixels in a scan. In V007, a new algorithm at L1B is applied that identifies the non-spike pixels for L2 retrievals in a scan. This algorithm also makes spike-removal corrections to the interferograms that has spikes away from the kernel where near zero optical path difference occurs. These corrected pixels are also made available to L2 retrievals.

In V007 the throughputs of CO retrievals are therefore increased compared to that of V006. Figure 6-2 shows the time series of the percent of monthly good quality CO retrievals for V007 (R14.1) and V006 (R13). The drop of the throughputs since 2011 is mainly due to the worsening of the ICS performance. The throughputs in V007 are much improved over V006 for the post 2011 times. In the recent V008 data, these better throughputs are kept.

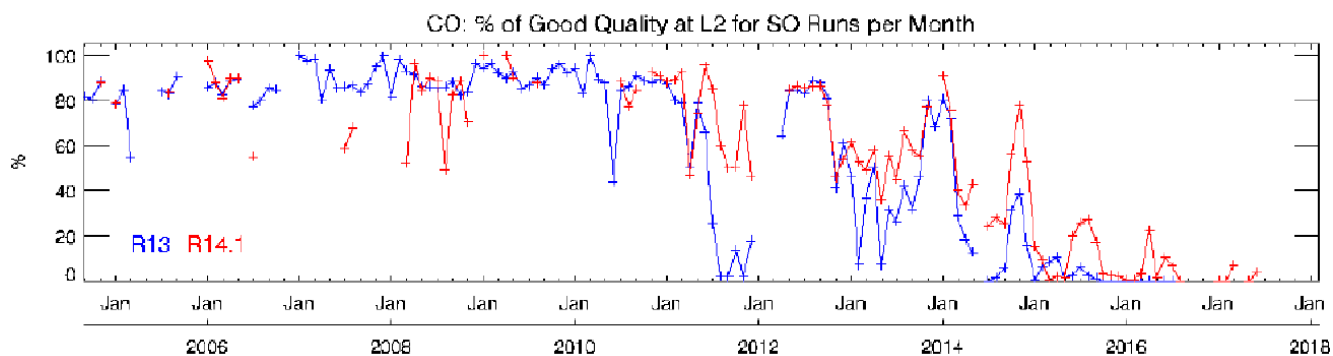


Figure 6-2 Time series of the percentage of ‘good quality CO retrievals’ per month. Note that V007 data processing was still in progress when this figure was prepared.

6.4 Comparisons of TES V008 to V007 in CO retrieval

There are no changes made in CO step retrieval and the a priori data used in TES V008 data processing. The MOZART-4 model data provided to TES from the NCAR (National Center for Atmospheric Research) group are used as the CO a priori state. These model results for CO VMR were averaged monthly in 10 degree latitude by 60 degree longitude boxes as the TES CO a priori. The constraint matrix for TES CO retrievals is by adopting the same algorithm provided by the MOPITT team for deriving their V4/V5/V6/V7 data (Deeter et al., 2010). The slight changes in TES V008 and V007 are due to changes made in other retrieval.

We examine the differences between TES V008 and V007 to document the magnitude of the changes in CO retrievals. We also perform the comparisons of TES and MOPITT CO to evaluate their statistical differences by removing the known a priori effects as it has been done previously.

Figure 6-3 shows that V008 retrievals are almost identical to that of V007 in the troposphere. Figure 6-4 statistical comparison for a Global Survey run at 681 and 215 hPa pressure levels also show almost no change in CO in V008 from that of V007.

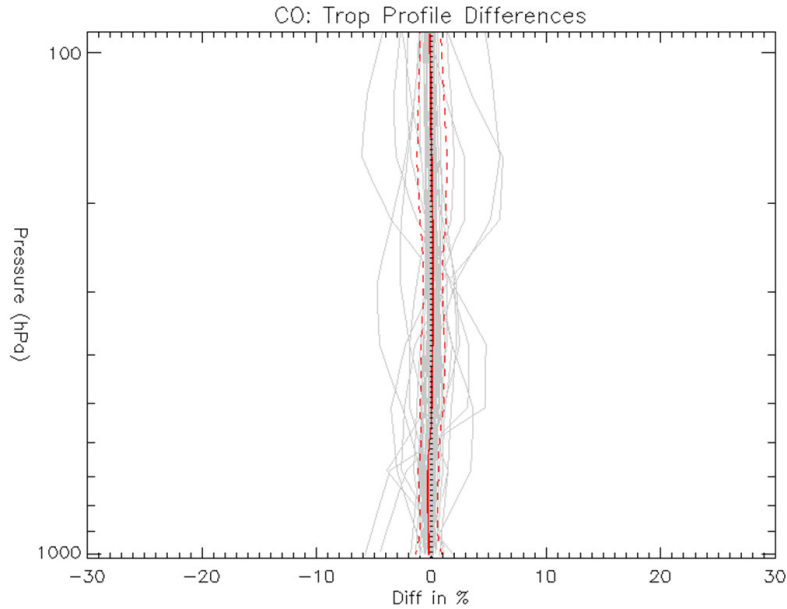


Figure 6-3 TES CO Volume Mixing Ratio V008 minus V007 in percent for run 5800, an along track Step and Stare observation campaign taken 2007-07-26 over mid-east Asia and E Europe.

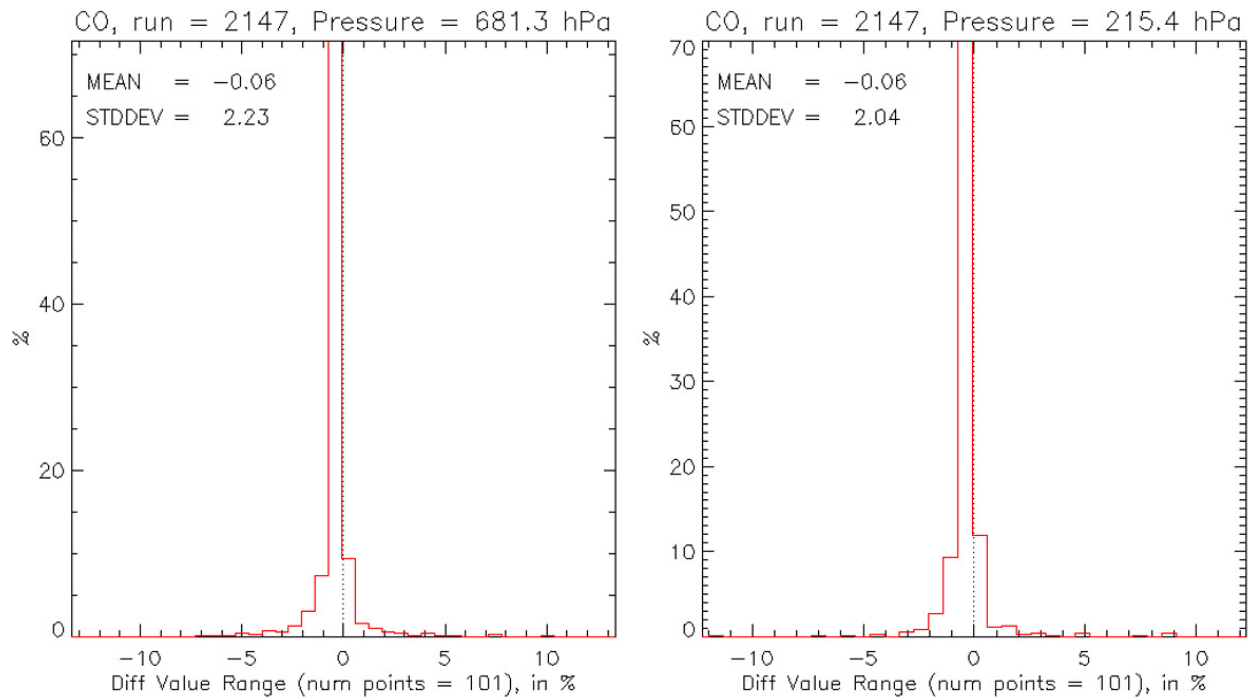


Figure 6-4 Histograms of percent differences between TES CO V008 and V007 from Global Survey run2147 taken 2004-09-20/21.

6.5 Global distributions of CO from TES measurements

Carbon monoxide is a by-product of incomplete combustion of fossil fuels and biomass, and is produced by oxidation of methane (CH₄) and other hydrocarbons. The global distributions of TES CO fields reflect this basic understanding, e.g., the enhanced CO regions and their seasonal variations are co-located with the known combustion source regions. Figure 6-5 shows TES CO monthly mean distributions at 681.3 hPa for Jan, Apr, July, and Oct 2009. In general, the northern hemisphere (and the tropics) show much more CO than the southern hemisphere due to the known distribution of natural and industrial sources. CO values in the winter/spring are larger than summer/fall due to the longer lifetime in seasons with less photochemical activity.

In central Africa, the enhanced CO corresponding to biomass burning occurs in two time periods, in Dec/Jan/Feb for latitudes north of the equator and in Jul-Oct south of the equator, corresponding to the local dry seasons. In South America, the biomass burning induced maximum in CO concentration occurred during Aug/Sep/Oct near equator. Enhanced levels of CO over E. China can be related local pollution and can be seen throughout the year in the TES observations.

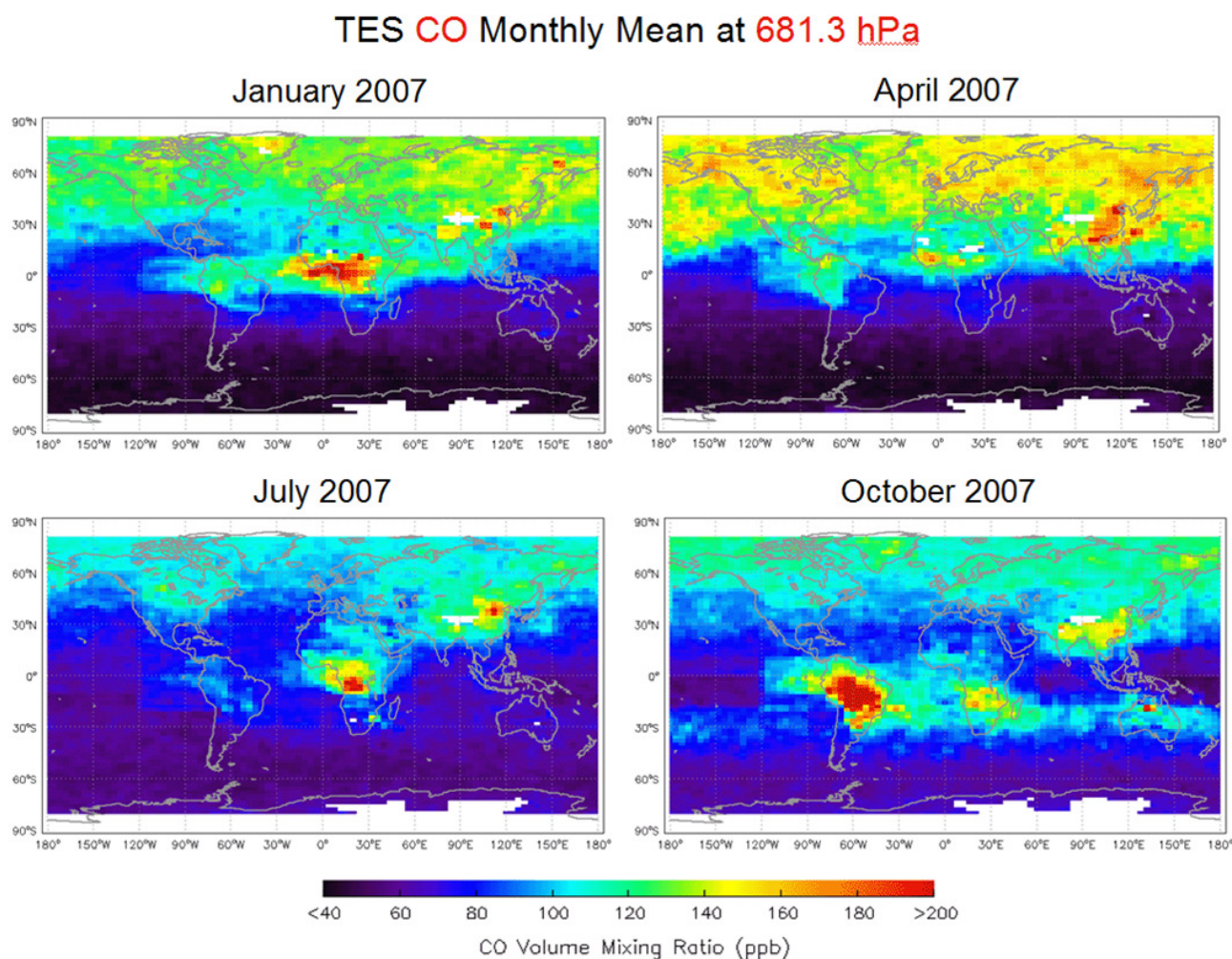


Figure 6-5 TES CO Global Distributions at 681.3 hPa for the Four Typical Months, Jan, April, July, and Oct 2007.

6.6 CO validation: Comparisons to in situ Aircraft Measurement

During the TES mission operation years, several aircraft campaigns were conducted to study tropospheric chemistry and transport, and provide data for validation of the measurements made by the instruments on the Aura satellite. The TES team participated in the Aura Validation Experiment (AVE) campaigns: Oct-Nov 2004 based near Houston, Jan-Feb 2005 based in Portsmouth, NH (PAVE), and in Jan-Feb 2006 based in Costa Rica (CR-AVE). TES also participated in INTEX-B (International Chemical Transport Experiment), which had deployments in Houston, Honolulu and Anchorage in March-May 2006. The TES CO data from the time periods of these campaigns were compared with the in situ measurements for the aircraft flights when there are the best coincidences between TES measurement location and the aircraft CO profiles. Most validation results are reported in papers by M. Luo et al. (2007b) and J. Lopez et al. (2008). Here we give a brief review of the aircraft data validation for previous version TES CO data.

In all aircraft campaigns, TES made a series of step and stare nadir observations with some footprints coinciding with the aircraft tracks and the spiral profiling locations. During the AVE and CR-AVE campaigns, CO was measured by the NASA Ames Research Center Argus instrument on the WB-57 aircraft. The CO profiles were also measured by Aircraft Laser Infrared Absorption Spectrometer (ALIAS) of JPL during CR-AVE. During the INTEX-B campaign the DACOM instrument by the NASA Langley Research Center was on board to measure CO.

For the TES and aircraft CO comparisons, all possible aircraft profiles, including profiles taken while taking-off and landing, and the vertical spirals, are extracted to match with TES profiles closest in times and locations. A few aircraft profiles and ~2-4 TES CO profiles per aircraft profile can be identified per campaign station, normally within a couple of hours and a couple to a few hundred kilometers. The next procedure is to apply TES retrieval operator to the in-situ profile, x_{aircraft} , to obtain the simulated aircraft profile as seen by TES, $x_{\text{simul-aircraft}}$,

$$x_{\text{simul-aircraft}} = Ax_{\text{aircraft}} + (I - A)x_a \quad (\text{Equation 6-1})$$

where x_a is the TES CO retrieval a priori profile from the MOZART model, and A is the averaging kernel. This profile as seen by TES is then compared to the TES retrieved CO profile.

In summary, the averaged comparisons are the best in the Houston region for the two campaigns in Oct 2004 and March 2006. The differences between Argus and TES CO profiles are within TES retrieval errors and equivalent to CO spatial/temporal variability detected in both TES and Argus measurements. The comparisons of TES and DACOM CO profiles near Hawaii and Anchorage in April-May 2006 are not as good. In these regions, the aircraft DACOM CO profiles are characterized by plumes or enhanced CO layers, consistent with known features in the tracer fields due to transpacific transport of polluted air parcels originating from East Asia. In the newer version TES CO comparisons, the effects of a priori should be removed and these conclusions should remain the same.

6.7 CO validation: comparisons to MOZAIC, ACE, MLS, and AIRS data sets

Some preliminary results are obtained in TES CO data validation using the CO data sets of MOZAIC (Measurements of Ozone and water vapor by In-service Airbus aircraft, <http://mozaic.aero.obs-mip.fr>), ACE (Atmospheric Chemistry Experiment), MLS (Microwave Limb Sounder), and AIRS (Atmospheric Infrared Sounder). Detailed results are documented either

in the TES Validation Report (V003) (Osterman et al., 2007) or papers (Rinsland et al., 2008; Warner et al., 2007).

6.8 CO Validation: Comparisons to MOPITT Data

Both TES and MOPITT (Measurements Of Pollution In The Troposphere) have updated CO data products to the new versions (V008 for TES and V008 for MOPITT). The a priori data used by the two teams are from the same MOZART model simulation results. TES uses 10 degree latitude by 60 degree longitude monthly bins of the model data as the a priori. TES also uses the same algorithm as that of MOPITT to compute the constraint matrix used for all profile retrievals (Deeter et al., 2010), e.g., 0.3 diagonals in lnVMR (~30%) and 100 hPa vertical correlation distances. In theory, different a priori or constraints will affect final CO products and to change their global distributions from previous versions, but when proper a priori, averaging kernels, and error estimates are considered in applications, the different version data should be consistent. Here we make comparisons between new versions of TES and MOPITT CO data using the technique that was applied in a previous study (Luo et al., 2007a). We did three TES Global Surveys, Sept 20-21, 2004, the original GS for the publication, a TES GS taken June 5-6, 2009, and a TES GS taken June 6-7, 2010 after the new instrument calibration scheme was adopted.

The retrieval results of TES 16-orbit global survey measurements in Sept 20-21, 2004 (Run ID 2147) have been examined extensively by the TES science team. In CO comparisons, MOPITT data are down-sampled to near the TES geolocations. Figure 6-6 shows TES and down-selected MOPITT CO VMR at 681 hPa and interpolated spatially to illustrate the distribution more clearly. The two CO distribution fields are very similar partially due to the usage of the same a priori. This is an improvement from Luo et al. (2007a) using older versions of TES and MOPITT CO data.

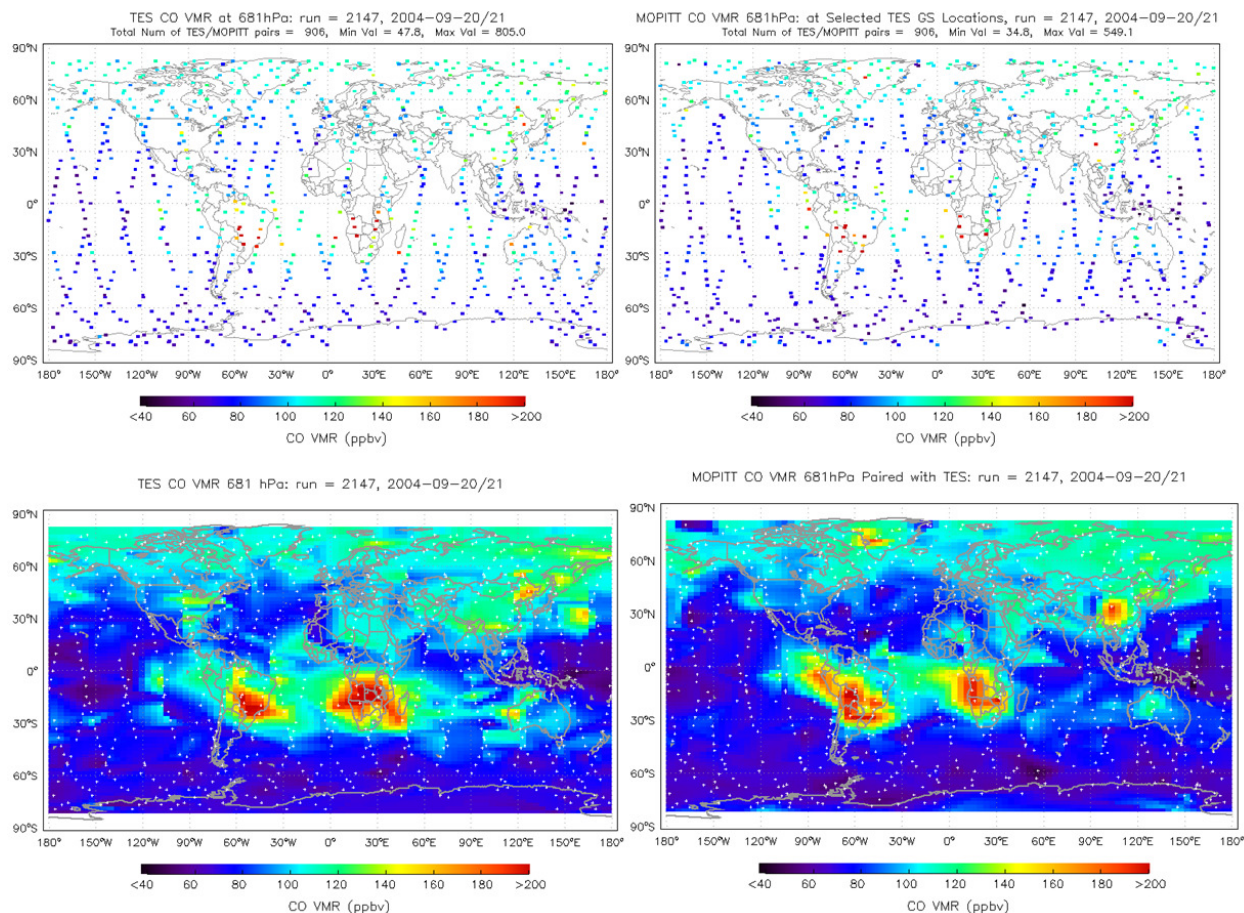


Figure 6-6 TES (left column) and down-sampled MOPITT (right column) CO VMRs at 681 hPa. The corresponding date is one TES Global Survey, Sept 20-21, 2004. Top panels are TES and MOPITT CO VMRs at or near TES geolocations. Bottom panels are horizontally interpolated CO VMR maps with footprints in white dots. TES data version is V008 and MOPITT data is V008 Thermal Infrared (TIR) only.

Quantitative comparisons between TES and MOPITT CO at low, mid and upper troposphere and total column for this day are carried out. Three steps are performed in the comparison, direct comparison, adjusting TES CO profiles to MOPITT a priori profile, and applying TES averaging kernels to MOPITT retrieved profiles. The final comparison is to compare TES retrieved CO profiles adjusted to MOPITT a priori and the MOPITT retrieved CO profiles adjusted to TES averaging kernel. The agreement between the two CO fields becomes better in all tropospheric levels and the total column, especially in the lower and upper troposphere where both instruments do not have much sensitivity in their measurements. Figure 6-7 shows the direct and final comparisons of the CO VMRs at 681 hPa and 215 hPa between TES and MOPITT. The final comparisons show TES CO is slightly higher than that of MOPITT at 681 hPa, and TES CO is slightly lower than that of MOPITT at 215 hPa.

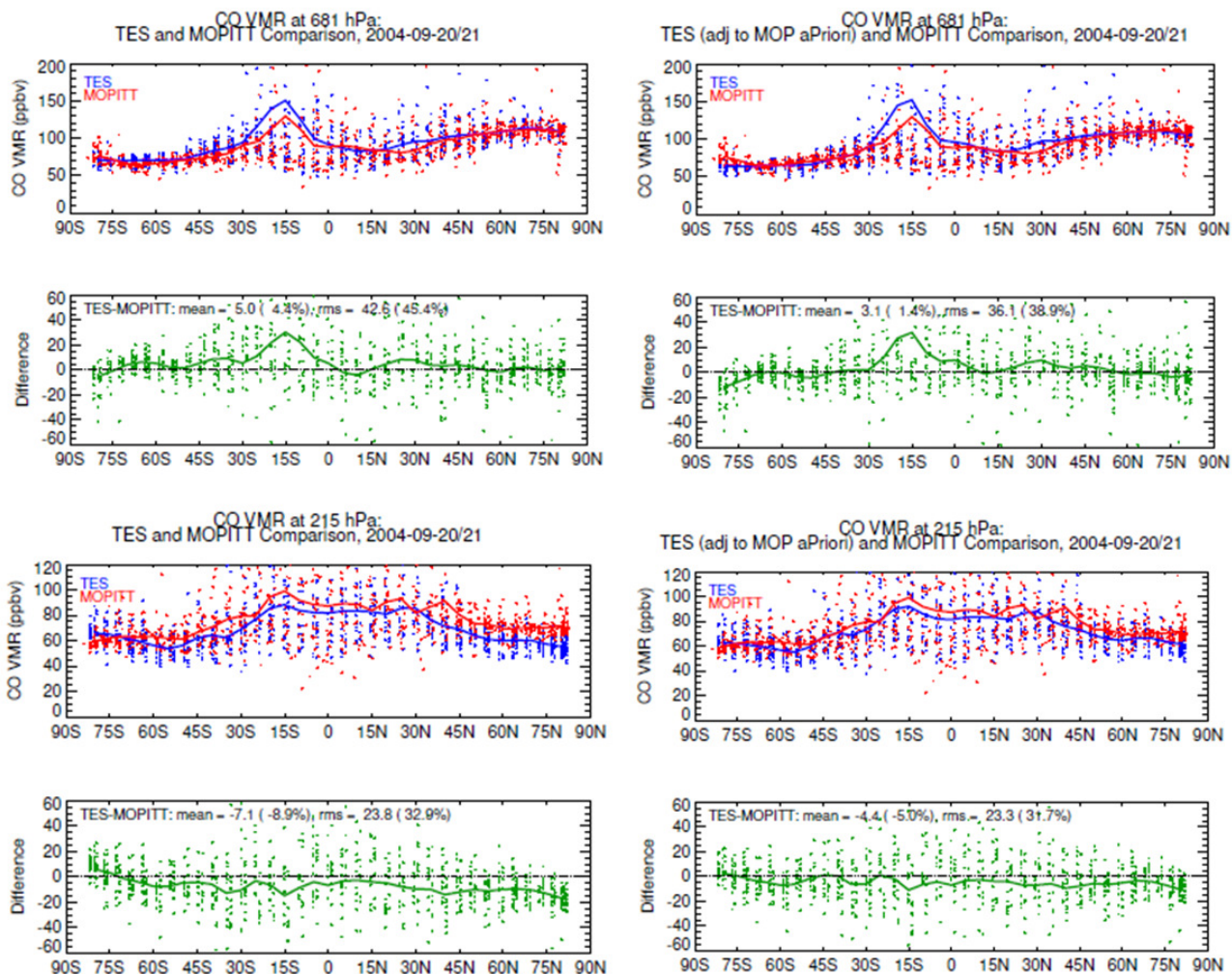


Figure 6-7 Comparisons of CO VMR reported by TES and MOPITT at 681 hPa and 215 hPa respectively. The left panels are the ‘direct’ comparisons. The right panels are the comparisons after the TES CO being adjusted to MOPITT a priori profile and MOPITT CO profiles being adjusted by applying TES averaging kernels (Luo et al., 2007a).

To summarize the comparison results for Sept 20-21, 2004 and two other TES GS periods, three tables (Table 6-1, Table 6-2, and Table 6-3) are used below.

Table 6-1 TES-MOPITT CO comparisons for Sept 20-21, 2004

	681 hPa		215 hPa		Total Column	
	Mean Diff (%)	RMS of Diff (%)	Mean Diff (%)	RMS of Diff (%)	Mean Diff (%)	RMS of Diff (%)
Direct Compare	4.4%	45%	-9%	33%	-1.3%	22%
TES adj to MOP aPriori vs MOP	1.4%	39%	-5%	32%		
TES adj to MOP aPriori vs MOP adj to TES AK	2%	37%	-3.3%	25%		
Mean RMS of MOP in 500km/24hrs of TES location	MOP at 700hPa 12-17% (land) 10-12% (ocean)		MOP at 200hPa 1-15% (land) 2-8% (ocean)			
TES Retrieval Err	10-20%		10-30%		10-30%	
MOP Retrieval Err	25-30%		25-30%		5-12%	

Table 6-2 TES-MOPITT CO comparisons for June 5-6, 2009

	681 hPa		215 hPa		Total Column	
	Mean Diff (%)	RMS of Diff (%)	Mean Diff (%)	RMS of Diff (%)	Mean Diff (%)	RMS of Diff (%)
Direct Compare	2.1%	21%	-8.1%	31%	-1.5%	17%
TES adj to MOP aPriori vs MOP	3%	18%	-4.8%	30%		
TES adj to MOP aPriori vs MOP adj to TES AK	2%	16%	-3%	21%		
Mean RMS of MOP in 500km/24hrs of TES location	700hPa 1-20%		200hPa 1-10%			
TES Retrieval Err	10-20%		8-15%		3-20%	
MOP Retrieval Err	25-30%		20-30%		3-15%	

Table 6-3 TES-MOPITT CO comparisons for June 6-7, 2010

	681 hPa		215 hPa		Total Column	
	Mean Diff (%)	RMS of Diff (%)	Mean Diff (%)	RMS of Diff (%)	Mean Diff (%)	RMS of Diff (%)
Direct Compare	2.6%	25%	-7.5%	33%	-0.7%	19%
TES adj to MOP aPriori vs MOP	4.1%	21%	-5.4%	32%		
TES adj to MOP aPriori vs MOP adj to TES AK	3.6%	18%	-2.8%	23%		
Mean RMS of MOP in 500km/24hrs of TES location	700hPa 10-20%		200hPa 10-25%			
TES Retrieval Err	10-20%		8-15%		8-15%	
MOP Retrieval Err	25-30%		20-30%		5-10%	

In all comparisons, the RMS (root-mean-square) of the TES-MOPITT differences are seen reducing from direct comparisons to the comparisons with slight differences in a priori and averaging kernels considered as described in Luo et al. (2007a). For TES GS run2147, Sept 20-21, 2004 in Table 6-1, the comparison conclusions are similar to that of Luo et al. (2007a) made for TES and MOPITT earlier version data. When separating ocean from land scenes, we see that the mean differences and the RMSs between TES and MOPITT data on all levels agree better over ocean scenes. Here we add the calculation of the variability (RMS) of MOPITT CO within 500km/24hrs of TES location and time. This number indicates that the comparison RMS can partially be explained by the miss-matches between the two instruments in space and time. We also listed estimated retrieval errors by the two instrument teams that also contribute to the explanations of the final RMS in the differences. We notice that in average, TES CO is less than 5% higher in the lower troposphere (681 hPa) while TES CO is less than 5% lower in the upper troposphere (215 hPa) comparing to MOPITT CO.

6.9 CO validation: summary

Carbon Monoxide: TES final version V08 CO retrievals are almost identical to that of V07 in the troposphere. Comparisons have been carried out between TES carbon monoxide retrievals and those from a variety of satellite and aircraft instruments. Global patterns of carbon monoxide as measured by TES are in good qualitative agreement with those seen by MOPITT on the NASA Terra satellite. Comparisons of profiles of CO between TES and MOPITT show better agreement when a priori information is accounted for correctly. TES carbon monoxide agrees to within the estimated uncertainty of the aircraft instruments, including both errors and the variability of CO itself. This is also reflected in TES-MOPITT comparisons. The global averaged TES V08 CO agree with that of MOPITT V08 CO within 5%, with the lower-troposphere being slightly lower and upper-troposphere being slightly higher.

6.10 References

6.10.1 TES Carbon Monoxide References

- [1] Deeter, M.N., D.P. Edwards, J.C. Gille, L.K. Emmons, G. Francis, S.-P. Ho, D. Mao, D. Masters, H. Worden, James R. Drummond, and Paul C. Novelli (2010), The MOPITT version 4 CO product: Algorithm enhancements, validation, and long-term stability, *J. Geophys. Res.: Atmospheres*, Vol. 115 Issue D7, D07306, doi:10.1029/2009JD013005, April 15, 2010.
- [2] Lopez, J.P., M. Luo, L.E. Christensen, M. Loewenstein, H. Jost, C.R. Webster, and G. Osterman (2008), TES carbon monoxide validation during two AVE campaigns using the Argus and ALIAS instruments on NASA's WB-57F, *Journal of Geophysical Research*, Vol. 113, D16S47, (doi:10.1029/2007JD008811) August 2, 2008.
- [3] Luo, M., C.P. Rinsland, C.D. Rodgers, J.A. Logan, H. Worden, S. Kulawik, A. Eldering, A. Goldman, M.W. Shephard, M. Gunson, and M. Lampel (2007a), Comparison of carbon monoxide measurements by TES and MOPITT: the influence of a priori data and instrument characteristics on nadir atmospheric species retrievals, *J. Geophys. Res.*, 112, D09303, (doi:10.1029/2006JD007663) May 3, 2007a.
- [4] Luo, M., C. Rinsland, B. Fisher, G. Sachse, G. Diskin, J. Logan, H. Worden, S. Kulawik, G. Osterman, A. Eldering, R. Herman and M. Shephard (2007b), TES carbon monoxide validation with DACOM aircraft measurements during INTEX-B 2006, *J. Geophys. Res.*, 112, D24S48, (doi:10.1029/2007JD008803) December 20, 2007b.
- [5] Osterman, G., (editor), K. Bowman, K. Cady-Pereira, T. Clough, A. Eldering, B. Fisher, R. Herman, D. Jacob, L. Jourdain, S. Kulawik, M. Lampel, Q. Li, J. Logan, M. Luo, I. Megretskaia, R. Nassar, G. Osterman, S. Paradise, V. Payne, H. Revercomb., N. Richards, M. Shephard, D. Tobin, S. Turquety, F. Vilnrotter, H. Worden, J. Worden, and L. Zhang (2007), Earth Observing System (EOS) Tropospheric Emission Spectrometer (TES) Data Validation Report (Version F04_04 data), Version 3.0, JPL Internal Report D-33192, November 5, 2007.
- [6] Rinsland, C.P., M. Luo, J.A. Logan, R. Beer, H.M. Worden, J.R. Worden, K. Bowman, S.S. Kulawik, D. Rider, G. Osterman, M. Gunson, A. Goldman, M. Shephard, S.A. Clough, C. Rodgers, M. Lampel, and L. Chiou (2006), Nadir Measurements of carbon monoxide distributions by the Tropospheric Emission Spectrometer onboard the Aura Spacecraft: Overview of analysis approach and examples of initial results, *Geophys. Res. Lett.*, 33, (L2280610.1029/2006GL027000) November 22, 2006.
- [7] Rinsland, C.P., M Luo, M.W. Shephard, C. Clerbaux, C.D. Boone, P.F. Bernath, L. Chiou, and P.F. Coheur (2008), Tropospheric Emission Spectrometer (TES) and atmospheric chemistry experiment (ACE) measurements of tropospheric chemistry in tropical southeast Asia during a moderate El Niño in 2006, *Journal of Quantitative Spectroscopy and Radiative Transfer*, Vol. 109, Issue 10, pp. 1931-1942, July, 2008, <http://dx.doi.org/10.1016/j.jqsrt.2007.12.020>.
- [8] Warner, J.X., Z. Sun, A. Tangborn, C. Barnett, M. Luo, D. Glenn (2007), Improved Tropospheric Carbon Monoxide Profiles Using AIRS and TES Measurements, *Eos Trans. AGU (American Geophysical Union)*, 88(52), 2007 Fall Meeting Suppl., Abstract A52D-07. <https://abstractsearch.agu.org/meetings/2007/FM/A52D-07.html>

7. Validation of TES nadir Temperature Retrievals with Radiosondes

7.1 Executive Summary

TES V008 nadir temperature (TATM) retrievals have been compared with nearly coincident radiosonde measurements from the NOAA ESRL global radiosonde database. Generally, V008 TATM is very similar to the previous V007 data.

To evaluate the retrieval stability, the monthly mean and standard deviation of the TATM residual between TES V005 and the Global Modeling and Data Assimilation Office (GMAO) GEOS-5.2 model, which provides the first guess and a priori for the TATM retrieval, were calculated. The statistics for both Tropical Pacific and Northern Atlantic Ocean regions indicate only minor month-to-month variability and no substantial trends over the entire five-and-a-half-year period. The standard deviation of the residual was generally smaller than the standard deviation of the GMAO GEOS-5.2 but larger than the TES estimated measurement error. Overall, based on this analysis it appears that the TES retrieval quality has remained stable over the years inspected, 2006 through 2011.

7.2 Details of TES V008 TATM retrieval

For V008 TATM, there are two retrieval steps. First, for latitudes between 40° S and 40° N, there is a simultaneous retrieval of TATM, O₃, and CO₂. Second, there is a sequential retrieval of TATM using the 2B1 filter. The microwindows selected for temperature retrieval are within the CO₂ ν_2 band, spanning 671.32 to 901.48 cm⁻¹ (14.896 μ m to 11.093 μ m wavelength). Constraints are altitude-dependent Tikhonov constraints (Kulawik et al., 2006). Changes in V008 compared to V007 are due to updated CO₂ and H₂O spectroscopy in ABSCO v3.0 tables, which are based on the tes_v2.0 line file and the Line-by-Line Radiative Transfer Model (LBLRTM) v12.4.

The TES level 2 retrieval processes use a CO₂ climatology that incorporates improved seasonal and geographic variations in CO₂, as well as scaling to account for the annual increase in global CO₂ levels. This is highly relevant to temperature retrievals from the CO₂ ν_2 band because inaccurate assumptions about atmospheric CO₂ concentrations may lead to significant errors in atmospheric temperature retrievals, up to 0.5 K (see Figure 14 of Divakarla et al., 2006). The climatology is based on model results for the year 2004 from a chemical transport model (CTM) used in conjunction with a variety of other models to provide CO₂ surface fluxes (David Baker, pers. comm.). The CTM used to create the time-varying three-dimensional CO₂ fields (longitude, latitude and pressure) is the Model of Atmospheric Transport and Chemistry (MATCH) (Nevison et al., 2008). Key surface CO₂ fluxes are derived from models including biospheric fluxes from the Carnegie Ames Stanford Approach (CASA) land biosphere model, oceanic fluxes from the WHOI model and a realistic, annually-varying fossil fuel source scheme (Nevison et al., 2008). The CO₂ fields generated by the model compare well to GLOBALVIEW atmospheric CO₂ data. Model results were provided to the TES team for the year 2004. Monthly mean profiles were calculated for two longitude bins and 10-degree latitude bins. This binned monthly mean climatology for 2004 was then scaled upward yearly (by 1.0055) to match the annual increase in CO₂.

7.3 A priori constraint vector

For each individual sequence and scan, the initial guess in the TES retrieval algorithm is set equal to an a priori profile (constraint vector). The TES V008 a priori constraint vectors come from

NASA's Goddard Earth Observing System (GEOS) data assimilation system GEOS-5 (Rienecker et al., 2008). What is new in TES V008 is that the temperature initial guess and constraint comes from GEOS-5.12.4. GEOS-5 data are produced by the Global Modeling and Assimilation Office (GMAO) at the NASA Goddard Space Flight Center (GSFC) on a 0.625° longitude by 0.5° latitude grid. GEOS-5 data are then interpolated to the locations and pressure levels of TES retrievals. The a priori covariance matrices used for retrieval regularization are described in Bowman et al. (2006). GEOS-5 assimilates a wide range of operational satellite data and in situ radiosonde measurements. Radiosonde profiles are strong constraints on the thermal structure and winds throughout the troposphere, with an emphasis on continental regions where the observing network is denser. Space-based observations include the High Resolution Infrared Sounders (HIRS) and Advanced Microwave Sounders (AMSU) instruments on NOAA's operational sounders, which directly constrain temperature and moisture. GEOS-5 includes a direct assimilation of radiances from AMSU and HIRS in a three-dimensional variational assimilation, as well as radiances from the Advanced Infrared Sounder (AIRS) and AMSU instruments on NASA's EOS Aqua platform (Zhu and Gelaro, 2008).

7.4 Validation Status of V008 nadir temperature

This section summarizes the latest validation comparisons for V008 TES nadir TATM retrievals. TES retrievals have been filtered by the master quality flag (see TES Data Users Guide, Herman and Kulawik, 2013). The TES observation operator has been applied to the radiosonde profiles, and differences are shown as TATM minus $T_{\text{radiosonde}}$ (with averaging kernel). Levels where TES has no sensitivity to temperature (i.e., where the sum of the row of the averaging kernel equals zero) are not included in the calculation of the mean difference.

The TES V008 TATM retrievals are compared with a global radiosonde database from the National Oceanic and Atmospheric Administration (NOAA) Earth System Research Laboratory (ESRL) Global Systems Division (https://ruc.noaa.gov/raobs/General_Information.html, M. Govett, pers. comm.). The advantage of this database is that it includes the exact radiosonde release time, which improves the temporal coincidence between TES and radiosonde, and the temperature rms. The NOAA ESRL database combines the Integrated Global Radiosonde Archive (IGRA) data with North American Global Telecommunications Service (GTS) radiosonde data. Both undergo extensive checks for errors and hydrostatic consistency.

TES global surveys from 2005-2009 are matched with radiosonde profiles from the NOAA ESRL database within 100 km and -0.5 hr to +1.5 hr. The tightly constrained time match is possible because the exact radiosonde release time is known. Times are offset so that, on average, the radiosonde has ascended to the middle troposphere by the time of the Aura overpass and TES retrieval.

Figure 7-1 shows comparisons of TES V008 TATM with NOAA ESRL radiosondes. The solid red line is the temperature bias (TES TATM minus $T_{\text{radiosonde}}$ with averaging kernel) and the dashed red line is the temperature rms. For TES V008 TATM minus $T_{\text{radiosonde}}$ (with averaging kernel applied), TES is biased 1 K high in the lower troposphere, decreasing to -1 K in the upper troposphere. The rms is less than 1 K in the stratosphere and upper troposphere, increasing to 2 K in the lower troposphere.

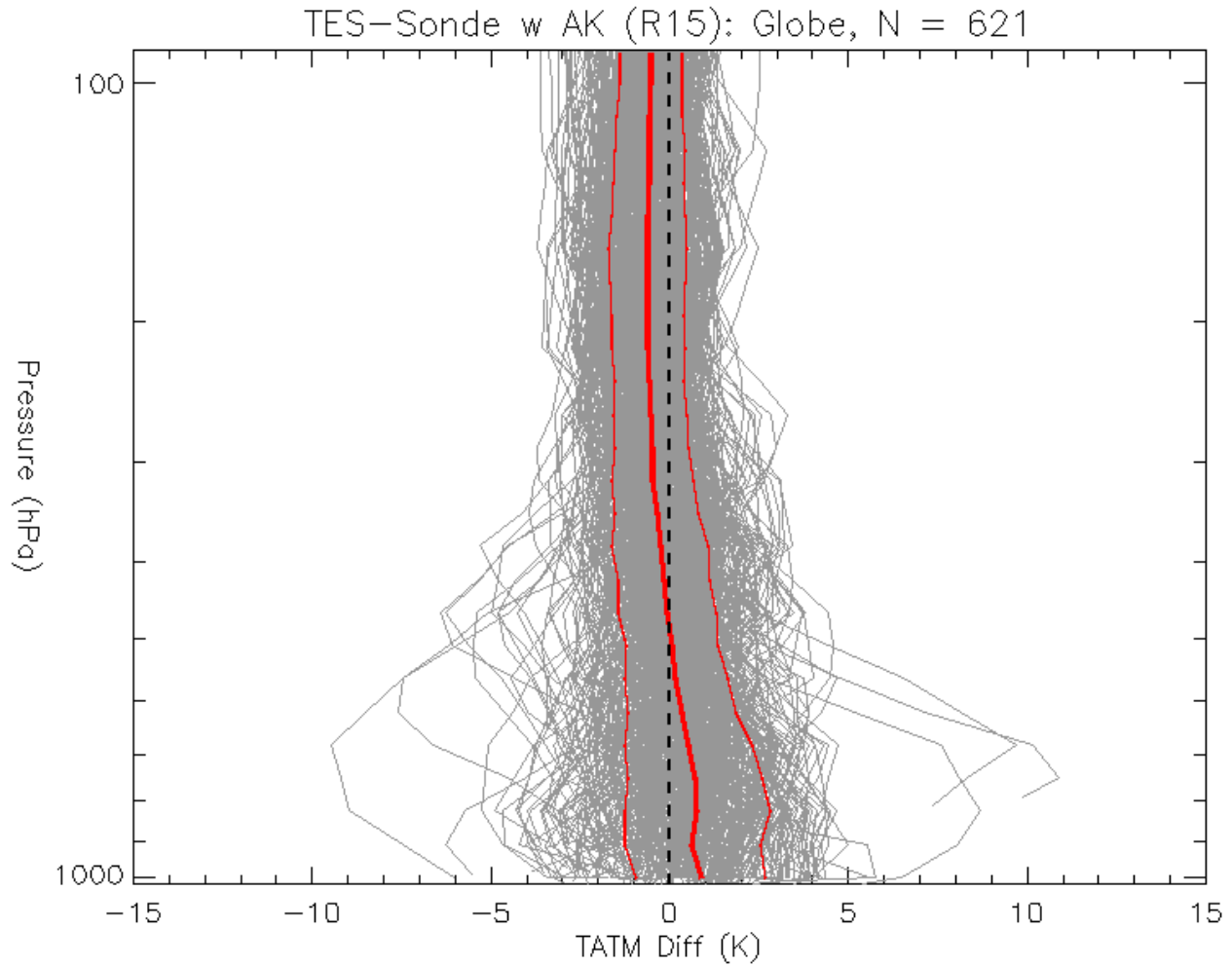


Figure 7-1 Temperature differences between TES V008 TATM and NOAA ESRL radiosondes with observation operator applied: (left) all good quality comparisons, (right) comparisons filtered by average cloud effective optical depth < 0.1 . Shown are individual temperature differences (thin grey lines), bias (solid red line), rms (dashed red line), and the TES observation error (solid blue line).

7.5 Comparison of TES V008 nadir temperature with V007 nadir temperature

For one TES Global Survey run id 2147 (September 20 to September 21, 2004), TES retrievals of V008 TATM have been compared to V007 TATM. In a direct comparison, individual TATM measurements differ, but the mean differences are very small. Figure 7-2 shows that for this global survey, the mean difference between V008 and V007 TATM is 0.04 K at 681.3 hPa in the lower troposphere, and -0.08 K at 215.4 hPa in the upper troposphere.

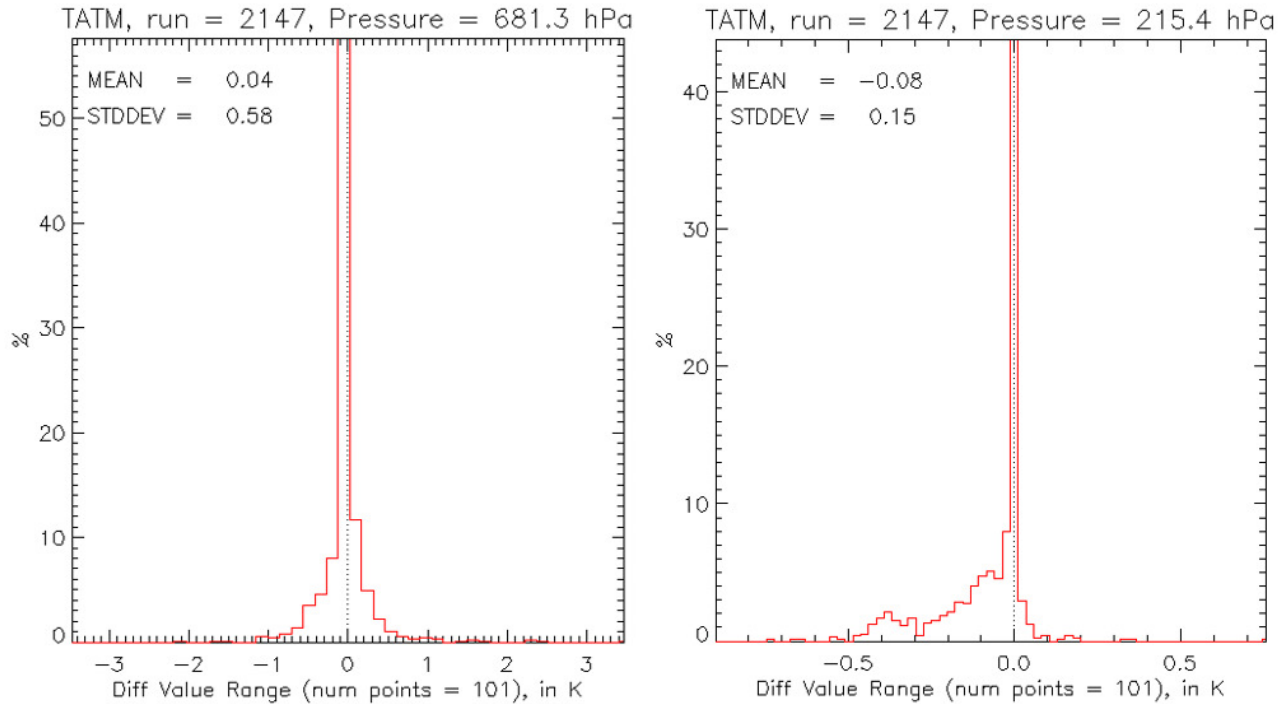


Figure 7-2 Histogram of nadir temperature differences between TES V008 and V007 retrievals for TES Global Survey run id 2147 at (left) the 681.3 hPa pressure level and (right) 215.4 hPa pressure level. Figure prepared by Ming Luo using code developed by Mark Montero.

7.6 TES Temperature Retrieval Stability 2006-2011

A recent design file memorandum (DFM A&M 838) by J. Hegarty et al. (2012) presented an analysis of TES TATM retrieval stability over the lifetime of the TES instrument. Overall, based on that analysis it appears that the TES retrieval quality has remained stable from 2006 - 2011.

7.7 References

7.7.1 TES Temperature References

- [1] Hegarty, J., S.S. Kulawik, V.H. Payne, K.E. Cady-Pereira, TES Temperature Retrieval Stability 2006-2011, TES internal DFM A&M 838, 2012.

7.7.2 TES References

- [2] Bowman, K. W., J. Worden, T. Steck, H. M. Worden, S. Clough, and C. Rodgers (2002), Capturing time and vertical variability of tropospheric ozone: A study using TES nadir retrievals, *J. Geophys. Res.*, *107*, No. D23, 4723, (doi:10.1029/2002JD002150) December 14, 2002.
- [3] Bowman, K. W., C. D. Rodgers, S. S. Kulawik, J. Worden, E. Sarkissian, G. Osterman, T. Steck, M. Luo, A. Eldering, M. W. Shephard, H. Worden, M. Lampel, S. A. Clough, P. Brown, C. Rinsland, M. Gunson, R. Beer (2006), Tropospheric emission spectrometer:

- Retrieval method and error analysis, *IEEE Trans. Geosci. Remote Sens.*, 44(5), 1297-1307, May 2006.
- [4] Connor, T.C., M.W. Shephard, V.H. Payne, K.E. Cady-Pereira, S.S. Kulawik, M. Luo, G. Osterman, M. Lampel (2011), Long-term stability of TES satellite radiance measurements, *Atmospheric Measurement Techniques*, 4, doi:10.5194/amt-4-1481-2011, 1481–1490, July 25, 2011.
- [5] Herman, Robert and Susan Kulawik (editors), Kevin Bowman, Karen Cady-Pereira, Annmarie Eldering, Brendan Fisher, Dejian Fu, Robert Herman, Daniel Jacob, Line Jourdain, Susan Kulawik, Ming Luo, Ruth Monarrez, Gregory Osterman, Susan Paradise, Vivienne Payne, Sassaneh Poosti, Nigel Richards, David Rider, Douglas Shepard, Mark Shephard, Felicia Vlnrotter, Helen Worden, John Worden, Hyejung Yun, Lin Zhang (2018), Earth Observing System (EOS) Tropospheric Emission Spectrometer (TES) Level 2 (L2) Data User's Guide (Up to & including Version 7 data), Version 7.0, JPL Internal Report D-38042, September 27, 2018.
- [6] Herman, Robert and Gregory Osterman (editors), Christopher Boxe, Kevin Bowman, Karen Cady-Pereira, Tony Clough, Annmarie Eldering, Brendan Fisher, Dejian Fu, Robert Herman, Daniel Jacob, Line Jourdain, Susan Kulawik, Michael Lampel, Qinbin Li, Jennifer Logan, Ming Luo, Inna Megretskaja, Ray Nassar, Gregory Osterman, Susan Paradise, Vivienne Payne, Hank Revercomb, Nigel Richards, Mark Shephard, Dave Tobin, Solene Turquety, Felicia Vlnrotter, Kevin Wecht, Helen Worden, John Worden, Lin Zhang (2012), Earth Observing System (EOS) Tropospheric Emission Spectrometer (TES) Data Validation Report (Version F06_08, F06_09 data), Version 5.0, JPL Internal Report D-33192, April 8, 2012.
- [7] Kulawik, S. S., G. B. Osterman, D. B. A. Jones, and K. W. Bowman (2006), Calculation of Altitude-Dependent Tikhonov Constraints for TES Nadir Retrievals, *IEEE Transactions on Geoscience and Remote Sensing*, 44 (No.5), Special Issue on Aura, 1334-1342, May 2006.
- [8] Nassar, R., J.A. Logan, H.M. Worden, I.A. Megretskaja, K.W. Bowman, G.B. Osterman, A.M. Thompson, D.W. Tarasick, S. Austin, H. Claude, M.K. Dubey, W.K. Hocking, B.J. Johnson, E. Joseph, J. Merrill, G.A. Morris, M. Newchurch, S.J. Oltmans, F. Posny, F.J. Schmidlin, H. Vömel, D.N. Whiteman, J.C. Witte (2008), Validation of Tropospheric Emission Spectrometer (TES) Nadir Ozone Profiles Using Ozone Sonde Measurements, *J. Geophys. Res.* 113, D15S17, (doi:10.1029/2007JD008819), May 7, 2008.
- [9] Osterman, G., S.S. Kulawik, H.M. Worden, N.A.D. Richards, B.M. Fisher, A. Eldering, M.W. Shephard, L. Froidevaux, G. Labow, M. Luo, R.L. Herman, K.W. Bowman, A.M. Thompson (2008), Validation of Tropospheric Emission Spectrometer (TES) Measurements of the Total, Stratospheric and Tropospheric Column Abundance of Ozone, *J. Geophys. Res.*, 113, D15S16, (doi:10.1029/2007JD008801) May 7, 2008.
- [10] Osterman, G. B. (editor), K. Bowman, K. Cady-Pereira, T. Clough, A. Eldering, B. Fisher, R. Herman, D. Jacob, L. Jourdain, S. Kulawik, M. Lampel, Q. Li, J. Logan, M. Luo, I. Megretskaja, R. Nassar, G. Osterman, S. Paradise, V. Payne, H. Revercomb., N. Richards, M. Shephard, D. Tobin, S. Turquety, F. Vlnrotter, H. Worden, J. Worden, and L. Zhang (2007), Earth Observing System (EOS) Tropospheric Emission Spectrometer

(TES) Data Validation Report (Version F04_04 data), Version 3.0, JPL Internal Report D-33192, November 5, 2007, available at:

<https://eosweb.larc.nasa.gov/project/tes/validation>

- [11] Richards, N.A.D., G.B. Osterman, E.V. Browell, J.W. Hair, M. Avery and Q.Li, Validation of Tropospheric Emission Spectrometer ozone profiles with aircraft observations during the Intercontinental Chemical Transport Experiment–B, *J. Geophys. Res.*, *113*, D16S29, (doi:10.1029/2007JD008815) May 23, 2008.
- [12] Worden, J., S. S. Kulawik, M. W. Shephard, S. A. Clough, H. Worden, K. Bowman, and A. Goldman (2004), Predicted errors of tropospheric emission spectrometer nadir retrievals from spectral window selection, *J. Geophys. Res.*, *109*, D09308, May 15, 2004.

7.7.3 General References

- [13] Bloom, S., A. da Silva, D. Dee, M. Bosilovich, J.-D. Chern, S. Pawson, S. Schubert, M. Sienkiewicz, I. Stajner, W.-W. Tan, M.-L. Wu (2005). Documentation and Validation of the Goddard Earth Observing System (GEOS) Data Assimilation System - Version 4. *Technical Report Series on Global Modeling and Data Assimilation 104606, Vol. 26*, 187 pages, April 2005. Available from (paste entire link including pdf into browser):
http://ntrs.nasa.gov/archive/nasa/casi.ntrs.nasa.gov/20050175690_2005173043.pdf.
- [14] Divakarla, M. G., C. D. Barnet, M. D. Goldberg, L. M. McMillin, E. Maddy, W. Wolf, L. Zhou, and X. Liu (2006), Validation of Atmospheric Infrared Sounder temperature and water vapor retrievals with matched radiosonde measurements and forecasts, *J. Geophys. Res.*, *111*, D09S15, (doi: 10.1029/2005JD006116) April 6, 2006.
- [15] Nevison, C. D., N. M. Mahowald, S. C. Doney, I. D. Lima, G. R. van der Werf, J. T. Randerson, D. F. Baker, P. Kasibhatla, and G. A. McKinley (2008), Contribution of ocean, fossil fuel, land biosphere and biomass burning carbon fluxes to seasonal and interannual variability in atmospheric CO₂, *J. Geophys. Res.*, *113*, G01010, (doi:10.1029/2007JG000408) February 12, 2008.
- [16] Rienecker, M. M., M. J. Suarez (editor), R. Todling, J. Bacmeister, L. Takacs, H.-C. Liu, W. Gu, M. Sienkiewicz, R. D. Koster, R. Gelaro, I. Stajner and J.E. Nielson (2008), The GEOS-5 Data Assimilation System- Documentation of Versions 5.0.1, 5.1.0, and 5.2.0 *NASA Technical Report Series on Global Modeling and Data Assimilation 104606, Vol.27.*, December 2008.
- [17] Tobin, D. C., H. E. Revercomb, R. O. Knuteson, B. M. Lesht, L. L. Strow, S. E. Hannon, W. F. Felt, L. A. Moy, E. J. Fetzer, and T. S. Cress (2006), Atmospheric Radiation Measurement site atmospheric state best estimates for Atmospheric Infrared Sounder temperature and water vapor retrieval validation, *J. Geophys. Res.*, *111*, doi: 10.1029/2005JD006103.
- [18] Zhu, Y., and R. Gelaro (2008), Observation Sensitivity Calculations Using the Adjoint of the Gridpoint Statistical Interpolation (GSI) Analysis System, *Monthly Weather Review, Volume 136, Issue 1*, pp. 335-351, (DOI:10.1175/MWR3525.1) January 2008 – follow link at https://gmao.gsfc.nasa.gov/GEOS_systems/geos5/index_pubs.php

8. Sea Surface Temperature

TES retrievals of sea surface temperature rely on validation of previous data versions, as described in detail in the TES Validation Report V003 (Osterman et al., 2007). V003 sea surface temperature (SST) was compared with Reynolds Optimally Interpolated (ROI) weekly SST for the time period Jan 2005 through July 2008. In clear sky conditions, TES SST versus ROI has a bias of -0.04 K (daytime) and -0.20 K (nighttime). The day/night difference is within the uncertainty of the predicted value based on ocean skin versus ocean bulk SST [D. Kerola, pers. comm.].

8.1 References

8.1.1 TES References

- [1] Osterman, G., (editor), K. Bowman, K. Cady-Pereira, T. Clough, A. Eldering, B. Fisher, R. Herman, D. Jacob, L. Jourdain, S. Kulawik, M. Lampel, Q. Li, J. Logan, M. Luo, I. Megretskiaia, R. Nassar, G. Osterman, S. Paradise, V. Payne, H. Revercomb., N. Richards, M. Shephard, D. Tobin, S. Turquety, F. Vilnrotter, H. Worden, J. Worden, and L. Zhang (2007), Earth Observing System (EOS) Tropospheric Emission Spectrometer (TES) Data Validation Report (Version F04_04 data), Version 3.0, JPL Internal Report D-33192, November 5, 2007

9. Water Vapor

The main objectives for obtaining retrieved water vapor from TES are to measure the isotopic ratio of HDO/H₂O and to obtain the most likely state of the atmosphere within the field-of-view. This applies whether water vapor is a tracer of air mass, of chemical interest, or whether it is an interferent. TES V008 H₂O has been compared with V007 H₂O. More than most species retrieved by TES, tropospheric water vapor is highly variable over short distances. Therefore, the key to water validation is to perform statistics on large datasets to determine possible biases. Once more V008 runs have been processed, the H₂O validation comparisons will be rerun with a large set of radiosondes for comparison.

9.1 Executive Summary

TES V008 H₂O has been compared to V007 H₂O. Individual retrievals show insignificant differences between V008 and V007: these changes are largely due to updated spectroscopy. Compared to radiosondes, TES V008 has a dry bias of 0% to -13% in the lower troposphere. The user should select data using the master data quality flag ("speciesretrievalquality"=1) and filter by degreesoffreedomforsignal (DOFS) greater than 2.

9.2 Background and Recommendation

TES uses an optimal estimation non-linear least squares retrieval (Bowman et al., 2006). All TES versions since V005 use a wide band retrieval (1100 to 1330 cm⁻¹) to jointly estimate the mixing ratios of four species: HDO, H₂O, CH₄, and N₂O (Worden et al., 2012). This retrieval dramatically improves the vertical resolution in the lower troposphere for water vapor, compared to V004. Changes in V008 compared to V007 are due to new ABSCO v3.0 tables, which are based on the tes_v2.0 line file and LBLRTM v12.4. TES V008 H₂O retrievals have degreesoffreedomforsignal (DOFS) that vary by latitude, from 2.5 in the polar regions to 6 in the tropics. The user is recommended to select H₂O data using the master data quality flag ("speciesretrievalquality"=1) and filter by degreesoffreedomforsignal (DOFS) greater than 2.

9.3 A priori constraint vector

For each individual sequence and scan, the initial guess in the TES retrieval algorithm is set equal to an a priori profile (constraint vector). The TES V008 a priori constraint vectors come from NASA's Goddard Earth Observing System (GEOS) data assimilation system GEOS-5 (Rienecker et al., 2008). The a priori constraint comes from the new GMAO GEOS version 5.12.4 processing stream. GEOS-5 data are produced by the Global Modeling and Assimilation Office (GMAO) at the NASA Goddard Space Flight Center (GSFC), on a 0.625° longitude by 0.5° latitude grid. GEOS-5 data are then interpolated to the locations and pressure levels of TES retrievals. The a priori covariance matrices used for retrieval regularization are described in Bowman et al. (2006). GEOS-5 assimilates a wide range of operational satellite data and in situ radiosonde measurements. Radiosonde profiles are strong constraints on the thermal structure and winds throughout the troposphere, with an emphasis on continental regions where the observing network is denser. Space-based observations include the High Resolution Infrared Sounders (HIRS) and Advanced Microwave Sounders (AMSU) instruments on NOAA's operational sounders, which directly constrain temperature and moisture. GEOS-5 includes a direct assimilation of radiances from AMSU and HIRS in a three-dimensional variational assimilation, as well as radiances from

the Advanced Infrared Sounder (AIRS) and AMSU instruments on NASA's EOS Aqua platform (Zhu and Gelaro, 2008).

9.4 Comparison of TES V008 Water Vapor with in situ Radiosondes

Radiosonde data come from a global database from the National Oceanic and Atmospheric Administration (NOAA) Earth System Research Laboratory (ESRL) Global Systems Division [https://ruc.noaa.gov/raobs/General_Information.html, M. Govett, pers. comm.]. The NOAA ESRL database combines the Integrated Global Radiosonde Archive (IGRA) global data with the North American Global Telecommunications Service (GTS) radiosonde data. This merged database features the exact radiosonde launch time, which improves the temporal coincidence between TES and radiosonde significantly. The disadvantage of radiosondes is the spatial mismatch between the satellite retrieval footprint (8 km by 5 km for TES) and the radiosonde data (a vertical profile of in situ measurements with no horizontal information). Coincidence constraints are TES-radiosonde matches within 100 km and -0.5 hours to +1.5 hours. The tightly constrained time match is possible because the exact launch time of the radiosonde is known. Times are offset so that, on average, the radiosonde has ascended to the middle troposphere by the time of the Aura overpass and TES retrieval. The TES observation operator (averaging kernel) and the master data quality flag ("speciesretrievalquality"=1) have been applied to the radiosonde profiles.

Figure 9-1 below shows the comparison between TES V008 water vapor and radiosondes. Most of the matches are in the Arctic (56 to 90 N) and the Northern midlatitudes (35 to 56 N). In the Arctic, 293 TES-radiosonde matches indicate that TES has a dry bias of -4% to -12% in the lower troposphere and RMS of approximately 30%. The lower troposphere is where TES has greatest sensitivity to H₂O/H₂O. TES has a greater dry bias in the upper troposphere, altitudes less relevant to H₂O/H₂O. In Northern midlatitudes, 279 matches indicate a TES dry bias of 0 to -13% and 40% RMS, and a smaller upper tropospheric dry bias. These TES V008 versus radiosonde results are nearly indistinguishable from TES V007 versus radiosonde results.

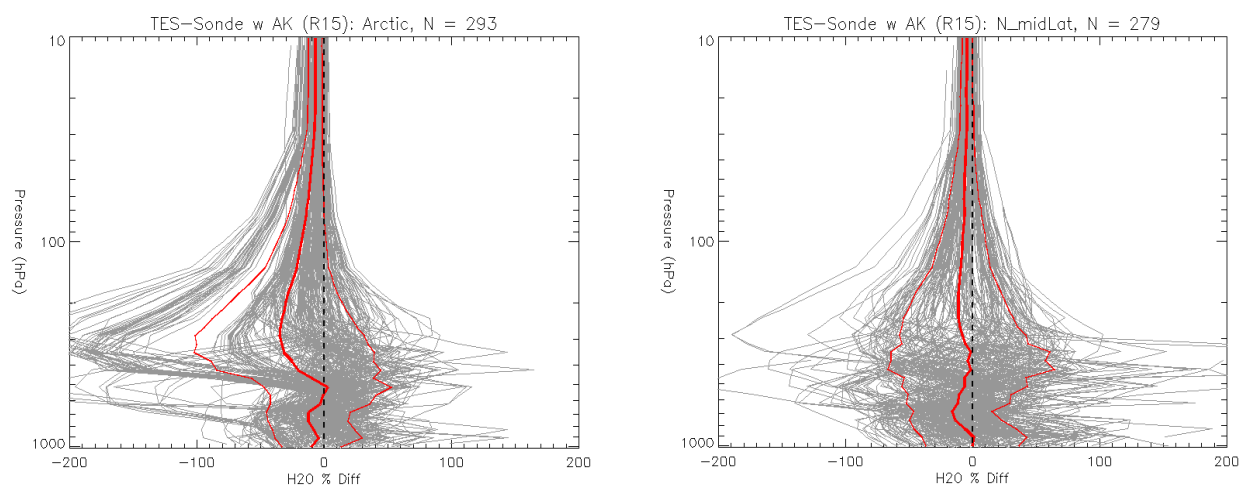


Figure 9-1 Water vapor percent differences between TES V008 retrievals and radiosondes (with averaging kernel applied) from the NOAA ESRL database for two latitude ranges, the Arctic (left) and Northern midlatitudes (right). Matches are selected for TES geolocation coincidence within 100 km distance and -0.5 to +1.5 hours of radiosonde launch time. In each panel, N individual

matches are shown (thin grey lines) with bias (thick red line) and bias \pm rms (thin red lines). Percent differences are calculated as $100(\text{TES}-\text{radiosonde})/\text{TES}$. Figure prepared by Ming Luo.

9.5 Comparison of TES V008 Water Vapor with V007 Water Vapor

For one TES Global Survey run id 2147 (September 20 to September 21, 2004), TES retrievals of V008 H₂O have been compared to V007 H₂O. In a direct comparison, individual water vapor measurements differ, but the mean differences are small. As shown below in Figure 9-2 the mean difference of V008 and V007 H₂O at 681.3 hPa is -0.15% with a standard deviation of 7.21%. In the upper troposphere, the mean difference of V008 and V007 H₂O at 215.4 hPa is -0.57% with a standard deviation of 2.81%. TES has greater sensitivity to water vapor in the lower to middle troposphere (including 681 hPa) than in the upper troposphere. The mean difference between V008 and V007 is negligible.

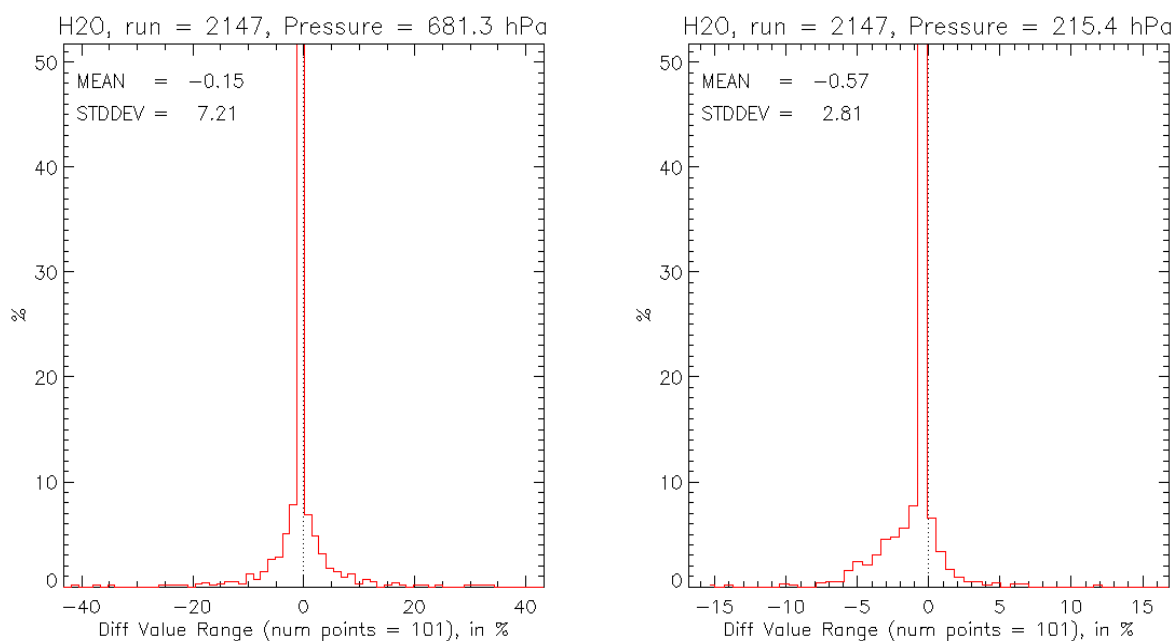


Figure 9-2 Histogram of water vapor percent differences between TES V008 and V007 retrievals for TES Global Survey run id 2147 at (left) the 681.3 hPa pressure level and (right) 215.4 hPa pressure level. Figure prepared by Ming Luo using code developed by Mark Montero.

9.6 References

9.6.1 TES H₂O References

- [1] Worden, J., S. Kulawik, C. Frankenberg, V. Payne, K. Bowman, K. Cady-Peirara, K. Wecht, J.-E. Lee, D. Noone (2012), Profiles of CH₄, HDO, H₂O, and N₂O with improved lower tropospheric vertical resolution from Aura TES radiances, *Atmospheric*

Measurement Techniques, 5, 397–411, 2012, doi:10.5194/amt-5-397-2012, February 20, 2012.

9.6.2 TES References

- [2] Bowman K. W., C. D. Rodgers, S. S. Kulawik, J. Worden, E. Sarkissian, G. Osterman, T. Steck, M. Lou, A. Eldering, M. Shephard, H. Worden, M. Lampel, S. A. Clough, P. D. Brown, C. P. Rinsland, M. Gunson, and R. Beer (2006), Tropospheric emission spectrometer: Retrieval method and error analysis, *IEEE Transactions on Geoscience and Remote Sensing*, 44(5), 1297-1307, May 2006.
- [3] Herman, Robert and Susan Kulawik (editors), Kevin Bowman, Karen Cady-Pereira, Annmarie Eldering, Brendan Fisher, Dejian Fu, Robert Herman, Daniel Jacob, Line Jourdain, Susan Kulawik, Ming Luo, Ruth Monarrez, Gregory Osterman, Susan Paradise, Vivienne Payne, Sassaneh Poosti, Nigel Richards, David Rider, Douglas Shepard, Mark Shephard, Felicia Vilnrotter, Helen Worden, John Worden, Hyejung Yun, Lin Zhang (2018), Earth Observing System (EOS) Tropospheric Emission Spectrometer (TES) Level 2 (L2) Data User's Guide (Up to & including Version 7 data), Version 7.0, JPL Internal Report D-38042, September 27, 2018.
- [4] Shephard, M. W., R.L. Herman, B.M. Fisher, K.E. Cady-Pereira, S. A. Clough, V. H. Payne, D.N. Whiteman, J. P. Comer, H. Vömel, L.M. Miloshevich, Ricardo Forno, M. Adam, G. B. Osterman, A. Eldering, J. R. Worden, L. R. Brown, H. M. Worden, S. S. Kulawik, D. M. Rider, A. Goldman, R. Beer, K. W. Bowman, C. D. Rodgers, M. Luo, C. P. Rinsland, M. Lampel, M. R. Gunson (2008), Comparison of Tropospheric Emission Spectrometer nadir water vapor retrievals with in situ measurements, *J. Geophys. Res.*, 113, D15S24, (doi:10.1029/2007JD008822) May 16, 2008.

9.6.3 General References

- [5] Bloom, S., A. da Silva, D. Dee, M. Bosilovich, J.-D. Chern, S. Pawson, S. Schubert, M. Sienkiewicz, I. Stajner, W.-W. Tan, M.-L. Wu (2005). Documentation and Validation of the Goddard Earth Observing System (GEOS) Data Assimilation System - Version 4. *Technical Report Series on Global Modeling and Data Assimilation 104606*, Vol. 26, 187 pages, April 2005. Available from (paste entire link including pdf into browser):
http://ntrs.nasa.gov/archive/nasa/casi.ntrs.nasa.gov/20050175690_2005173043.pdf
- [6] Miloshevich, L.M., H. Voemel, D.N. Whiteman, B.M. Lesht, F.J. Schmidlin, and F. Russo (2006), Absolute accuracy of water vapor measurements from six operational radiosonde types launched during AWEX-G, and implications for AIRS validation. *J. Geophys. Res.*, 111, D09S10, doi:10.1029/2005JD006083, 2006.
- [7] Rienecker, M. M., M. J. Suarez (editor), R. Todling, J. Bacmeister, L. Takacs, H.-C. Liu, W. Gu, M. Sienkiewicz, R. D. Koster, R. Gelaro, I. Stajner and J.E. Nielson (2008), The GEOS-5 Data Assimilation System- Documentation of Versions 5.0.1, 5.1.0, and 5.2.0



NASA Technical Report Series on Global Modeling and Data Assimilation 104606, Vol.27., December 2008.

- [8] Voemel, H., H. Selkirk, L. Miloshevich, J. Valverde-Canossa, J. Valdes, E. Kyro, R. Kivi, W. Stolz, G. Peng, and J.A. Diaz (2007), Radiation Dry Bias of the Vaisala RS92 Humidity Sensor, *J. Atmos. Ocean. Tech.*, 24, pp. 953-963, doi: 10.1175/JTECH2019.1, 2007.
- [9] Zhu, Y., and R. Gelaro (2008), Observation Sensitivity Calculations Using the Adjoint of the Gridpoint Statistical Interpolation (GSI) Analysis System, *Monthly Weather Review, Volume 136, Issue 1*, pp. 335-351, (DOI:10.1175/MWR3525.1) January 2008 – follow link at https://gmao.gsfc.nasa.gov/GEOS_systems/geos5/index_pubs.php

10. HDO/H₂O

10.1 Comparison of V008 to V007 HDO/H₂O

TES V008 estimates of HDO/H₂O have been compared to V007. By standard convention, the isotopic abundance is reported as δD (per mil) = $[(\text{HDO}/\text{H}_2\text{O})_{\text{obs}}/(\text{HDO}/\text{H}_2\text{O})_{\text{std}} - 1] * 1000$, where $(\text{HDO}/\text{H}_2\text{O})_{\text{std}} = 3.11 \times 10^{-4}$ based on the D/H standard ratio for Vienna Standard Mean Ocean Water. As shown in Figure 10-1 below, there is essentially a zero-mean difference between the versions: the mean bias (V008 versus V007) over 500 hPa to 825 hPa levels is 0.02 per mil, with 4 per mil RMS. The uncertainty calculation between versions are consistent. We note that, in prior versions, V006 was biased lower than V005 by -1.1 per mil in the free troposphere, and biased *higher* than V005 by +6 per mil in the boundary layer.

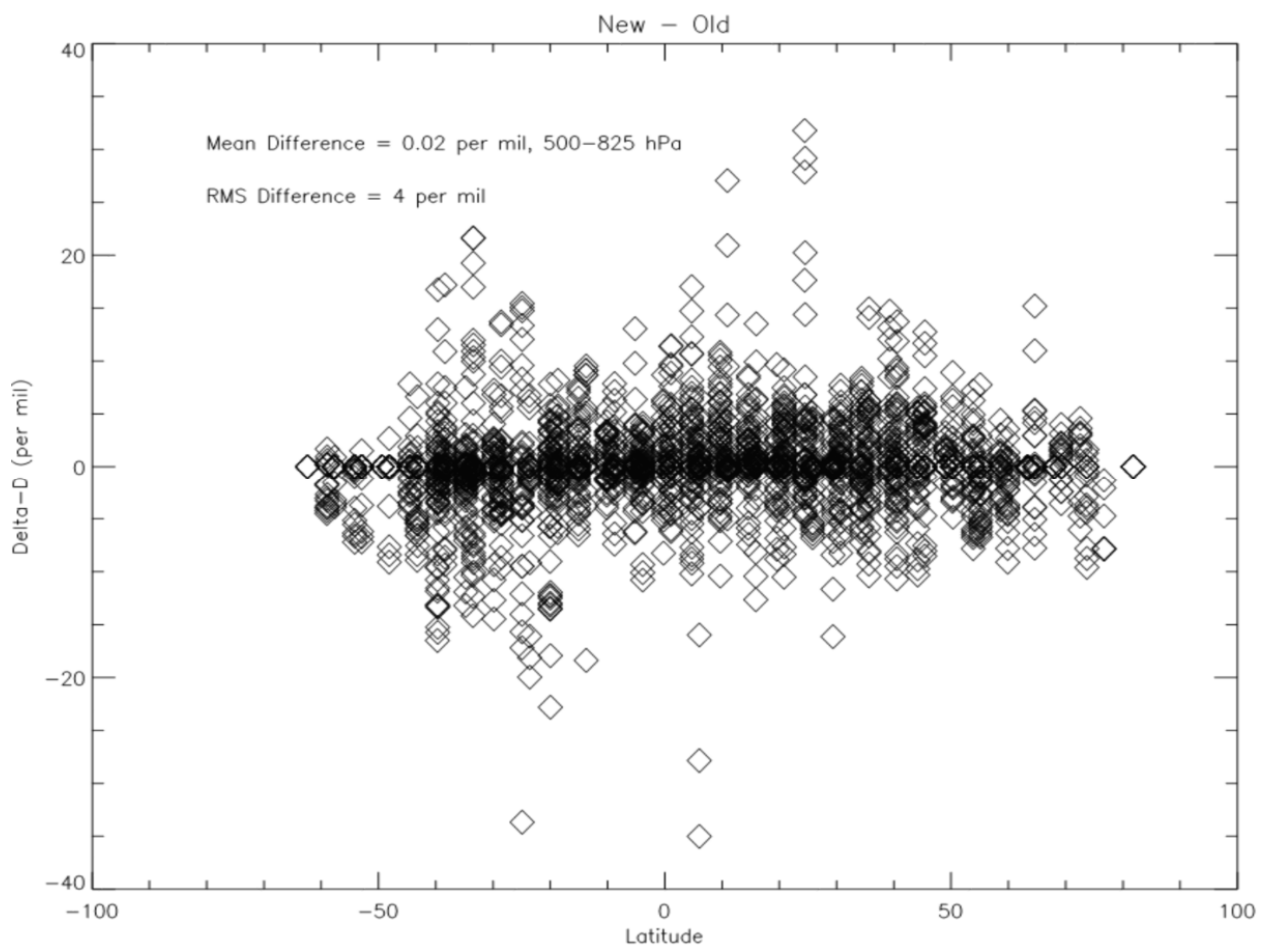


Figure 10-1 TES V008 Delta-D minus V007 Delta-D as a function of latitude.

V008 estimates of HDO/H₂O show considerable sensitivity to the isotopic composition of water vapor with typically DOFS~2 in the tropics and DOFS~1 at high latitudes. This increased sensitivity allows the TES estimates to resolve lower tropospheric and mid-tropospheric variability

of the HDO/H₂O vapor ratio (see Worden et al., 2012; Herman et al., 2014) with the expense of increased uncertainty over tropical oceans.

We find that the HDO/H₂O estimates are consistent with the previous TES release within the altitude range where the sensitivity overlaps. Comparisons with Alaska aircraft data for V008 and V007 shown virtually zero difference between the TES data versions. For validation of V005 HDO/H₂O, we refer the reader to Herman et al. (2014). For validation of V004 HDO/H₂O, we refer the reader to Worden et al. (2011).

10.2 References

10.2.1 TES HDO/H₂O References

- [1] Herman, R. L., J. E. Cherry, J. Young, J. M. Welker, D. Noone, S. S. Kulawik, and J. Worden (2014), Aircraft validation of Aura Tropospheric Emission Spectrometer retrievals of HDO / H₂O, *Atmos. Meas. Tech. Discuss.*, 7, 3127-3138, 2014, <https://doi.org/10.5194/amt-7-3127-2014>.
- [2] Worden, J., D. Noone, J. Galewsky, A. Bailey, K. Bowman, D. Brown, J. Hurley, S. Kulawik, J. Lee, M. Strong (2011), Estimate of bias in Aura TES HDO/H₂O profiles from comparison of TES and in situ HDO/H₂O measurements at the Mauna Loa observatory, *Atmospheric Chemistry and Physics*, 11, pp. 4491–4503, doi:10.5194/acp-11-4491-2011, May 12, 2011.

10.2.2 TES References

- [3] Worden, J., S. Kulawik, C. Frankenberg, V. Payne, K. Bowman, K. Cady-Peirara, K. Wecht, J.-E. Lee, D. Noone (2012), Profiles of CH₄, HDO, H₂O, and N₂O with improved lower tropospheric vertical resolution from Aura TES radiances, *Atmospheric Measurement Techniques*, 5, pp. 397–411, 2012, doi:10.5194/amt-5-397-2012, February 20, 2012.

11. Validation of Nadir Methane

Previously, TES V006 methane (CH₄) was validated against aircraft observations from all five missions of the HIAPER Pole-to-Pole Observations (HIPPO) campaign. Comparisons were performed for both the CH₄ profiles reported in the Level 2 files, and for N₂O-corrected CH₄ profiles (see Worden et al. (2012) for details of the N₂O correction). These comparisons are described in Alvarado et al. (2015), who found a high overall bias in the TES V006 CH₄ retrievals. The bias for TES V006 CH₄ relative to HIPPO measurements between 50S and 50N was 56.9 ppbv (25.7 ppbv after the N₂O correction) for upper tropospheric representative values and 27.3 ppbv (28.4 ppbv after the N₂O correction) for lower tropospheric representative values.

Here, we reference the V008 (R15) results to the V006 (R13) results that were validated against HIPPO. Using 37 TES global surveys from the time periods of the HIPPO campaign, we find that the mean difference between V006 and V007 is less than 4 ppbv at all altitudes for both uncorrected and N₂O-corrected profiles, with standard deviation less than 37 ppbv at all altitudes. Therefore, the biases between V008 and V006 are relatively small compared to the biases with respect to the HIPPO aircraft profiles.

There were no changes in the a priori and initial guess for CH₄ or N₂O between V006 (R13) and V008 (R15). There were updates to the GMAO water vapor and temperature profiles used as initial guess and a priori for those quantities going from V006 to V007, but no further changes in the GMAO in going from V007 to V008. There were non-negligible changes in the spectroscopy for CH₄ and interfering gases (H₂O, HDO, N₂O) between V006 and V008. Therefore, the variability in the differences between V006 (used here as a reference) and V008 CH₄ could have arisen from the updates to the GMAO water vapor and temperature profiles and/or spectroscopy updates.

11.1 References

11.1.1 TES CH₄ References

- [1] Alvarado, M. J., V. H. Payne, K. E. Cady-Pereira, J. D. Hegarty, S. S. Kulawik, K. J. Wecht, J. R. Worden, V. Pittman and S. C. Wofsy (2015), Impacts of updated spectroscopy on thermal infrared retrievals of methane evaluated with HIPPO data, *Atmos. Meas. Tech.*, 8, pp. 965-985, 2015.
- [2] Worden, J., S. Kulawik, C. Frankenberg, V. Payne, K. Bowman, K. Cady-Pereira, K. Wecht, J.-E. Lee, and D. Noone (2012), Profiles of CH₄, HDO, H₂O, and N₂O with improved lower tropospheric vertical resolution from Aura TES radiances, *Atmospheric Measurement Techniques*, 5, pp. 397–411, doi:10.5194/amt-5-397-2012, February 20, 2012.

11.1.2 General References

- [3] Payne, V.H., S.A. Clough, M.W. Shephard, R. Nassar and J.A. Logan (2009), Information-centered representation of retrievals with limited degrees of freedom for signal: Application to methane from the Tropospheric Emission Spectrometer, *Journal of Geophysical Research: Atmospheres*, Vol. 114 Issue D10, May 27, 2009, D10307, (doi:10.1029/2008JD010155).

12. Cloud Products

TES retrievals of cloud products rely on validation of previous data versions, as described in detail in the TES Validation Report V004 (Herman et al., 2011).

12.1 References

12.1.1 TES References

- [1] Herman, Robert and Gregory Osterman (editors), Christopher Boxe, Kevin Bowman, Karen Cady-Pereira, Tony Clough, Annmarie Eldering, Brendan Fisher, Dejian Fu, Robert Herman, Daniel Jacob, Line Jourdain, Susan Kulawik, Michael Lampel, Qinbin Li, Jennifer Logan, Ming Luo, Inna Megretskaya, Ray Nassar, Gregory Osterman, Susan Paradise, Vivienne Payne, Hank Revercomb, Nigel Richards, Mark Shephard, Dave Tobin, Solene Turquety, Felicia Vilnrotter, Helen Worden, John Worden, Lin Zhang (2011), Earth Observing System (EOS) Tropospheric Emission Spectrometer (TES) Data Validation Report (Version F05_05, F05_06, F05_07 data), Version 4.0, JPL Internal Report D-33192, November 23, 2011. Available online at: <https://eosweb.larc.nasa.gov/project/tes/validation>.

13. Carbon Dioxide Validation

13.1 Overview of current validation status of TES V008 CO₂

TES CO₂ is retrieved between 40S and 45N, with average cloud optical depth < 0.5, among other tests, for good quality. Errors tend to be correlated for close locations and times, and it is recommended to use TES data averaged in 10 degree by 10 degree by 1 month averages, both to mitigate correlated errors and reduce errors to useful levels. On average, TES CO₂ has an average of 0.65 degree of freedom for signal (DOFS) – with the most DOFS for daytime land cases (which can be on the order of 1 DOFS) and the least for nighttime or winter land cases (which can be on the order of 0.3 DOFS). Ocean targets (day or night) have intermediate DOFS with about 0.8 DOFS. The averaging kernel indicates sensitivity between the surface to above 100 hPa, with the most sensitivity between about 700 and 300 hPa, peaking at about 650 hPa. Although a profile is retrieved, there is very little independent information at the different profile levels and it is necessary to utilize the provided averaging kernel when using TES data. Most of the validation has been performed at the 510 hPa pressure level. TES V008 CO₂ is compared with aircraft vertical profiles over the Pacific from the HIAPER Pole-to-Pole Observation (HIPPO) program (Wofsy, 2011). The error assessment follows Kulawik et al. (2019), which estimates systematic and random errors, such that the error for an average of n observations equals $\sqrt{\text{systematic}^2 + \text{random}^2/n}$. The TES observations have an overall bias of -1.1 ppm versus HIPPO, a systematic error of 1.4 ppm, and random error of 7.3 ppm. This is similar to the previous V007 errors, which were estimated to be a random error of 6 ppm, and a correlated error of 1.7 ppm.

13.2 References

13.2.1 TES CO₂ References

- [1] Kulawik, S.S., J.R. Worden, S.C. Wofsy, S.C. Biraud, R. Nassar, D.B.A. Jones, E.T. Olsen, G.B. Osterman, (2012), Comparison of improved Aura Tropospheric Emission Spectrometer (TES) CO₂ with HIPPO and SGP aircraft profile measurements, *Atmospheric Chemistry and Physics Discussions*, 12, 6283 – 6329, February 29, 2012.
- [2] Kulawik, S.S., J.R. Worden, S.C. Wofsy, S.C. Biraud, R. Nassar, D.B.A. Jones, E.T. Olsen, R. Jimenez, S. Park, G. W. Santoni, B. C. Daube, J. V. Pittman, B. B. Stephens, E. A. Kort, G. B. Osterman, and TES team (2013), Comparison of improved Aura Tropospheric Emission Spectrometer (TES) CO₂ with HIPPO and SGP aircraft profile measurements, *Atmospheric Chemistry and Physics*, 13, 3205–3225, 2013, doi:10.5194/acp-13-3205-2013, March 18, 2013.
- [3] Kulawik, S.S., S. Crowell, D. Baker, J. Liu, K. McKain, C. Sweeney, S.C. Biraud, S. Wofsy, C.W. O'Dell, P.O. Wennberg, D. Wunch, C. M. Roehl, N.M. Deutscher, M. Kiel, D.W.T. Griffith, V.A. Velazco, J. Notholt, T. Warneke, C. Petri, M. De Mazière, M.K. Sha, R. Sussmann, M. Rettinger, D.F. Pollard, I. Morino, O. Uchino, F. Hase, D.G. Feist, S. Roche, K. Strong, R. Kivi, L. Iraci, K. Shiomi, M.K. Dubey, E. Sepulveda, O.E.G. Rodriguez, Y. Té, P. Jeseck, P. Heikkinen, E.J. Dlugokencky, M.R. Gunson, A. Eldering, D. Crisp, B. Fisher and G.B. Osterman, (2019), Characterization of OCO-2 and ACOS-GOSAT biases and errors for CO₂ flux estimates, *Atmos. Meas. Tech. Discuss.*, <https://doi.org/10.5194/amt-2019-257>, in review, 2019.

- [4] Nassar, R., D.B.A. Jones, S.S. Kulawik, J.R. Worden, K.W. Bowman, R.J. Andres, P. Suntharalingam, J.M. Chen, C.A.M. Brenninkmeijer, T.J. Schuck, T.J. Conway, D.E. Worthy (2011), Inverse modeling of CO₂ sources and sinks using satellite observations of CO₂ from TES and surface flask measurements, *Atmos. Chem. Phys.*, **11**, (12), 6029-6047, June 24, 2011.

13.2.2 General References

- [5] Wofsy, S.C., the HIPPO Science Team and Cooperating Modellers and Satellite Teams (2011), HIAPER Pole-to-Pole Observations (HIPPO): Fine grained, global scale measurements of climatically important atmospheric gases and aerosols, *Phil. Trans. of the Royal Society A2011 vol. 369 (no. 1943)*, 2073-2086, DOI: 10.1098/rsta.2010.0313, April 18, 2011.

14. Minor Species: Ammonia (NH₃), Methanol (CH₃OH) and Formic Acid (HCOOH)

14.1 Objectives and Data

The objective of this validation exercise was to determine the magnitude of the differences between the V007 and V008 TES NH₃, CH₃OH and HCOOH products. This analysis used data from a Step and Stare (run 5800) over western Asia on July 26, 2007 and from a Global Survey (run 2147) on September 20, 2004.

The retrieval algorithms for NH₃, HCOOH and CH₃OH were not updated between V007 and V008. V007 uses the ABSCO_v2.4 absorption coefficients, while V008 uses ABSCO_v3.0. The spectroscopic parameters used to create these tables were updated for many species, including NH₃, but not CH₃OH or HCOOH. However these changes had an insignificant impact on the signal in the NH₃ spectral feature at 967 cm⁻¹ used for retrievals. Any changes in the retrieved profiles of these minor trace species will come from changes in the algorithms for the parameters needed as inputs for these retrievals, e.g., atmospheric temperature and water vapor, surface temperature and emissivity, and ozone (for CH₃OH), or from changes in the forward model or spectroscopy of these parameters.

All three species are characterized by large uncertainties in the retrieved profiles; direct comparisons against aircraft data and estimated retrieval errors can range from 5% to 60% (Shephard et al., 2015), depending on a number of factors: amount, thermal contrast, clouds, co-location, magnitude of cross-state errors.

The changes in retrieved surface temperature between V007 and V008 (Figure 14-1) are on average significantly less than 0.5K, but there are differences as large as 3K. There is no bias between the temperature profiles from V007 and V008, but once again a few profiles show differences as great as 4K (Figure 14-2). Water vapor retrievals on average show also show little or no bias (Figure 14-3), depending on the latitude; on average the differences are within 15%, but can range as high as 40%. These results suggest that V008 retrievals for the minor species will be unbiased with respect to V007 and that the differences in the retrieved profiles will in general (though not always) be insignificant.

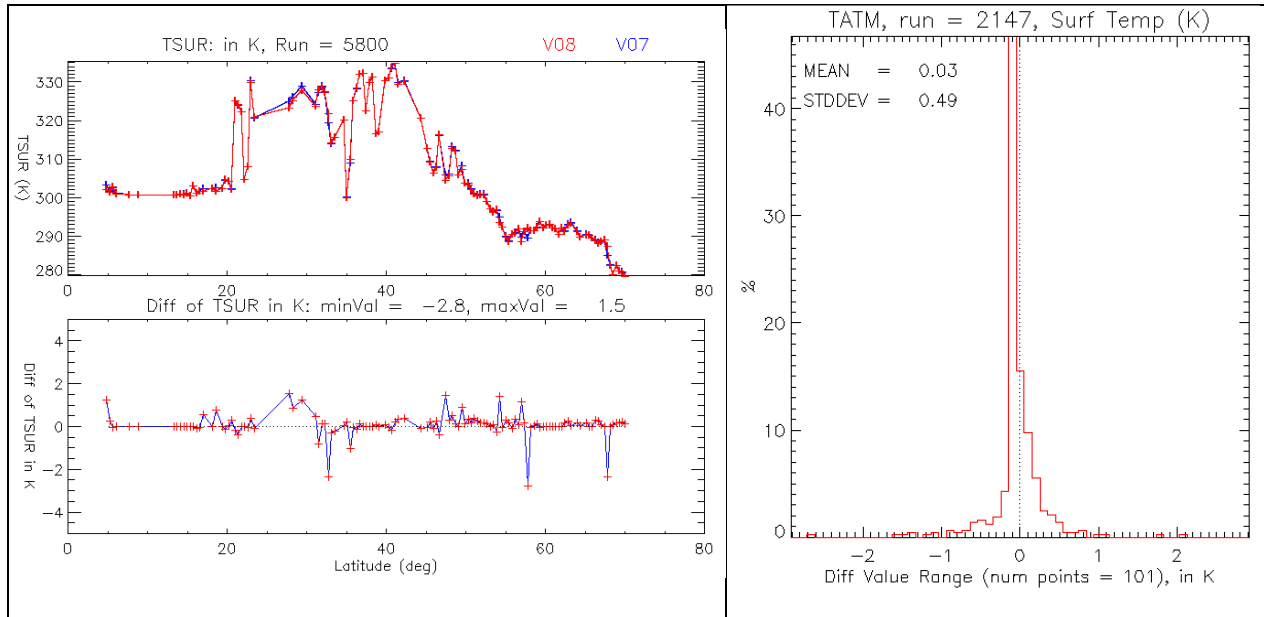


Figure 14-1 Surface temperature from V007 and V008 for run 5800 (Step and Stare) vs latitude: (left, top) and the difference between V008 and V007 (left, bottom). Histogram of the V008-V007 differences for run 2147 (GS) (right)

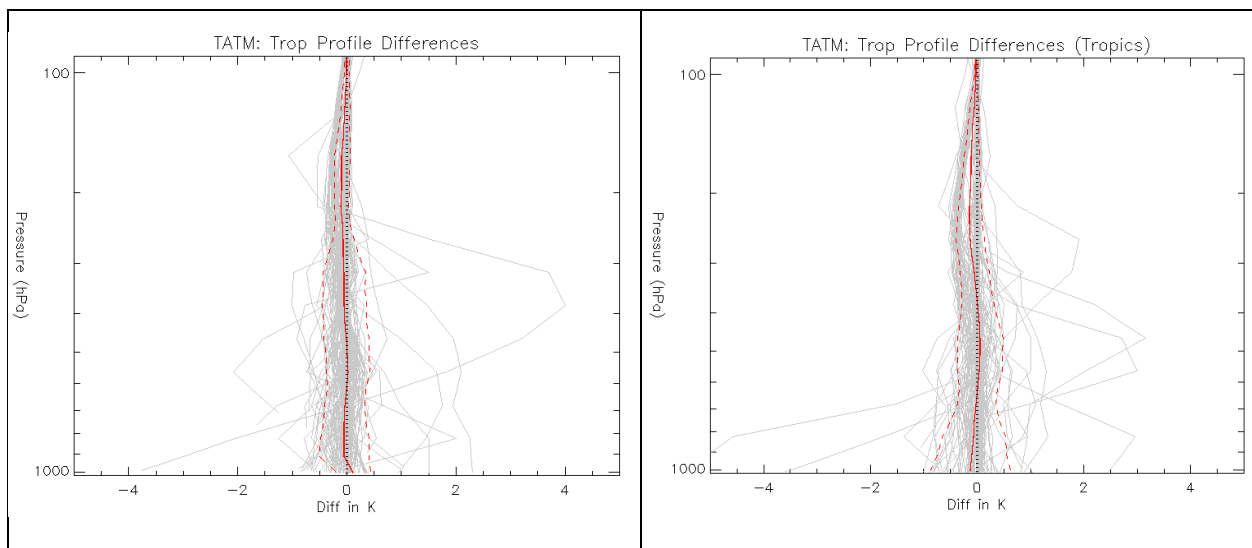


Figure 14-2 Atmospheric temperature differences between V008 and V007 for run 5800 (Step and Stare) (left) and for run 2147 (GS) (right).

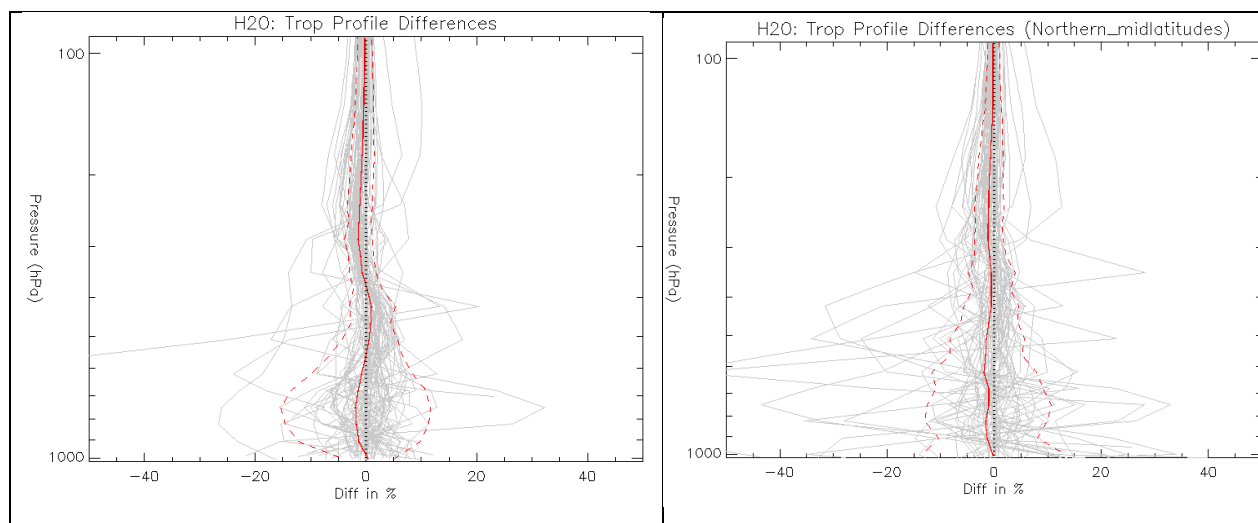


Figure 14-3 Water vapor differences between V008 and V007 for run 5800 (Step and Stare) (left) and for run 2147 (GS) (right).

14.2 Ammonia (NH₃) Analysis

Based on the differences in the input parameters to the NH₃ retrieval shown above it is expected that the differences in the NH₃ retrievals will be small, with some exceptions. The differences in DOFs (Figure 14-4, left) are trivial for the cases with meaningful DOFs, and show little change in information content; the total column differences (Figure 14-4, right) are at most 4%, much less than the estimated uncertainties in the NH₃ total column, which can range from 10% to 60%. Similar uncertainties apply to NH₃ profile retrievals: the overall differences between V007 and V008 profiles from run 5800 (Figure 14-5, left) are well within these bounds and are also unbiased. At 825 mbar the NH₃ from run 2147 (GS) (Figure 14-5, right) is for all effects unbiased; the spread in the differences is high given that the maximum value for this series is 5.32 ppbv, but large uncertainties are expected at these lower amounts. In summary, based on the analysis of these two runs, the changes included in V008 had little impact on the NH₃ retrievals, and should not alter the validity of the statement included in the V006 and V007 validation reports that TES captures the spatial variability of NH₃ over regions with strong NH₃ signals. (see TES V006 Validation report (Herman et al., 2014), and TES V007 Validation Report (Herman et al., 2018), and references therein).

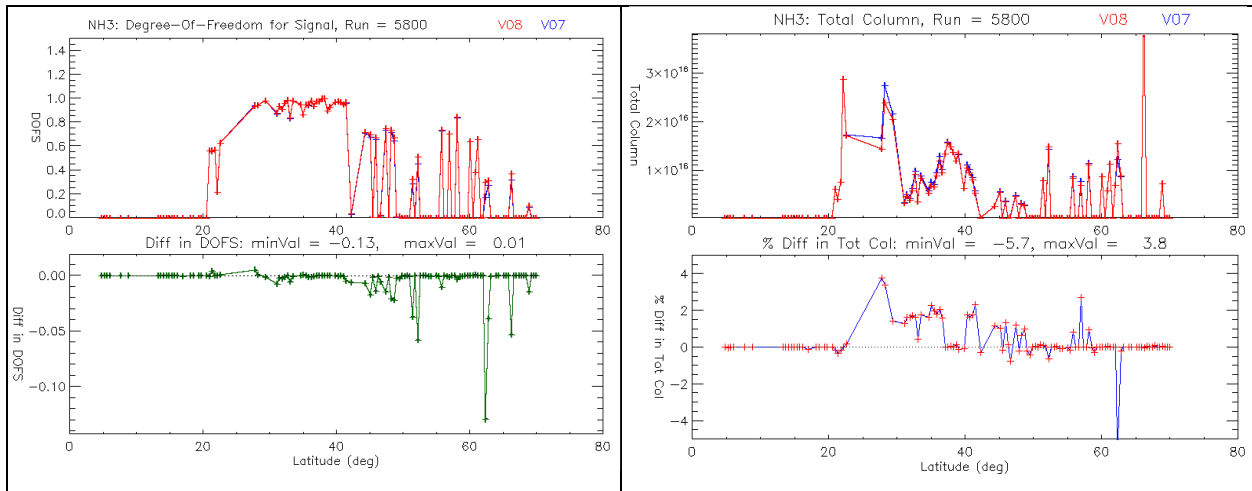


Figure 14-4 NH₃ Information from V007 and V008 vs latitude for run 5800 (Step and Stare): DOFs (left, top) and the difference between V008 and V007 (left, bottom). Total column NH₃ (right, top) and the differences between V007 and V008 (right, bottom).

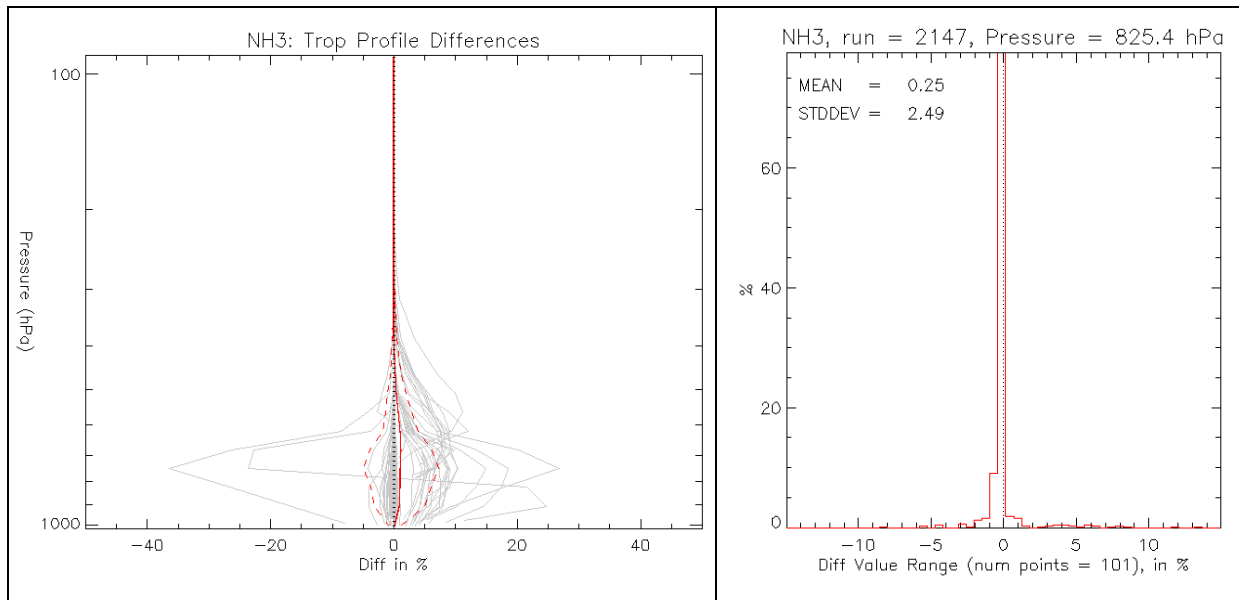


Figure 14-5 NH₃ differences between V008 and V007 for run 5800 (Step and Stare) (left) and histogram of differences for run 2147 (GS) at 825 hPa (right)

14.3 Methanol (CH₃OH) Analysis

CH₃OH is radiatively active in the O₃ band, thus changes to O₃ retrievals will propagate into the CH₃OH retrieval. Comparisons of V007 and V008 O₃ retrievals (Figure 14-6) show no bias in the lower troposphere, where CH₃OH is concentrated, and on average the differences are within 5% of the O₃ amounts, with a few exceptions. As expected, CH₃OH from V008 is unbiased with respect to V007 (Figure 14-7), and the differences are mostly within 5%, with fewer outliers than in the O₃ retrievals. The information content is nearly identical (Figure 14-8) and the differences in total column are negligible given the uncertainties in the CH₃OH retrievals (Figure 14-9).

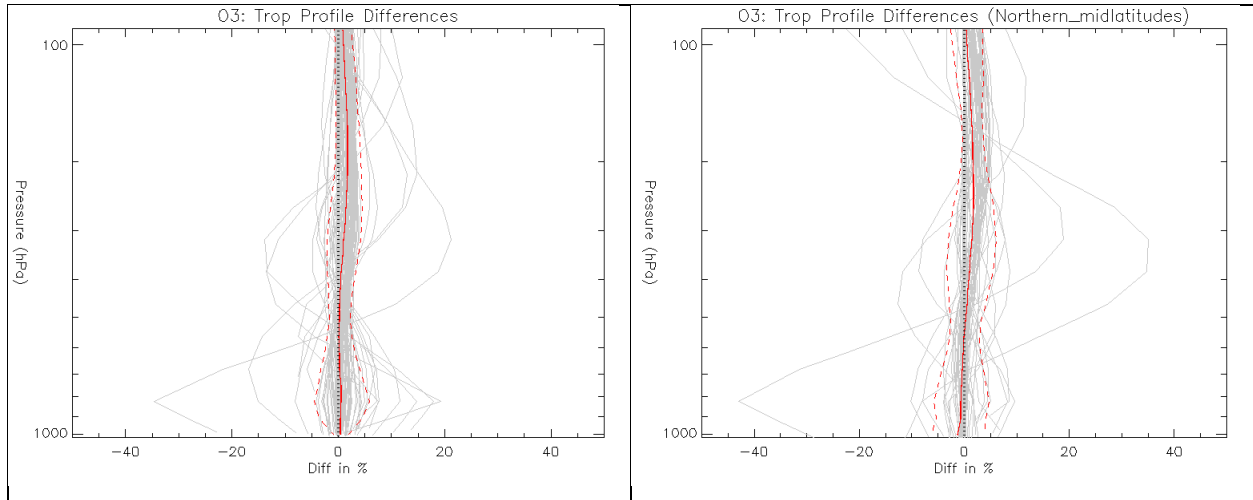


Figure 14-6 Ozone differences between V008 and V007 for run 5800 (Step and Stare) (left) and for run 2147 (GS) (right)

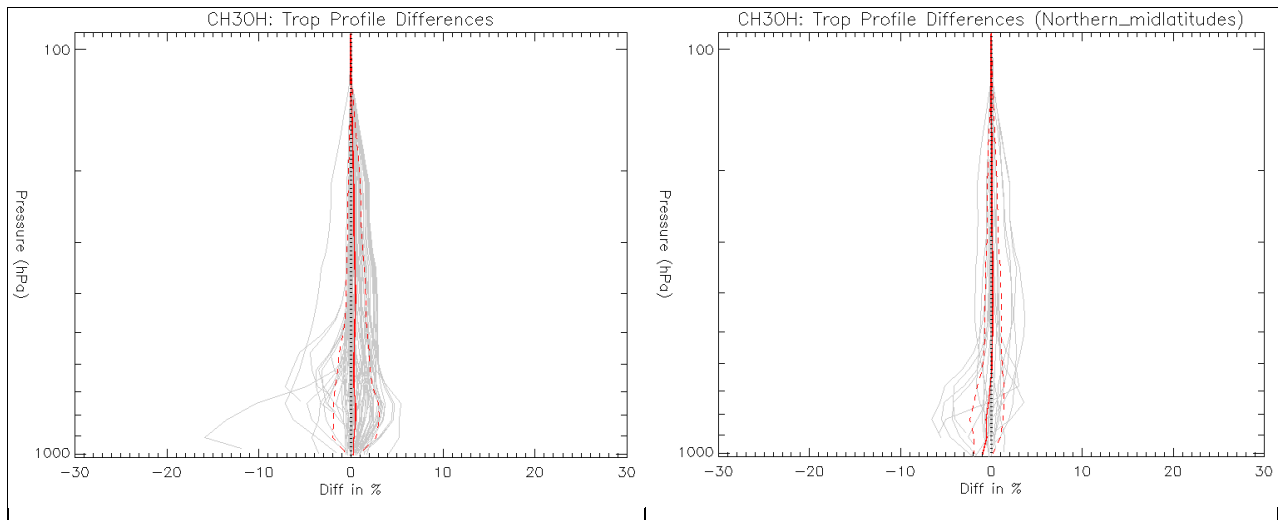


Figure 14-7 CH₃OH differences between V008 and V007 for run 5800 (Step and Stare) (left) and for run 2147 (GS) (right)

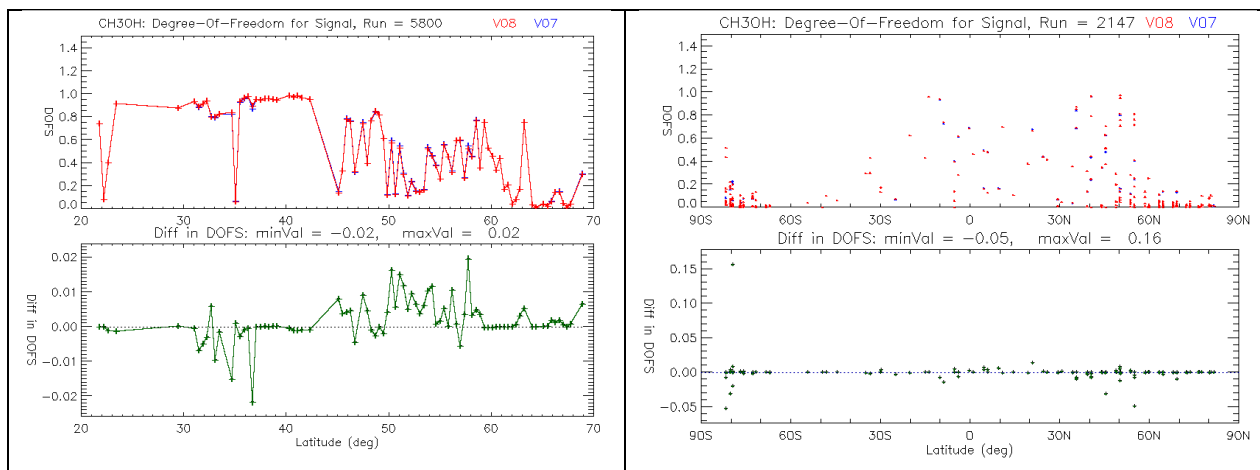


Figure 14-8 CH₃OH information from V007 and V008 vs latitude: DOFs (top) and the difference between V008 and V007 (bottom); run 5800 (left) and run 2147 (right)

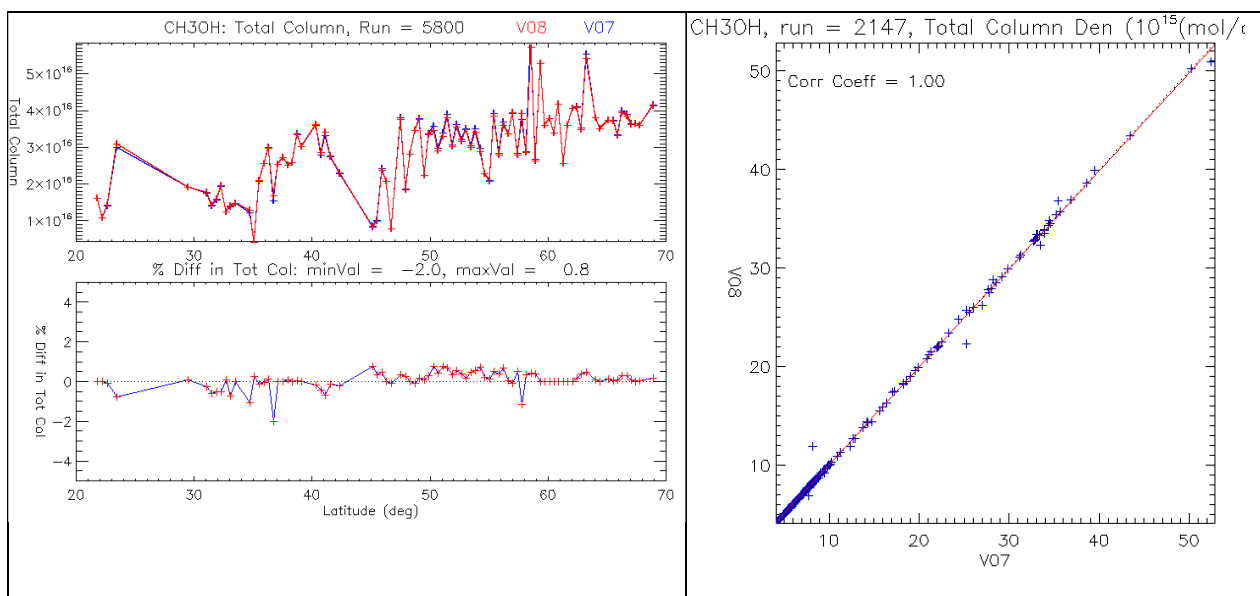


Figure 14-9 CH₃OH total column from V007 and V008 vs latitude for run 5800 (Step and Stare): total column (left, top) and the difference between V008 and V007 (left, bottom); total column scatter plot for run 2147 (GS) (right): red line is linear fit, dashed line is 1:1.

There has been little validation of any version of the TES CH₃OH retrievals. The V006 TES Validation report (Herman et al., 2014), and references therein, described a validation of the prototype algorithm against aircraft data taken during a number of campaigns (e.g., Megacity Initiative: Local and Global Research Observations (MILAGRO), ARCTAS, INTEX-B) using the

GEOS-Chem CTM as a transfer function. This analysis and the posterior use of TES data to constrain emissions showed that TES CH_3OH could provide useful information over relatively large scales. Limited comparisons of the prototype retrieval and V006 and V007 were carried out, but were hampered by varying throughput from each algorithm. An attempt to use DISCOVER-AQ data was also made, but the TES CH_3OH throughput during this time was very low. The CH_3OH signal is weak and is deep within the ozone band, making CH_3OH retrievals very sensitive to errors in ozone retrievals. Thus validation requires large amounts of data to obtain meaningful results. The differences between V007 and V008 are thus minor given the current uncertainties in the retrieval quality of individual profiles

14.4 Formic Acid (HCOOH) Analysis

The spectral feature used for HCOOH retrievals is around 1105 cm^{-1} , in a region with weak water vapor and ozone lines, so changes between V007 and V008 will most likely be due to changes to the retrieved temperature profile, which were shown in Figure 14-2 to be small for most profiles but significant for some. Therefore it is expected that the differences between V007 and V008 HCOOH will be similar. Indeed, the bias between V007 and V008 HCOOH profiles is negligible and only a few profiles differ by more than a few percent (Figure 14-10). The information content is nearly identical (Figure 14-11) and the differences in total column are negligible given the uncertainties in the CH_3OH retrievals, in almost all cases (Figure 14-12).

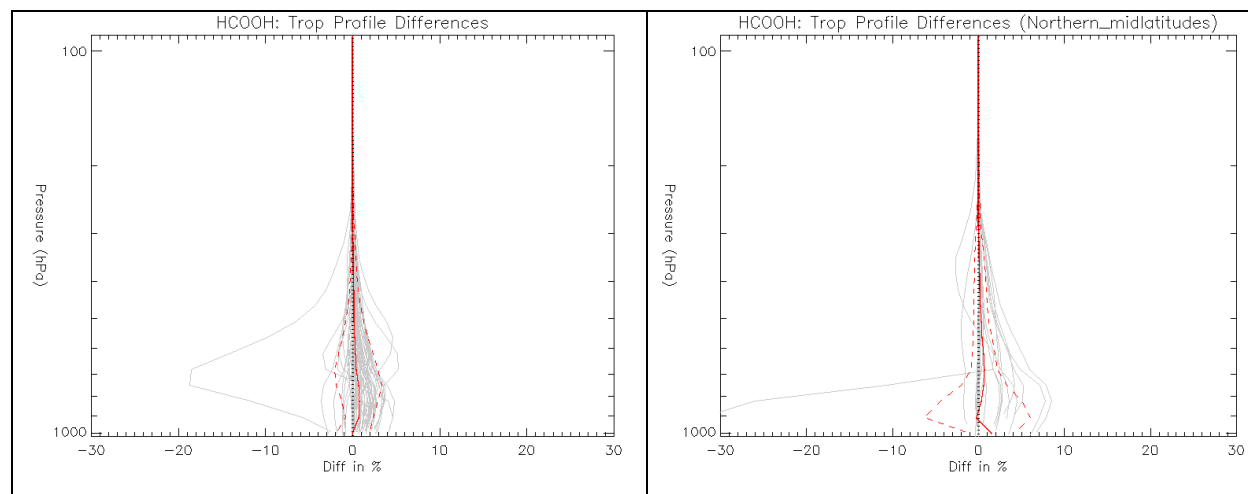


Figure 14-10 HCOOH differences between V008 and V007 for run 5800 (Step and Stare) (left) and for run 2147 (GS) (right)

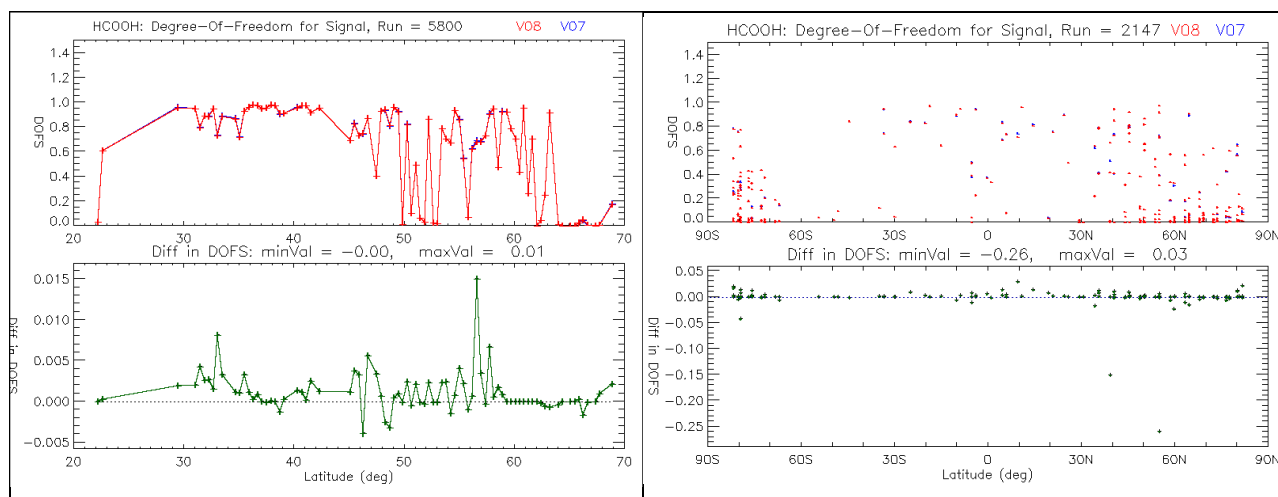


Figure 14-11 HCOOH information from V007 and V008 vs latitude: DOFs (top) and the difference between V008 and V007 (bottom); run 5800 (left) and run 2147 (right)

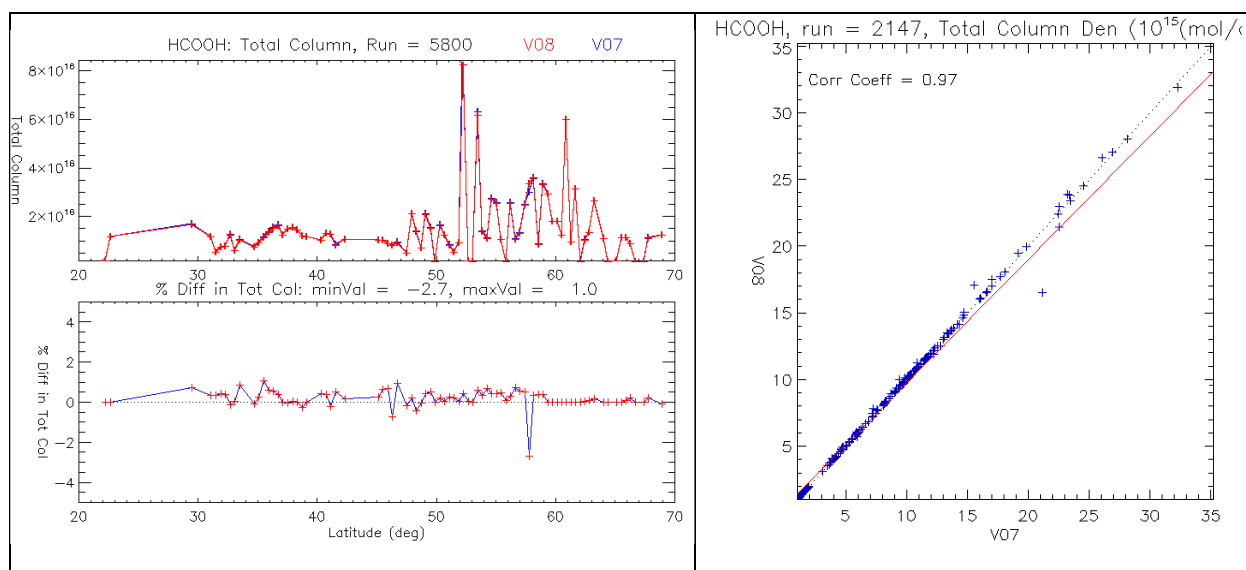


Figure 14-12 HCOOH total column from V007 and V008 vs latitude for run 5800 (Step and Stare): total col (left, top) and the difference between V008 and V007 (left, bottom); total column scatter plot for run 2147 (GS) (right): red line is linear fit, dashed line is 1:1.

The V006 TES Validation report (Herman et al., 2014), and references therein, described a validation of the prototype HCOOH algorithm against aircraft data taken during a couple of campaigns (MILAGRO, INTEX-B) using the GEOS-Chem CTM as a transfer function. Both aircraft measurements and TES data showed that GEOS-Chem HCOOH correlated well with the MILAGRO data, but underestimated the INTEX-B data. Limited comparisons of the prototype retrieval and V006 were carried out, but showed good correlation with each other, and no significant bias. Given the low bias between V006 and V007, and V007 and V008, it is expected

that V008 data would provide similar results. An attempt to use DISCOVER-AQ data was also made, but the HCOOH levels in this region/period were too close to the detectability level (0.5 ppbv) to provide useful TES data.

14.5 References

14.5.1 TES NH₃, CH₃OH and HCOOH References

- [1] Herman, Robert and Gregory Osterman (editors), Matthew Alvarado, Christopher Boxe, Kevin Bowman, Karen Cady-Pereira, Tony Clough, Annmarie Eldering, Brendan Fisher, Dejian Fu, Robert Herman, Daniel Jacob, Line Jourdain, Susan Kulawik, Michael Lampel, Qinbin Li, Jennifer Logan, Ming Luo, Inna Megretskaja, Ray Nassar, Gregory Osterman, Susan Paradise, Vivienne Payne, Hank Revercomb, Nigel Richards, Mark Shephard, Dave Tobin, Solene Turquety, Felicia Vilnrotter, Kevin Wecht, Helen Worden, John Worden, Lin Zhang, Earth Observing System (EOS) Tropospheric Emission Spectrometer (TES) Data Validation Report (Version F07_10 data), Version 6.0, Jet Propulsion Laboratory Internal Report D-33192, June 20, 2014. Available online at: <https://eosweb.larc.nasa.gov/project/tes/validation>.
- [2] Herman, Robert and Gregory Osterman (editors), Matthew Alvarado, Christopher Boxe, Kevin Bowman, Karen Cady-Pereira, Tony Clough, Annmarie Eldering, Brendan Fisher, Dejian Fu, Robert Herman, Daniel Jacob, Line Jourdain, Le Kuai, Susan Kulawik, Michael Lampel, Qinbin Li, Jennifer Logan, Ming Luo, Inna Megretskaja, Ray Nassar, Gregory Osterman, Susan Paradise, Vivienne Payne, Hank Revercomb, Nigel Richards, Mark Shephard, Dave Tobin, Solene Turquety, Felicia Vilnrotter, Kevin Wecht, Helen Worden, John Worden, Lin Zhang (2018), Earth Observing System (EOS) Tropospheric Emission Spectrometer (TES) Data Validation Report (Version F08_11 data), Version 7.0, JPL Internal Report D-33192, May 30, 2018. Available online at: <https://eosweb.larc.nasa.gov/project/tes/validation>.
- [3] Shephard, M. W., C. A. McLinden, K. E. Cady-Pereira, M. Luo, S. G. Moussa, A. Leithead, J. Liggio, R. M. Staebler, A. Akingunola, P. Makar, P. Lehr, J. Zhang, D. K. Henze, D. B. Millet, J. O. Bash, L. Zhu, K. C. Wells, S. L. Capps, S. Chaliyakunnel, M. Gordon, K. Hayden, J. R. Brook, M. Wolde, and S.-M. Li (2015), Tropospheric Emission Spectrometer (TES) satellite observations of ammonia, methanol, formic acid, and carbon monoxide over the Canadian oil sands: validation and model evaluation, *Atmos. Meas. Tech.*, *Volume 8, Issue 12*, 5189-5211, doi:10.5194/amt-8-5189-2015, December 10, 2015.

15. Peroxylacetyl nitrate (PAN) Validation

Peroxyacetyl nitrate (PAN) may show large variation on relatively small spatial scales. Ideally, the PAN product would be validated using comparisons with coincident in situ measurements. Sufficient coincidences for robust TES PAN validation are not available. However, TES PAN retrievals have been previously examined for the existence of expected features in the PAN fields. PAN was first introduced as a TES product in V007 (R14). The V007 retrievals (as well as prototype results that preceded V007) have been extensively utilized in peer-reviewed publications. Therefore, we have performed a preliminary assessment of the V008 (R15) PAN product by (1) comparing to TES observations/time periods that have previously been utilized in publications and (2) checking consistency between V007 and V008.

The PAN algorithm has not changed between V007 and V008, but there have been updates to the spectroscopy of interfering species that could cause minor changes to the retrieved PAN. Payne et al. (2014) showed that the dominant sources of error in the TES PAN retrievals are instrument noise, water vapor and ozone. V007 uses the ABSCO v2.5 tables, while V008 uses ABSCO v3.0.

Payne et al. (2014) showed examples of elevated CO and PAN in boreal burning plumes (previously identified by Alvarado et al. (2010)) seen in TES special observations made during the July 2008 phase of the ARCTAS campaign. These plume examples showed strong evidence for PAN enhancements in fire plumes and demonstrated that it was possible for adjacent TES pixels to show sharply different PAN volume mixing ratios. Although coincident aircraft data were not available, the retrieved PAN values, between zero and 1.5 ppbv, were deemed to be reasonable, given the range of PAN values measured from aircraft during the campaign (Alvarado et al., 2010; Roberts et al., 2009). Figure 15-1 shows the V008 results for the same example boreal fire plumes that were shown in Payne et al. (2014), clearly showing the expected spatial correlation between enhancements in TES CO and PAN. Note that these plots are very similar for V008 and V007 (not shown).

Payne et al. (2017) showed prototype PAN retrieval results for the Tropics in austral spring, showing a maximum in PAN over the tropical Atlantic, a feature that had been predicted by models and also previously observed using limb-sounding satellite measurements. Figure 15-2 shows global maps of V007 and V008 PAN for October 2006, a time period highlighted in Payne et al. (2017). Figure 15-2 shows elevated PAN in the tropical south Atlantic, as expected, and also shows overall good agreement between the two sets of results, providing further confidence in the V008 PAN product.

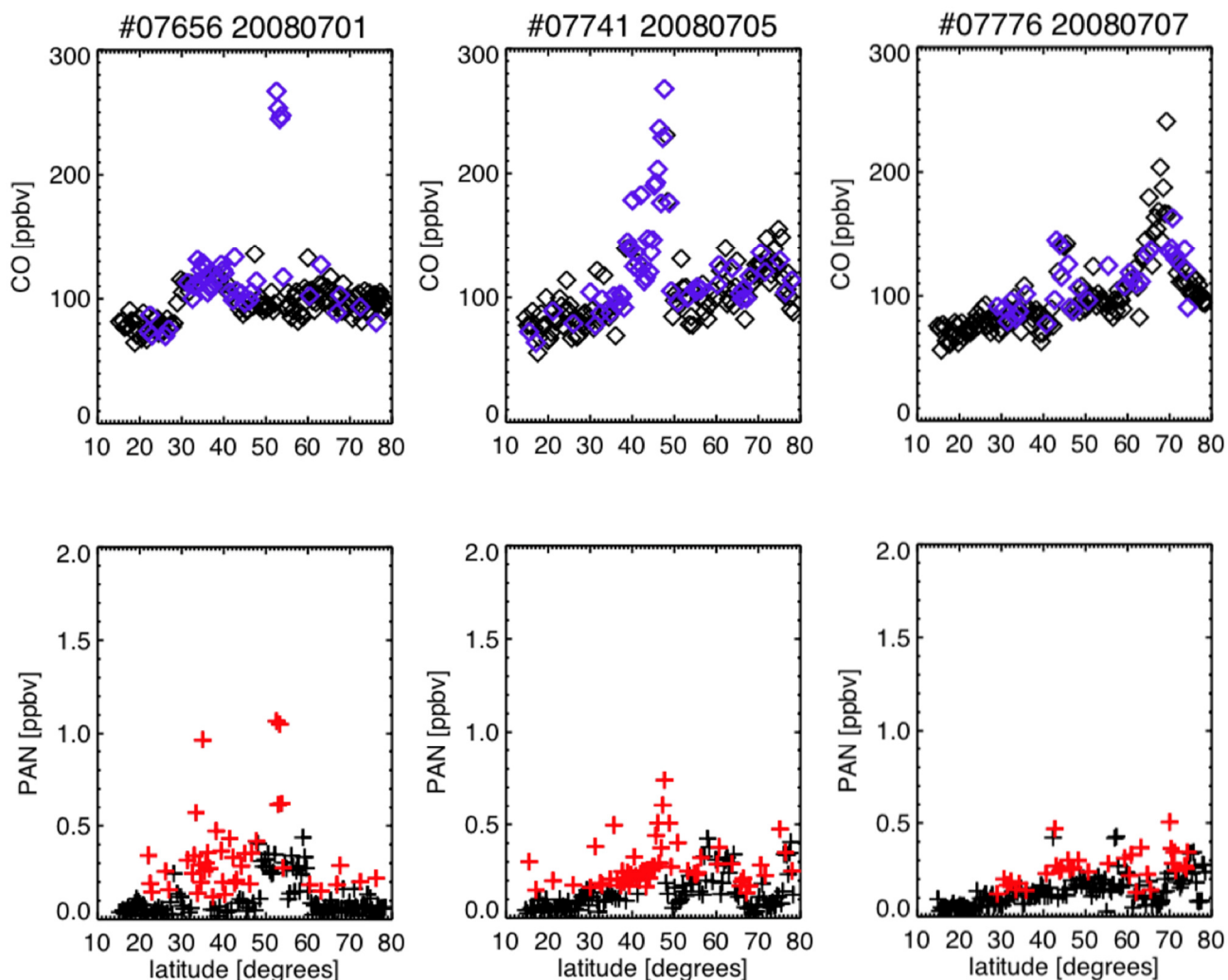


Figure 15-1 Examples of elevated CO and PAN in boreal burning plumes (previously identified by Alvarado et al. (2010) and shown in Payne et al. (2014)) seen in TES special observations made during the July 2008 phase of the ARCTAS campaign. These are the V008 retrievals. CO plots show the retrieved CO at 510 mbar, while PAN plots show the average retrieved VMR for retrieval levels between 800 hPa and the tropopause. Colored points show the cases where the degrees of freedom for signal (DOFS) was greater than 0.6 for the PAN retrieval.

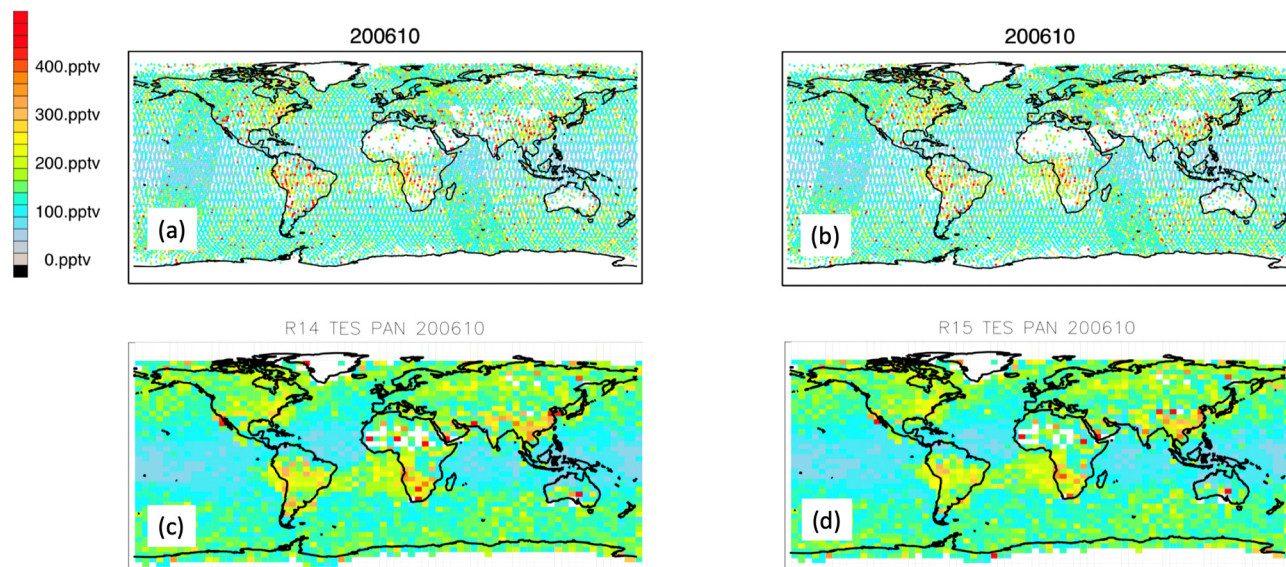


Figure 15-2 Comparison between V007 and V008 global PAN results for October 2006. PAN values shown here represent the average VMR for retrieval levels between 800 mbar and the tropopause. Panels (a) and (b) show individual PAN retrievals for V007 and V008 respectively, while panels (c) and (d) show gridded results for V007 and V008 respectively.

15.1 References

15.1.1 TES PAN References

- [1] Alvarado, M.J., J. A. Logan, J. Mao, E. Apel, D. Riemer, D. Blake, R. C. Cohen, K.-E. Min, A. E. Perring, E. C. Browne, P. J. Wooldridge, G. S. Diskin, G. W. Sachse, H. Fuelberg, W. R. Sessions, D. L. Harrigan, G. Huey, J. Liao, A. Case-Hanks, J. L. Jimenez, M. J. Cubison, S. A. Vay, A. J. Weinheimer, D. J. Knapp, D. D. Montzka, F. M. Flocke, I. B. Pollack, P. O. Wennberg, A. Kurten, J. Crouse, J. M. St. Clair, A. Wisthaler, T. Mikoviny, R. M. Yantosca, C. C. Carouge, and P. Le Sager (2010), Nitrogen oxides and PAN in plumes from boreal fires during ARCTAS-B and their impact on ozone: an integrated analysis of aircraft and satellite observations, *Atmospheric Chemistry and Physics*, *10*, doi:10.5194/acp-10-9739-2010, 2010
- [2] Payne, V. H., M. J. Alvarado, K. E. Cady-Pereira, J. R. Worden, S. S. Kulawik, and E. V. Fischer (2014), Satellite observations of peroxyacetyl nitrate from the Aura Tropospheric Emission Spectrometer, *Atmospheric Measurement Techniques*, *7/3737/2014/*, doi:10.5194/amt-7-3737-2014, November 12, 2014
- [3] Payne, V. H., E.V. Fischer, J.R. Worden, Z. Jiang, L. Zhu, Thomas P. Kurosu, and S.S. Kulawik (2017), Spatial variability in tropospheric peroxyacetyl nitrate in the tropics from infrared satellite observations in 2005 and 2006, *Atmospheric Chemistry and Physics*, *17*, 6341-6351, <https://doi.org/10.5194/acp-17-6341-2017>, 2017.

- [4] Roberts, J. M., J. Neuman, J. B. Nowak, T. B., Ryerson, J. W. Peischl, J. Holloway, C. Warneke, and J. A. de Gouw, (2009), Measurements of Acylperoxynitrates (PANs) in Biomass Burning Plumes over the Arctic in Spring 2008, *Eos Trans. AGU*, 90(52), American Geophysical Union, Fall Meeting Suppl., Abstract A43A-0231, 2009

16. Nadir Carbonyl Sulfide (OCS) Validation

Carbonyl sulfide (OCS) product was added as a standard product in TES V007. Now we have TES V008. Here we evaluate the data quality in V008 by comparing V008 with V007 and checking the representation of the special global pattern and the comparison with the observations by HIPPO campaign for the latitudinal gradient over different months of the year.

16.1 Sampling density

Similar to V007, we grid the OCS product into 5° by 10° (lat x lon) grid box so that the sampling density is at least above 50 observations per pixel between $+50^\circ$ and -50° latitudinal range for four seasons. V008 currently has lower sampling density, especially for the December-January-February (DJF) seasonal average (Figure 16-1).

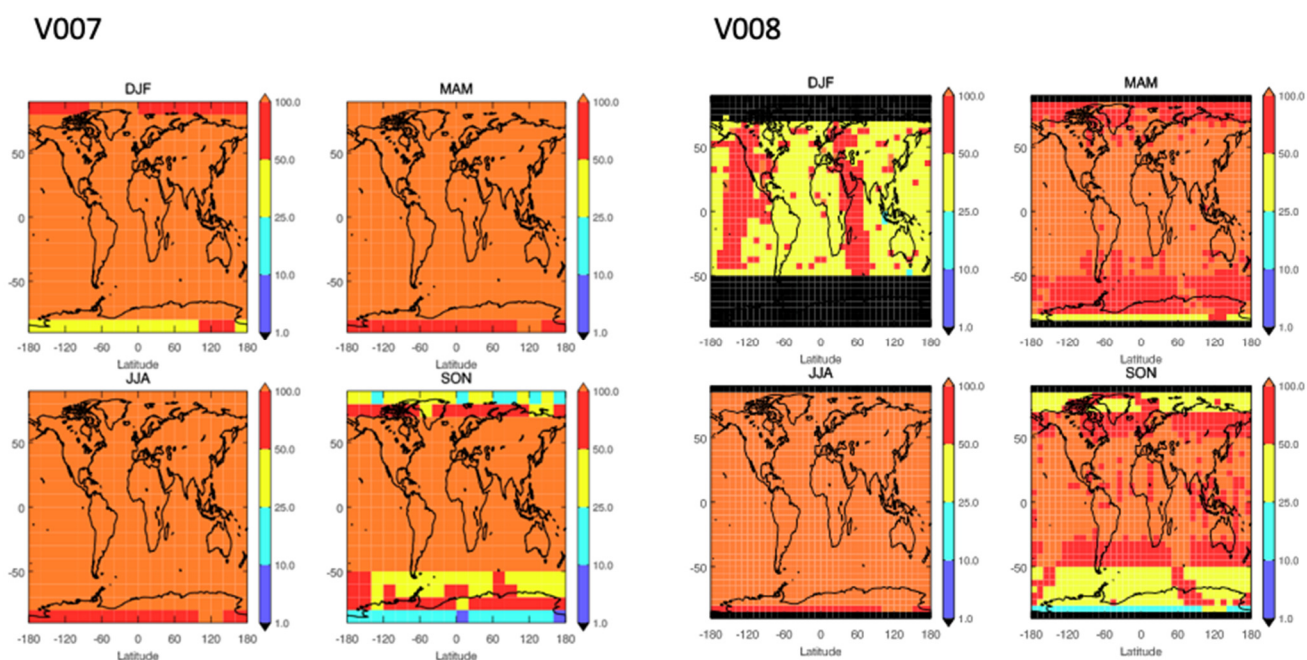


Figure 16-1 The maps of the sampling density for four seasons. Left for V007 and right for V008.

16.2 Global pattern

The spatial patterns of the higher OCS from the tropical Western Pacific warm pool region exist in V008 but have a relative weaker maximum in a smaller area compared with V007 for all four seasonal averages (Figure 16-2). The lower sampling density in V008 data might be one of the reasons.

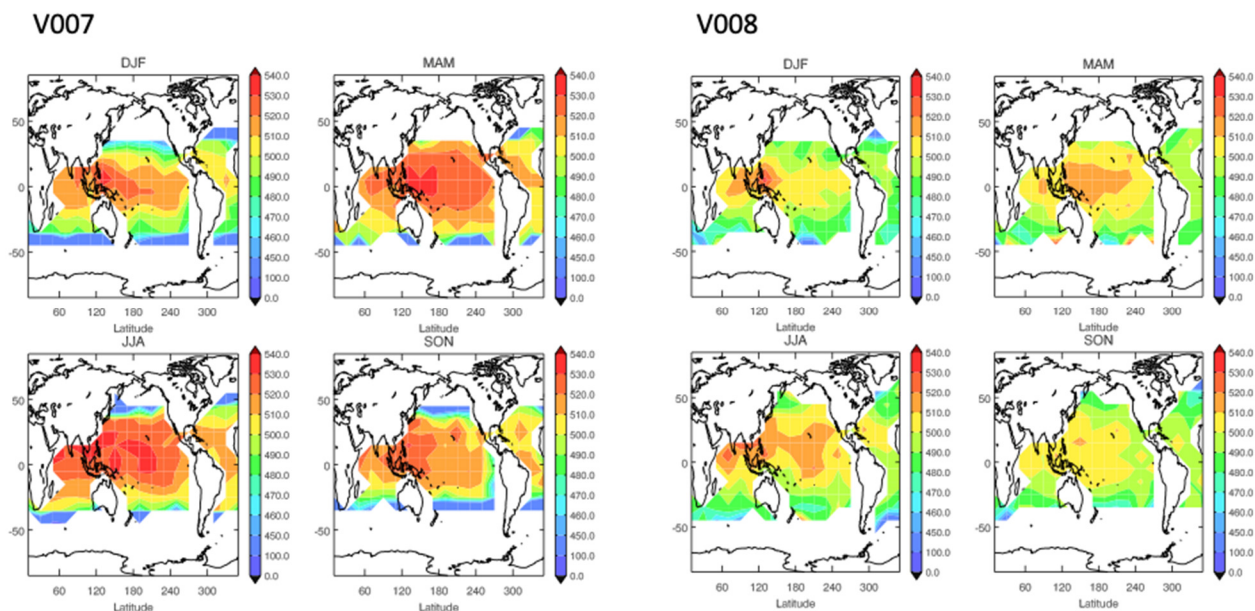


Figure 16-2 The global data with quality control in four seasons.

16.3 Comparison with HIPPO observation data

Figure 16-3 compares the HIPPO observed free tropospheric OCS across the central Pacific from north to south with the two version of TES products. The left column shows the path of the observations in the months of January, November, April, July, and September through the two years of the campaign. The blue highlighted path is the data over land, which are not included in the comparison with TES ocean data. We took the HIPPO free troposphere profiles averaged between 200 and 900 hPa to compare with TES OCS product. The blue curves with light blue shade in the plots of the middle and right column are the same HIPPO grid data along latitudes with one standard deviation. The red lines with yellow shade are the TES OCS product (V007 in the middle columns and V008 in the right column) matched to the HIPPO path.

The V008 TES OCS product shows a reasonably consistent latitudinal gradient over different seasons but shows slight low bias. The correlation coefficients are lower in V008 than V007, especially in the months of January and April. Not enough sampling density will be the reason for the differences between the two versions of the products.

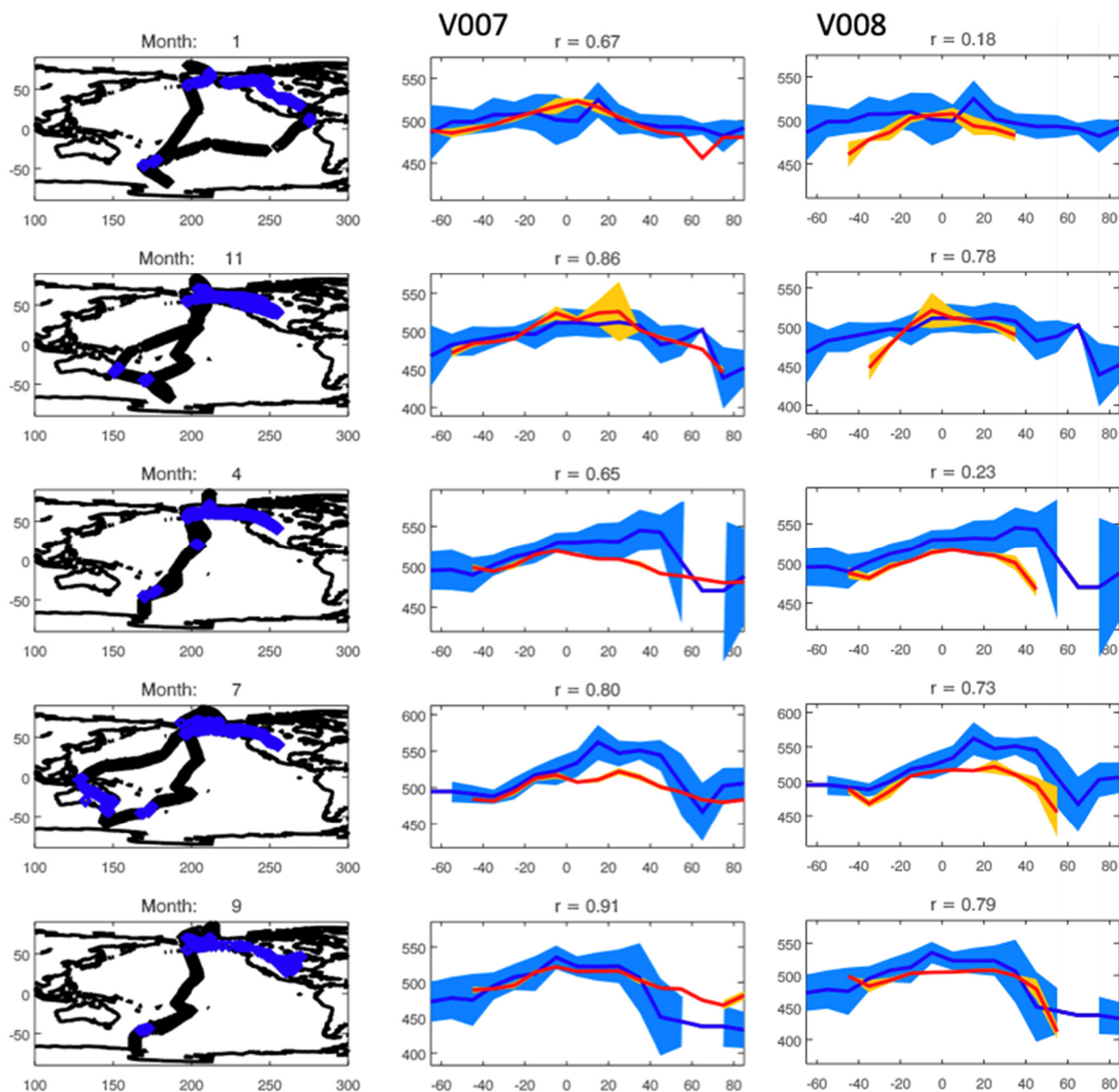


Figure 16-3 Comparisons between HIPPO and TES matched OCS in V007 and V008. Left column is the HIPPO path during each campaign. The middle and right column shows the HIPPO free tropospheric OCS in blue and TES OCS in red.

16.4 References

16.4.1 TES OCS References

- [1] Kuai, L., J. Worden, S.S. Kulawik, S.A. Montzka, and J. Liu (2014), Characterization of Aura TES carbonyl sulfide retrievals over ocean, *Atmos. Meas. Tech.*, 7, 163-172, <https://doi.org/10.5194/amt-7-163-2014>, 2014.

17. Hydrogen Cyanide (HCN) Validation

Hydrogen cyanide (HCN) is a new product in TES V008. TES is sensitive to HCN in the upper troposphere (e.g. 200 hPa) and therefore will primarily observe fire signatures with high injection heights. TES HCN is the first product to be retrieved in linear volume mixing ratio (VMR). This has the advantage of resulting in very consistent sensitivity over the large range of retrieved HCN, but also may result in negative HCN values. The initial guess and a priori for HCN are set to a constant value of 100 parts per trillion.

Validation of HCN is from the global distribution of HCN for October, 2006. The large Indonesian fires in October, 2006, should show up strongly in HCN (Lupu et al., 2009). Figure 17-1 for HCN shows this large signal. This figure is made off of partially processed TES data and includes run IDs 5047, 5050, 5053, 5055, 5058, 5061, 5064, 5066, 5069, 5072, 5075, 5077, 5080, 5083, 5086, 5088, 5090, 5093, 5095, 5097, 5099, 5101, 5103, 5105, 5107, 5110, 5112, 5115, 5117, 5119.

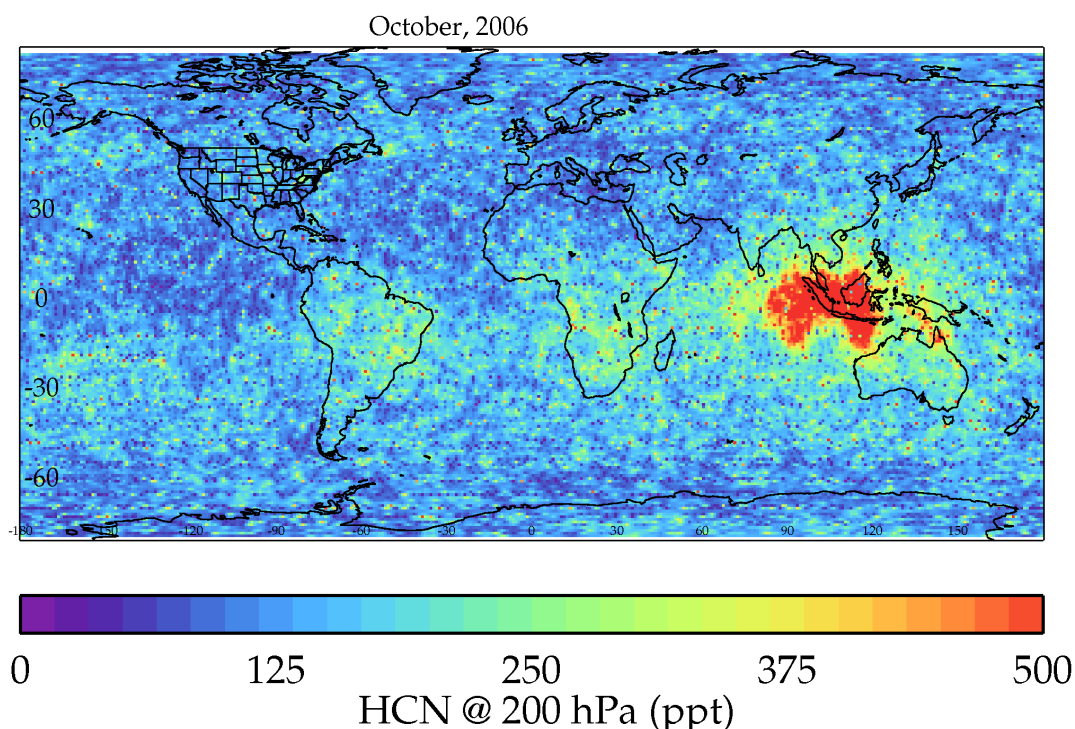


Figure 17-1 Retrieved TES HCN for October, 2006. A large HCN signal is expected over Indonesia.

17.1 References

17.1.1 TES HCN References

- [1] Lupu, J.W. Kaminski, L. Neary, J.C. McConnell, K. Toyota, C.P. Rinsland, P.F. Bernath, K.A. Walker, C.D. Boone, Y. Nagahama and K. Suzuki (2009), Hydrogen cyanide in the upper troposphere: GEM-AQ simulation and comparison with ACE-FTS observations, *Atmos. Chem. Phys.*, 9, 4301–4313, <https://doi.org/10.5194/acp-9-4301-2009>, 2009.

Appendices

A. Acronyms

ABSCO	Absorption Coefficient
ACE	Atmospheric Chemistry Experiment
AER	Atmospheric and Environmental Research
AGU	American Geophysical Union
AIRS	Atmospheric Infrared Sounder
AK	Averaging Kernel
AKVMR	Averaging Kernel weighted Volume Mixing Ratio
ALIAS	Aircraft Laser Infrared Absorption Spectrometer
AMoN	Ammonia Monitoring Network
AMSU	Advanced Microwave Sounding Unit
ASDC	Atmospheric Science Data Center
ARCIONS	Arctic Intensive Ozone Sonde Network Study
ARCPAC	Aerosol, Radiation, and Cloud Processes affecting Arctic Climate
ARCTAS	Arctic Research on the Composition of the Troposphere from Aircraft and Satellites
ARM	Atmospheric Radiation Measurement
ARM-SGP	Atmospheric Radiation Measurement – Southern Great Plains
ASHOE	Airborne Southern Hemisphere Ozone Experiment
AVE	Aura Validation Experiment
BL	Boundary Layer
CalNex	California Nexus
CAMNET	Coordinated Air Monitoring NETWORK
CASA	Carnegie Ames Stanford Approach
CFH	Cryogenic Frostpoint Hygrometer
CH ₃ OH	Methanol
CH ₄	Methane, Natural Gas
CIMS	Chemical Ionization Mass Spectrometer
CIT	California Institute of Technology
CMAQ	Community Multi-scale Air Quality

CO	Carbon Monoxide
CO ₂	Carbon Dioxide
COD	Cloud Optical Depth
CONTRAIL	CONDensation TRAIL
CR-AVE	Costa Rica Aura Validation Experiment
CTM	Chemical Transport Model
CTP	Cloud Top Pressure
DACOM	Differential-Absorption CO Monitor
DFM	Design File Memorandum
DISCOVER-AQ	Deriving Information on Surface conditions from Column and Vertically Resolved Observations Relevant to Air Quality
DJF	December-January-February
DN	Data Number
DOE	Department of Energy
DOF	Degrees of Freedom
DOFS	Degrees of Freedom for Signal
DPS	Data Products Specification
EMIS	Emissivity
EOS	Earth Observing System
EPA	Environmental Protection Agency
ESDT	Earth Science Data Type
ESRL	Earth System Research Laboratory
FM	Forward Model
FPH	Frost-Point Hygrometer
FTIR	Fourier Transform Infrared Spectrometer
FTP	File Transfer Protocol
FTS	Fourier Transform Spectrometer
GAW	Global Atmosphere Watch
GEOS	Global Earth Observing System
GEOS	Goddard Earth Observing System
GMAO	Global Modeling Assimilation Office
GMD-ESRL	Global Monitoring Division of the Earth System Research Laboratory
GoMACCS	Gulf of Mexico Atmospheric Composition and Climate Study

GSFC	Goddard Space Flight Center
GSI	Gridpoint Statistical Interpolation
GTS	Global Telecommunications Service
H ₂ O	Dihydrogen Monoxide (Water)
HCN	Hydrogen Cyanide
HCOOH	Formic Acid
HDF	Hierarchical Data Format
HDO	Hydrogen Deuterium Monoxide (“Heavy Water”)
HIAPER	High-Performance Instrumented Airborne Platform for Environmental Research
HIPPO	HIAPER Pole-to-Pole Observations
HIRDLS	High Resolution Dynamics Limb Sounder
HIRS	High Resolution Infrared Sounders
HIS	High-Resolution Interferometer Sounder
HITRAN	High-resolution TRANsmission molecular absorption database
hPa	Hectopascal, a unit used for air pressure
HYSPLIT	Hybrid Single-Particle Lagrangian Integrated Trajectory
IASI	Infrared Atmospheric Sounding Interferometer
ICS	Interferometer Control System
IDL	Interactive Data Language
IEEE	Institute of Electrical and Electronics Engineers
IGRA	Integrated Global Radiosonde Archive
INTEX	International Chemical Transport Experiment
INTEX-B	Intercontinental Transport Experiment-Phase B
ITCZ	InterTropical Convergence Zone
IONS	INTEX Ozonesonde Network Study
IRK	Instantaneous Radiative Kernel
ISM	Integrated Spectral Magnitude
JPL	Jet Propulsion Laboratory
K	Kelvin
L1B	Level 1B
L2	Level 2
LBLRTM	Line-by-Line Radiative Transfer Model

LIRK	Logarithm IRK
LT	Lower Troposphere
LWRE	Longwave Radiative Effect
MACPEX	Mid-Latitude Airborne Cirrus Properties EXperiment
MATCH	Model of Atmospheric Transport and Chemistry
MILAGRO	Megacity Initiative: Local and Global Research Observations
MISR	Multi-angle Imaging SpectroRadiometer
MLS	Microwave Limb Sounder
MODIS	Moderate Resolution Imaging Spectroradiometer
MOHAVE	Measurements of Humidity in the Atmosphere Validation Experiments
MOPITT	Measurement Of Pollution In The Troposphere
MOZAIC	Measurement of OZone by Airbus In-service airCRAFT
MOZART	Model for OZone And Related chemical Tracers
N ₂ O	Nitrous Oxide
NADP	National Atmospheric Deposition Program
NASA	National Aeronautics and Space Administration
NCAR	National Center for Atmospheric Research
NCEP	National Centers for Environmental Prediction
NDACC	Network for the Detection of Atmospheric Composition Change
NESR	Noise Equivalent Spectra Radiance
NH	New Hampshire
NH ₃	Ammonia
NOAA	National Oceanic and Atmospheric Administration
O ₃	Ozone
OCS	Carbonyl Sulfide
OD	Optical Depth
OEM	Optimal Estimation Method
OMI	Ozone Monitoring Instrument
PAN	Peroxyacetyl Nitrate
PAVE	Polar Aura Validation Experiment
PBL	Planetary Boundary Layer
PCS	Pointing Control System

PGE	Product Generation Executive
PI	Principal Investigator
PM	Particulate Matter
POLARIS	Photochemistry of Ozone Loss in the Arctic Region in Summer
PTR	Proton-Transfer-Reaction
PTR-MS	Proton-Transfer-Reaction Mass Spectrometry
QCL	Quantum Cascade Laser
RMS, rms	Root-Mean-Square
ROI	Reynolds Optimally Interpolated
RTVMR	Representative Tropospheric Volume Mixing Ratio
RVMR	Representative Volume Mixing Ratio
SCIAMACHY	Scanning Imaging Absorption Spectrometer for Atmospheric Cartography
SGP	Southern Great Plains
SHADOZ	Southern Hemisphere Additional Ozonesondes
SO	Special Observation
SRF	Spectral Response Function
SST	Sea Surface Temperature
Stdev	Standard Deviation
STRAT	Stratospheric Tracers of Atmospheric Transport
TATM	Temperature
TES	Tropospheric Emission Spectrometer
TexAQS-II	Second Texas Air Quality Study
TIR	Thermal Infrared
TOA	Top Of Atmosphere
TOPP	Tropospheric Ozone Pollution Project
TSUR	Surface Temperature
UT	Upper Troposphere
UTC	Universal Time Coordinated
VMR	Volume Mixing Ratio
WACCM	Whole Atmosphere Community Climate Model
WAVES	Water Vapor Validation Experiments
WMO	World Meteorological Organization

WOUDC World Ozone and Ultraviolet Radiation Data Centre
WP-3D Lockheed Research Aircraft used by NOAA